

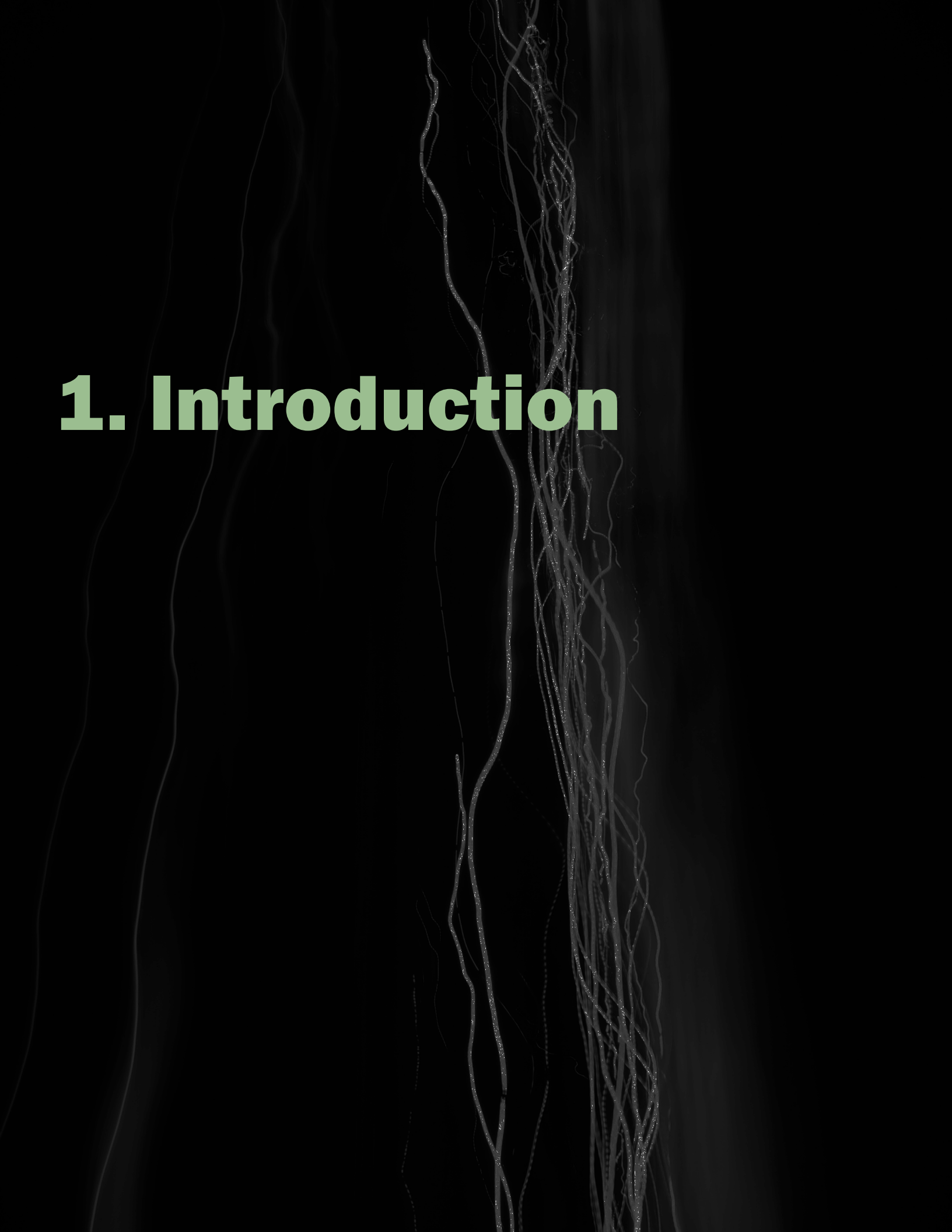
***UNDERSTANDING
MMWAVE SPECTRUM
FOR 5G NETWORKS***



Contents

1	Introduction	6
2	Status of Millimeter Wave Spectrum	9
2.1	Regional Status.....	9
2.2	Global Millimeter Wave Auctions	12
3	Millimeter Wave Technical Rules in the United States	15
3.1	Licensed Spectrum	15
3.2	Lightly Licensed	16
3.3	Unlicensed Spectrum	17
4	Millimeter Wave Challenges and Opportunities.....	19
4.1	Losses in Millimeter Wave	19
4.2	Opportunities in Millimeter Wave	29
5	Millimeter Wave Use Cases and Solutions.....	36
5.1	Use Case Considerations in mmWave Spectrum	36
5.2	5G mmWave Deployment Scenarios.....	36
5.3	5G mmWave Use Cases.....	38
5.4	Fixed Wireless Access	41
5.5	Backhaul	42
5.6	Distributed Antenna Systems	45
5.7	Repeaters.....	46

- 6 Enabling Technologies for Millimeter Wave..... 49
 - 6.1 RAN Architecture 49
 - 6.2 Antennas..... 52
 - 6.3 Beamforming 54
 - 6.4 Beam Acquisition and Tracking 60
 - 6.5 Standardization of Enabling Technologies For mmWave..... 61
- 7 Millimeter Wave Operational Aspects..... 66
 - 7.1 Multi-Connectivity 66
 - 7.2 Practical Deployment Challenges 70
 - 7.3 Hardware Impairments..... 71
 - 7.4 Handset Challenges..... 74
- 8 Link Budget and Performance Evaluation 79
 - 8.1 Outdoor Deployments 79
 - 8.2 Indoor Deployments 85
 - 8.3 Layer Management for Maximum Capacity..... 89
 - 8.4 Evolving Requirements for Future mmWave Technology Developments..... 93
- Conclusion 95
- Appendix..... 96
- Acknowledgments 108



1. Introduction

1 Introduction

The fifth generation (5G) of wireless communications technology is fundamentally transforming the telecommunications industry. The evolution of wireless data applications and the increasing popularity of smart devices have led to a massive proliferation of mobile data traffic, creating challenges and opportunities for mobile service providers. 5G is expected to enable further economic growth and digitization of a connected society of people and all possible things. 5G is gearing up to enable new use cases such as smart cities, smart agriculture, smart grids, energy, smart manufacturing, autonomous driving, logistics, public safety and numerous other verticals. New network requirements are on the rise due to the anticipated massive growth in connected devices and substantial increase in the data traffic in the near future. However, the daunting challenge to reach these heights and which has always been the case with mobile communications is the availability of useful and applicable spectrum.

5G systems are being planned for deployment in a variety of spectrum bands: below 1 GHz, between 1 and 6 GHz, and for the first time in spectrum beyond 6 GHz in the millimeter wave (mmWave) frequency range. The bandwidth shortage experienced by wireless communications has especially motivated the use of the underutilized mmWave bands (technically 30 to 300 GHz, but commonly used to refer to spectrum down to 24 GHz as well). These frequencies offer a vast amount of spectrum, including approximately 100 GHz has been defined for future 5G broadband mobile communication networks. This new foundation in mmWave spectrum, in combination with low- and mid-band spectrum, and the novel technologies to fully leverage this spectrum are expected to significantly boost the performance of the 5G cellular networks with increased spectrum

bandwidth, massive parallel communications and ultra-dense networks.

5G New Radio (NR) is the first mobile technology generation to make use of the mmWave spectrum. Although it has been years in the making, its characteristics and performance, as well as the status of the infrastructure and devices, are still not well understood by various stakeholders and the public. As the mobile communications industry continue to make strides in developing and deploying 5G NR systems in the mmWave band, a lot of new information is now available in terms of new methodologies, performance results and learning from various trials and deployments that can shed light on mmWave spectrum, its benefits and even challenges involved in this sphere.

As 5G NR systems in mmWave frequencies continue to advance, one of the most anticipated outcomes is its ready applicability in providing enhanced Mobile Broadband (eMBB) services, allowing operators to meet the growing demand for high speed data for typical outdoor deployment scenarios (e.g. dense urban micro, suburban, etc.). 5G NR mmWave promises a compelling complement to existing Wi-Fi deployments, both for indoor venues (e.g., convention centers, event halls, concert, indoor stadiums, etc.) as well as in enterprise deployments (e.g., office buildings, shop floors, meeting rooms, auditoriums, etc.). mmWave can provide new and enhanced experiences with multi-Gbps data rates, low latency and virtually unlimited capacity while supporting an array of devices beyond smartphones, tablets and laptops. It delivers on this promise through dense spatial reuse enabled by beamforming at both the cell site and device and vast amounts of spectrum.

The deployment of mobile communications in what is commonly referred to as millimeter wave spectrum requires dealing with the harsh radio frequency (RF) environment associated with high

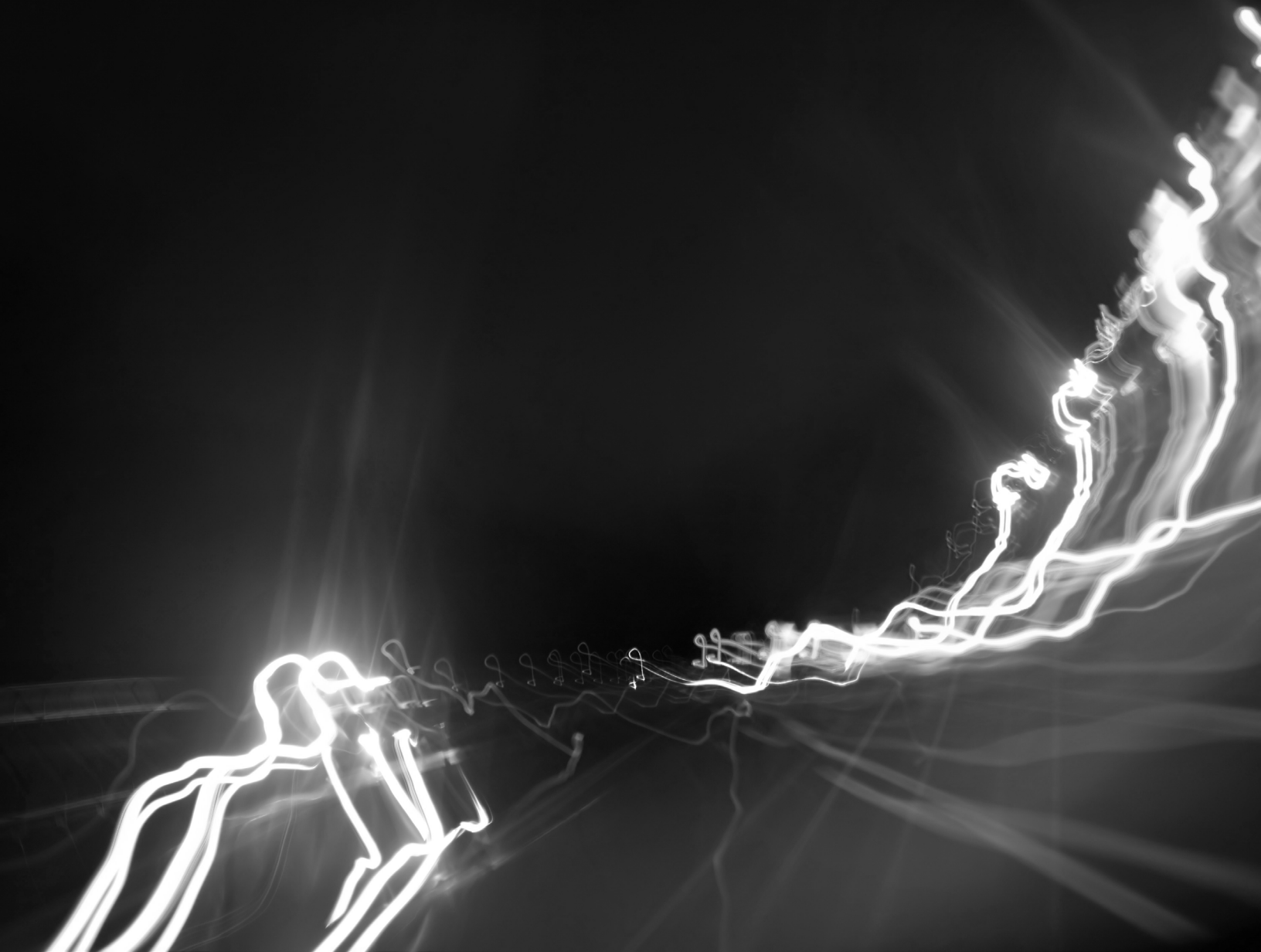
frequency bands. There is higher pathloss, reduced scattering, a resulting reduction in channel diversity, and increased blockage from weaker non-line-of-sight paths. These are serious issues that must be overcome for efficient mobile communications in millimeter wave spectrum. In addition, the effect of noise power is more pronounced in millimeter wave due to the usage of larger bandwidths.

Without question, there are several issues that need to be addressed to use this spectrum effectively. Massive MIMO, beamforming and the use of small cells or ultra-cell densification are seen as key solutions for future 5G mobile deployments in millimeter wave. Understanding and deploying these technologies effectively can unlock exciting new horizons in mobile broadband communications.

This whitepaper discusses the primary elements that are crucial for the development and deployment of 5G mmWave mobile communications. This paper also summarizes the understanding of the characteristics of the mmWave propagation channel, and highlights the main challenges, existing solutions and benefits associated with the use of mmWave spectrum. Most importantly, this paper will capture the lessons that are being learned in the ongoing mmWave deployments and defines the evolving requirements for the future mmWave technology developments. This whitepaper is organized as follows:

- **Chapter 2 provides a status of mmWave spectrum in the US and elsewhere in the world.**
- **Chapter 3 provides a look at the regulatory underpinnings of mmWave spectrum on 5G.**
- **Chapter 4 presents a detailed analysis of the mmWave channel.**
- **Chapter 5 presents several use cases for mmWave.**
- **Chapter 6 further discusses the technologies that allow mmWave to work.**
- **Chapter 7 discusses operational aspects of mmWave.**
- **Chapter 8 discusses the mmWave link budget and its performance characteristics.**

2. Status of Millimeter Wave Spectrum



2 Status of Millimeter Wave Spectrum

Millimeter wave spectrum falls in the range of 30 GHz to 300 GHz. The term millimeter wave describes the shortness of the radio wavelength, which is only a few millimeters or less. The 5G industry is also using spectrum that is a little longer than mmWaves, such as 24 GHz and 28 GHz – but these frequencies share a lot of the same operating characteristics. These bands, along with 39 GHz frequencies and higher, are referred to as millimeter wave.

The main attraction of mmWave spectrum is its large bandwidth, making it possible to deliver gigabit wireless services. Another advantage of this spectrum is that the antennas used to transmit and receive are so small that you can pack a large number of antenna elements into a small area, making it possible to achieve high antenna gain and beamforming, even in handsets. However, the primary drawback is the small target area used to receive a signal. Advances in silicon manufacturing have reduced the cost of mmWave hardware dramatically to a point where it is now feasible for consumer electronics. With further research and development currently ongoing, adaption of mmWave into 5G systems seem to be well on its way.

The following section details efforts that national and regional entities have undertaken to make spectrum 24 GHz and above available to 5G. While not exhaustive, it provides a decent look at the state of mmWave spectrum availability globally. It also addresses upcoming and already completed spectrum auctions.

2.1 Regional Status

2.1.1 United States

There has been an extensive push towards allocation of spectrum for 5G broadband services in the U.S.; progress has been made both below and above 24 GHz. Initially, the focus was exclusively on spectrum above 24 GHz, but since 2017 the FCC has increased its efforts to identify mid-band spectrum suitable for 5G applications as well.

The FCC has been driving the process of making spectrum above 24 GHz available for 5G since 2014. As a result, multiple bands, including 24 GHz (24.25 - 24.45/24.75 - 25.25 GHz), 37 GHz (37.6 - 38.6 GHz), 39 GHz (38.6 - 40 GHz), and 47 GHz (47.2 - 48.2 GHz) bands were designated for Upper Microwave Flexible Use Service (UMFUS), and the 64 - 71 GHz spectrum was designated for unlicensed use.

Auction of the UMFUS bands started in November 2018 and concluded in 2020. Through these auctions, 24 GHz, 28 GHz, 37 GHz, 39 GHz, and 47 GHz bands have been made available for 5G use in the United States. 5G systems are currently deployed in the US by all three major carriers using 28 GHz, 39 GHz or both.

The FCC has also proposed a number of new bands, including 26 GHz (25.25 - 27.5 GHz), 42 GHz (42 - 42.5 GHz), and 50 GHz (50.4 - 52.4 GHz) for flexible use service, and 70 GHz (71 - 76 GHz), and 80 GHz (81 - 86 GHz) for fixed services.

In February 2018, the FCC adopted a new Notice of Proposed Rulemaking (NPRM) called “Spectrum Horizons,” which makes the spectrum above 95 GHz more readily accessible for new innovative services and technologies.

2.1.2 Canada

Canada has also been active in identifying and designating new spectrum for 5G broadband services. In June 2018, Innovation, Science and Economic Development Canada (ISED) released a document entitled “Spectrum Outlook 2018 to 2022”, which outlined its plans to make additional spectrum resources available to support commercial mobile services, including 5G services, in several bands through 2022. Priority 1 bands identified in the document included the 600 MHz, 3500 MHz, 26 GHz, 28 GHz, 37-40 GHz, and 64-71 GHz bands.

In June 2017, ISED issued SLPB-001-17, Consultation on Releasing Millimeter Wave Spectrum to Support 5G,⁴ seeking comments on making millimeter wave (mmWave) spectrum available to support the deployment of 5G in the 28 GHz (27.50 - 28.35 GHz) and 37 - 40 GHz frequency bands for flexible fixed and mobile use, and the 64 - 71 GHz frequency band for license-exempt use. Subsequently, ISED released an addendum. ISED also sought comments of the importance of harmonizing the band plan for the 26.5 - 28.35 GHz band with the U.S. While a decision on this consultation has not yet been made, an auction of the 26.5 - 28.35 GHz and 37 - 40 GHz bands is expected to take place in 2021.

2.1.3 Latin America

Some of the larger Latin American countries are well-positioned to move forward with making mmWave spectrum available for 5G. The larger economies generally support mobile usage as a co-primary allocation across a range of frequencies, from 25 GHz to 96 GHz. Moreover, there is good alignment in allocations with the work ongoing in preparation for WRC-19 with respect to these bands.

To date, other than Brazil, Chile, Colombia, Costa Rica, Mexico, Peru, and Uruguay, no other Latin American country has initiated plans to utilize these frequency bands for mobile services with proceedings, such as planning to assign licenses.

Chile is the only country in the region that will assign mmWave spectrum during 2020 with 1500 MHz in the 26 GHz scheduled for assignment before the end of the year. Uruguay granted a temporary license to the state-owned operator Antel in the 28 GHz that is being used to provide commercial fixed broadband services. All other Latin American countries have postponed their mmWave spectrum assignment processes to at least 2021.

Brazil is considering an auction of 26 GHz and updated rules in 2021, as well as unlicensed access to the extended 60 GHz band (54 - 71 GHz). Relative to the WRC-19 agenda item on 5G (IMT 2020), Mexico is supporting 24.65 - 27 GHz for mobile broadband. Colombia and Uruguay have joined Brazil’s Draft Inter-American Proposal to identify the 26 GHz band for mobile broadband at the WRC. Brazil also has a proposal to identify the 39 GHz band (37 - 43 GHz) for mobile broadband, as does Mexico. In addition, Mexico supports identifying the 42 - 43.5 GHz, 47.2 - 48.2 GHz, and the 50.4 - 52.6 GHz bands for mobile broadband in the region at the WRC.

All nations in the region should now be focused on whether additional allocations to mobile will be needed for spectrum at 24 GHz and higher, considering harmonization with the larger markets in the region, as well as WRC-19 Agenda item 1.13. Nations may also consider taking steps to assign licenses, and possibly, seek to align spectrum regulations to U.S. decisions in the band, because equipment is already available in some of the bands identified and allocated by the U.S.

2.1.4 European Union

The Radio Spectrum Policy Group (RSPG) is a high-level advisory group that assists the European Commission of the European Union (EU) in the development of radio spectrum policy. The RSPG developed an opinion on spectrum bands for next generation wireless systems (5G) as agreed to in the RSPG Work Program for 2016. The opinion was finalized in November 2016 and identified a strategic roadmap for 5G in Europe. In particular, the roadmap identified the following main building blocks for 5G spectrum:

- **High-bandwidth spectrum at 24.25-27.50 GHz as the “pioneer” mmWave band to give ultra-high capacity for innovative new services, enabling new business models and sectors of the economy to benefit from 5G.**
- **The EU’s Conference of telecom regulators (CEPT) also proposes a mobile broadband identification for 40.5-43.5 GHz. This is a priority band for CEPT and already identified for future harmonization in Europe. According to its draft European Common Position for WRC-19, CEPT considers that 40.5-43.5 GHz has good potential for future harmonization in Europe.**

2.1.5 Asia

2.1.5.1 China

In July 2017, China’s Ministry of Industry and Information Technology (MIIT) approved the 24.75-27.5 GHz and 37-42.5 GHz bands for China’s 5G technology research and development testing in Beijing and Shenzhen. These tests were meant to verify various aspects of the 5G technologies and provide a foundation to facilitate early ecosystem development. MIIT has an ongoing consultation for the 24.75-27.5 GHz band.

2.1.5.2 Japan

The frequency ranges which currently have priority in Japan for 5G in the mmWave bands are 24.25-29.5 GHz, 37.0-40 GHz and 40.5-43.5 GHz, with 27.5-29.5 GHz receiving priority attention. The 27.0-28.2 GHz and 29.1-29.5 GHz bands have been assigned to MNOs and 28.2-28.3 GHz has been locally licensed.

2.1.5.3 South Korea

A national broadband plan was published early 2017 and indicates the possibility of extending the 28 GHz band by up to 2 GHz to provide access to a total of 3 GHz, 26.5 – 29.5 GHz. There is interest in more spectrum for 5G in the longer term, though it is not yet decided which frequency band. 24.5-29.5 GHz band has been under consideration for 5G technology. 26.5-28.9 GHz has been assigned and there is a planned assignment for the 25.7-26.5 GHz band.

2.1.5.4 Taiwan

5G can be expected to be commercialized in Taiwan in 2020. In May 2018, the telecom regulator for Taiwan, the NCC, revealed plans to auction 5G licenses no later than the end of 2019, although the specific frequencies are still up under discussion.

NCC is reportedly considering low-band spectrum for 5G, including the 700 MHz band and 800 MHz band, while the 28 GHz band is also expected to receive further consideration. The 27.9-29.5 GHz band has been assigned.

2.1.5.5 Hong Kong

The 26.55- 27.75 GHz has been nationally assigned to MNOs. In July 2019, Hong Kong's Communications Authority announced that it would be making 400 MHz in the 27.95–28.35 GHz range available for localized wireless broadband licenses (using 5G or other advanced mobile technologies) on a geographic-sharing basis.

2.1.5.6 India

The Indian government is strongly backing 5G deployment but 5G is still in early stages of reflection. The Department of Telecom (DoT) is harmonizing spectrum in the 3.3-3.6 GHz and 26 GHz bands, along with the 71-76 GHz, the 81-86 GHz and the 57-64 GHz frequencies as 5G candidate bands.

2.1.6 Australia

Australian Communication and Media Authority (ACMA) has announced plans to enable use of fixed wireless access services across the 28 GHz (27.5–29.5 GHz) band. Change to spectrum allocation expected by Q1 2021. A draft spectrum reallocation recommendation has been made to the Minister for Communications to enable use of spectrum in the 26 GHz (24.25–27.5 GHz) range for wireless broadband. Proposed allocations in Q1 2021.

2.2 Global Millimeter Wave Auctions

The European Union's 5G Observatory provides a comprehensive look at relevant activity among the 27 member states and produces a quarterly report tracking 5G in the EU. The latest report, published in April, recaps planned mmWave assignments:

2.2.1 Recent Auctions

Table 2.1 lists the recent (post 2015) auctions/allocations of spectrum above 6 GHz that have taken place. In addition to usage for 5G, spectrum above 6 GHz has also historically been awarded for fixed point-to-point and some FWA usage; those historic allocations are not listed here.

2.2.1.1 EU Upcoming Auctions

- **Cyprus pushed award of 26 GHz from November 2019 to May 2020.**
- **Denmark could award 26 GHz licenses in the third quarter 2020.**
- **Finland plans to allocate 26 GHz in 2020. Auction concluded.**
- **France plans to award 26 GHz in 2020.**
- **Latvia is expected to award 26 GHz in fall or winter of 2020.**
- **Lithuania is expected to award mmWave licenses October 2020.**
- **Luxembourg is expected to move in the first half of 2020.**
- **Malta is expected to act before 2021.**
- **Spain delayed its award process until later in 2020.**

- **Belgium 2021/2022** From 2021 26 GHz 5G. From 2022 to 2027 31.8–33.4 GHz and 40.5–43.5 GHz.
- **Cyprus’s auction is TBD; it was originally due March 2020** 26 GHz (24250–27500 MHz).
- **Denmark is expected to auction 2020: 26 GHz in 2020.**
- **Finland is expected to award 25.1-27.5 GHz in the summer of 2020.**
- **Norway is expected to award 24250–27500 MHz (26 GHz) in 2021/2022.**
- **Sweden is expected to award 24.25–27.5 GHz in 2020.** The Swedish Post and Telecom Authority (PTS) plans to assign 24.25-25.1 GHz spectrum by 2021 at the latest.
- **Slovenia is expected to award 26 GHz in 2020.**
- **Slovenia is expected to award 28 GHz and 32 GHz for fixed wireless broadband access in 2021/2022.**

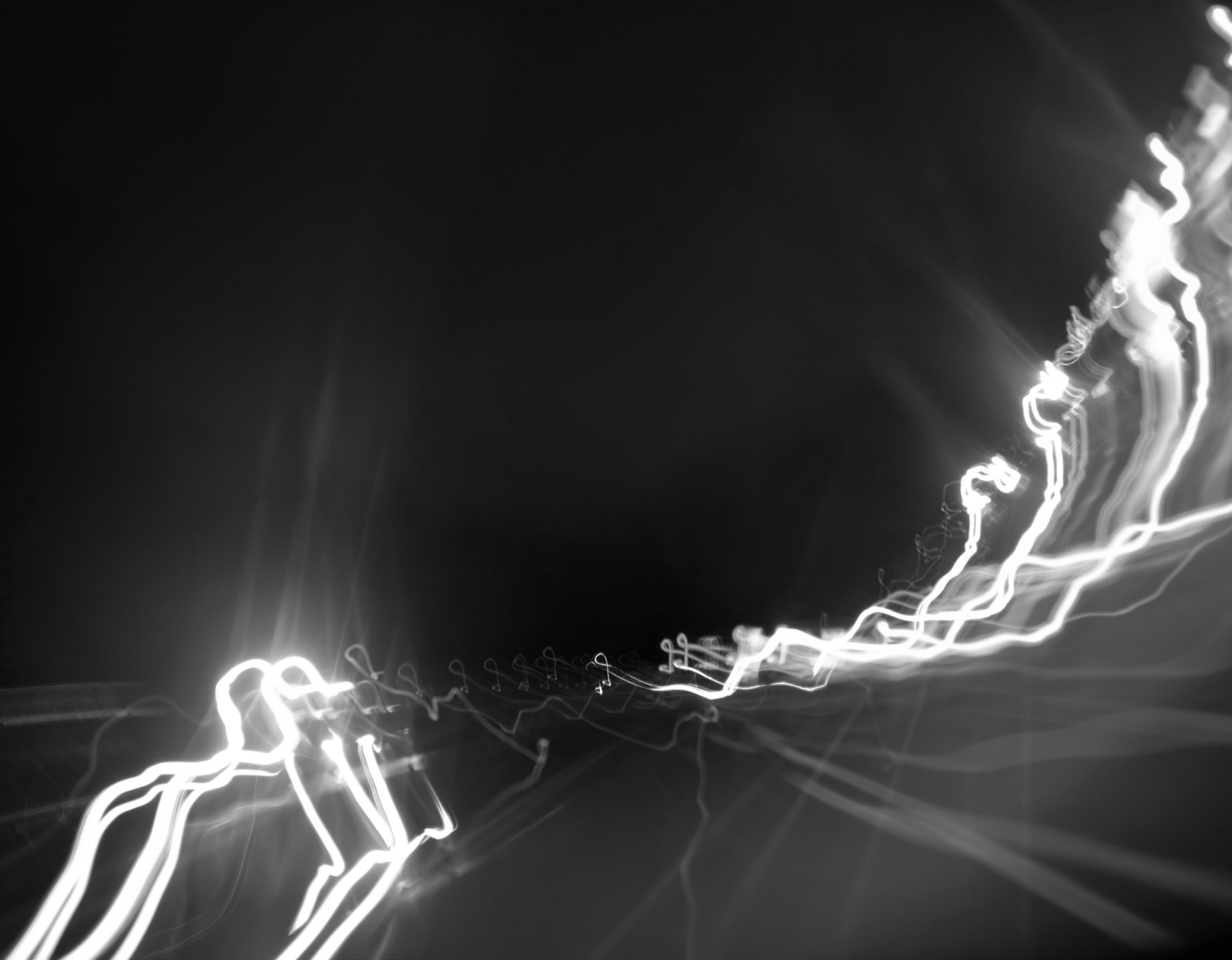
Table 2.1. Completed mmWave spectrum options

Region/Country	Spectrum Bands	Licensing basic (e.g. exclusively 5G, mobile broadband, etc.)	Auction/Award Date
Greece	24.5 – 26.5 GHz	Fixed wireless access	2017
Hong Kong	26.55 – 27.75 GHz	Public mobile and fixed wireless services (specifically including 5G)	March 2019
Italy	26 GHz	5G	October 2018
Japan	27.0 – 28.2 GHz 29.1 – 29.5 GHz	5G	April 2019
Republic of Korea	26.5 – 28.9 GHz	5G	June 2018
UK	24.25 – 26.6 GHz	Allocated for localized shared spectrum licenses (technology neutral, indoors only)	July 2019
Uruguay	27.5 – 28.35 GHz	Mobile services	May 2019
USA (inc. Guam)	28 GHz 24 GHz	Technology neutral Technology neutral	January 2019 May 2019

2.2.1.2 Asia Upcoming Auctions

- **Malaysia is expected to award 24.9–26.5 GHz in 2020 (possible delay due to COVID-19).** Malaysia is also expected to award 26.5–28.1 GHz in 2020 for Local/private 5G networks.
- **Singapore is in the process of awarding 28 GHz in 2020; winners have been announced.**

3. Millimeter Wave Technical Rules in the United States



3 Millimeter Wave Technical Rules in the United States

Millimeter wave spectrum usage is divided into three main areas:

- **Licensed band for mobile and fixed wireless access**
- **Lightly licensed bands for point to point backhaul application: 11, 13, 18, 23 GHz and E band (70/80 GHz)**
- **Unlicensed band in the 57-71 GHz (14 GHz of contiguous spectrum) for point to point and point to multi point application. This will be 15 times as much as all unlicensed Wi-Fi spectrum in lower bands.**
- **Shared access in the 37-37.6 GHz, makes available 600 MHz of spectrum for dynamic shared access between different commercial users and federal users.**

3.1 Licensed Spectrum

3.1.1 Maximum Emission Limits in Licensed Millimeter Wave Band

In U.S, the FCC has defined very high Effective Isotropic Radiated Power (EIRP) limits for millimeter bands. The challenge becomes manufacturing equipment that meets these targets within the cost, size, weight and power budget expected by the operators. FCC part 40 [1] defines rules and regulations to operate mmWave operation in the U.S. Transmit power limitations are as follows:

- **EIRP of 75 dBm/100 MHz for fixed and base stations**
- **EIRP of 43 dBm for mobile stations**
- **EIRP of 55 dBm for transportable stations**

EIRP is defined as the sum of total transmit power plus antenna gains. For an antenna array of n row and m columns, the antenna gain (G_{ANT}) is defined as $G_{ANT} = G_{element} + 10 \log (n * m)$, $G_{element}$ as stated by vendors.

For UEs, 3GPP [2] has defined four power classes for millimeter bands:

- **Power class 1 (PC1) for fixed access**
- **Power class 3 (PC3) for handheld UEs**
- **Power class 2 (PC2) for vehicular**
- **Power class 4 (PC4) for non-handheld**

In addition to different values, these power classes use different percentile CDF definition to reflect different use cases.

The minimum EIRP represents the EIRP at the highest gain angle in the spherical field. For handsets, a more representative of general use is the 50th percentile EIRP, meaning in 50% of angular direction, the EIRP will be less than 11.5 dBm.

Table 3.1. 3GPP device power class for FR1 (sub-6 GHz) and FR2 (mmWave).

Parameter	Sub 6 GHz (FR1)	Greater than 6 GHz (FR2)
Power class	PC2- HPUE handheld PC3- Handheld	PC1- Fixed Wireless Access PC2- Vehicular PC3- Handheld PC4- High powered non-handheld
Maximum Power	Conducted transmit power PC3- 23 dBm PC2- 26 dBm	EIRP (For PC1) Min peak- 20.6-22.4 dBm Max- 43 dBm Min 50percentile (8-11.5 dBm)

3.1.2 Out of Band Emissions

The FCC has authorized the following OOB levels for mmWave bands. The conductive power or the total radiated power of any emission outside a licensee’s frequency block should not exceed:

- 5 dBm/MHz in the band immediately outside and adjacent to the licensee’s frequency block, having a bandwidth equal to 10 percent of the channel bandwidth
- -13 dBm/MHz or lower elsewhere

3.2 Lightly Licensed

Lightly licensed millimeter bands are primarily used for point-to-point backhaul application. For these bands, one must obtain a license from the FCC by performing frequency coordination, filing a public notice, and submitting an application (601 form) with the FCC. This process is to ensure that no one else is already operating on the same frequency or a frequency that will inject interference into existing systems. Securing a license to operate a microwave link is inexpensive and can be obtained in a matter of weeks. Lightly licensed microwave link operators are permitted exclusive use of part of the band on a particular azimuth over an assigned geographic area. If licensed radios encounter interference, it is typically resolved with the assistance of the regulatory body.

Table 3.2. Lightly licensed mmWave bands.

	Antenna	Frequency range	Channelization
11 GHz	Min. 2 ft	10.7-11.7 GHz	80 MHz max (2x40 MHz)
18 GHz	Min 1 ft	17.7-19.7 GHz	50 MHz max
23 GHz	Min. 8 inches	21.2- 23.6 GHz	50 MHz max
70 - 80 GHz	Min, gain of 43 dBi *	71-76/ 81-86 GHz	

*Under consideration to relax to 38 dBi

The E band (71-76 GHz/81-86 GHz) has been made available for point-point microwave usage, enabling multi-gigabit per second data rates given the huge amount of spectrum available (10 GHz), with much less oxygen absorption (compared with 60 GHz), allowing longer distances compared with V band.

3.3 Unlicensed Spectrum

The use of 60 GHz (V band) is for point-point and point-to-multipoint backhaul and wireless access applications. Allocation of V band frequencies varies across countries. In the United States., V band is characterized by a continuous block of 14 GHz (57-71 GHz). In Europe, it consists of 9 MHz (57-66 GHz).

60 GHz is characterized by oxygen absorption that implies immunity to interference and enhanced frequency re-use, a favorable license regime, mostly unlicensed or lightly licensed (Country dependent).

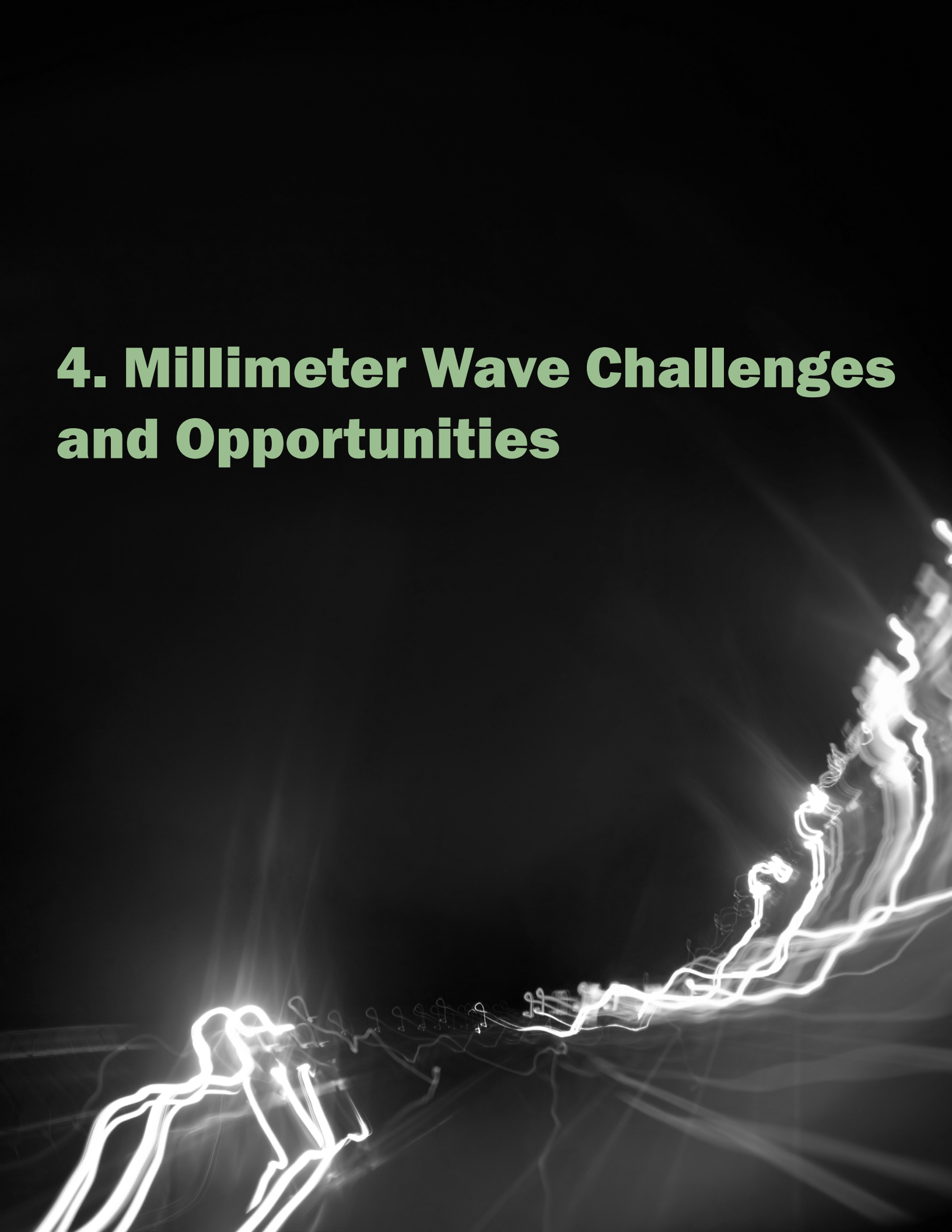
In the CEPT area (Europe), recommendations indicate the following limitations for V band [3]:

- **Maximum EIRP: + 55 dBm**
- **Minimum antenna gain: + 30 dBi**
- **Maximum transmit output power: + 10 dBm**

In the US, the FCC adopted a methodology (initially for E band) of limiting the maximum EIRP as a function of antenna gain (G) with a general formula. There is no minimum antenna gain requirement for V band. For the E band, there is a minimum antenna gain (G) of 43 dBi. Some companies are making a case to relax this requirement to 38 dBi. For V band, the antenna gain requirement is as follows:

$$\text{EIRP (dBm)} = 82 - 2 \cdot (53 - G)$$

4. Millimeter Wave Challenges and Opportunities



4 Millimeter Wave Challenges and Opportunities

4.1 Losses in Millimeter Wave

The increasing demand for faster data rates has brought significant 5G focus upon mmWaves, whose wide bandwidths hold tremendous promise. However, in order to optimally design a mmWave wireless system, it is essential to understand their propagation behavior. MmWaves behave differently in several key regards from the sub-6 GHz frequencies more commonly used by cellular systems today. Depending upon the specific use case, these differences can either pose challenges or opportunities.

4.1.1 Free Space Pathloss

Pathloss is the attenuation or reduction in power density of an electromagnetic wave as it propagates. It is a major consideration for all wireless communication systems, being fundamental the analysis and design of the link budget.

It is often stated that mmWaves suffer higher pathloss relative to lower frequencies, thereby limiting the range. However, this glosses over important details, hence it is useful to understand the origin of this frequency-dependent loss.

In the absence of atmospheric absorption or scattering, the radiated power density from an isotropic source falls off as $1/d^2$, where d is the distance from the transmitter. This square law decay arises from energy conservation and is independent of frequency.

The basic relationship between the transmit and receive power in line-of-sight conditions is given by the Friis equation:

$$P_R/P_T = G_T G_R (\lambda/4\pi d)^2$$

Here P_T is the transmitted power, P_R is the received power, d is the distance between transmitter and receiver, G_T is the antenna gain of the transmit antenna, G_R is the antenna gain of the receiver antenna, λ is the wavelength, with $d \gg \lambda$ assumed. The wavelength is inversely proportional to the frequency, i.e., $\lambda = c/f$ where c is the speed of light and f is the frequency.

The free-space pathloss (L_{FS}) is the loss in the Friis equation arising from distance and wavelength, for the case of isotropic unity-gain antennas (i.e., for $G_T = G_R = 1$, or 0 dB). Hence,

$$L_{FS} = \left[\frac{P_T}{P_R} \right]_{G_T=G_R=1} = \left(\frac{4\pi d}{\lambda} \right)^2$$

The $1/d^2$ comes from the expected square law behavior. The origin of the frequency dependence arises from the aperture (i.e., effective area) of the unity gain receive antenna at the chosen frequency. The receive aperture of a unity gain antenna is proportional to λ^2 , which decreases with frequency. Hence the higher pathloss at mmWave frequencies is a natural consequence of the smaller aperture. As is discussed in a subsequent section, this immediately motivates the use of antenna arrays at the transmitter and/or receiver to regain some of this frequency-dependent pathloss.

Written in dB, the free space pathloss becomes:

$$L_{FS}[dB] = 20 \log_{10}(d[km]) + 20 \log_{10}(f[GHz]) + 32.44$$

where the distance D is measured in km, and the frequency f in GHz. The frequency-dependent loss contribution is significant. Relative to 1 GHz, the free space pathloss at 28 GHz is 29 dB higher for the same distance. At 38 GHz, the free space pathloss is 31.6 dB higher.

Adding back the antenna gains, the line of sight pathloss becomes:

$$L_{LoS}[dB] = -G_T[dB] - G_R[dB] + 20 \log_{10}(d[km]) + 20 \log_{10}(f[GHz]) + 32.44$$

which is applicable only in the absence of scattering, diffraction, multipath, penetration losses, and atmospheric absorption.

4.1.2 Blockage (Shadowing Effects)

The large-scale variation in signal strength caused by objects in the physical environment between the mmWave transmitter and receiver is called blockage or shadowing.

In general, mmWave signals tend to be more sensitive to obstacles in the environment than sub-6 GHz signals because the mmWave wavelength is less than a centimeter, so most objects in the environment appear relatively larger. When in contact with these objects, mmWave signals may experience full or partial signal absorption, reflection, scattering, and/or diffraction.

Compared with sub-6 GHz signals, mmWave signals tend to experience more diffused scattering when in contact with large objects. With diffuse scattering, most reflected rays have different reflection angles; consequently, the signal strength in each direction is weakened, enabling the scattered paths to be easily shadowed by objects. mmWave diffuse scattering is in contrast with the specular reflection which is more commonly experienced by sub-6 GHz signals.

Furthermore, when in contact with large obstacles, mmWave signals tend to experience considerably less diffraction but more scattering and reflection than microwaves. This results in significant signal strength attenuation of mmWave compared to microwaves, where diffraction is more of a dominant means of propagation [4] [5].

The combined effect of increased diffuse scattering and reduced diffraction lead to more severe shadowing of mmWave signals when compared with sub-6 GHz signals [4]. To alleviate shadowing severity, mmWave communication systems tend to leverage high gain and narrow beamforming antenna arrays.

Since shadowing results in a large scale (typically on the order 10 meters to 100 meters) variation in signal strength, it is typically modeled as a large-scale variation around the pathloss. Hence, the composite large scaling propagation loss can be expressed as:

$$L_{Large-Scale}[dB] = L_{LoS}[dB] - S_{\sigma}[dB]$$

where L_{LoS} is the pathloss component given in the last equation in section 4.1.1, and S_{σ} is the shadowing loss with a given distribution which is typically log-normal in nature and σ is the standard deviation.

It is important to note that shadowing is an essential factor that must be considered when modeling the mmWave channel, and therefore it is needed to be considered in the link budget calculation and in determining the time variance of the mmWave channel [6].

4.1.2.1 Penetration Loss

mentioned in subsection 4.1.2, when a mmWave signal encounters reflective surfaces such as walls, tinted glass or elevators, these materials tend to exhibit high reflection coefficients. The reflected rays further bounce off objects in the environment, resulting in propagating multipath signals, and each multipath signal can then be further attenuated by the obstructions. In addition to reflection, the incident ray may partially travel through the obstructions, and in some cases are blocked or attenuated by the objects [4].

The aggregate attenuation caused by these obstructions is typically quantified as penetration loss, which is measured as the difference in power levels between the unobstructed and the obstructed path. This loss is measured as the excess of the free space pathloss discussed earlier in subsection 4.1.1. [7].

The major factors that impact penetration loss include signal frequency, material permittivity, the material thickness and surface roughness, the incident angle, and the polarization of the mmWave signal [4].

Studies of mmWave penetration losses at both 28 and 38 GHz have shown that while mmWaves tend to penetrate material like polystyrene with little to no reflections, some reflections are observed when incident on wood and walls, and materials such as tinted glass and brick cause extreme reflections, resulting in severe penetration loss. These studies also confirmed an increase in mmWave reflection coefficient as the thickness of the material increases [7].

Another study characterized 28 GHz mmWave penetration losses through measurements showing the impact of mmWave signals on different materials typically found in indoor and outdoor environments. A summary of the reflection coefficients and penetration losses are presented in Table 4.1 and Table 4.2, respectively.

Table 4.1. Reflection coefficient for different building materials at 28 GHz [4].

Environment	Material	Angle of Incidence (°)	Reflection Coefficient
Outdoor	Tinted Glass	10	0.896
	Concrete	10	0.815
		45	0.623
Indoor	Clear Glass	10	0.740
	Drywall	10	0.704
		45	0.628

Table 4.2. Penetration losses for different building materials at 28 GHz [4].

Environment	Material	Thickness (cm)	Penetration Loss (dB)
Outdoor	Tinted Glass	3.8	40.1
	Brick	185.4	28.3
Indoor	Clear Glass	<1.3	3.6 - 3.9
	Tinted Glass	<1.3	24.5
	Wall	38.1	6.8

Table 4.1 shows the reflection coefficient as a function of the indoor and outdoor building materials and the angle of incidence. Also, materials found in outdoor environment such as tinted glass showed higher reflection coefficient compared to the clear glass in indoors. In this case, the higher reflection coefficient is likely caused by the reflective coating which is used to reflect ultraviolet rays. Table 4.1 also shows higher reflection coefficient for outdoor building materials like concrete when compared to drywall in indoors. This higher reflection coefficient is likely a result of the difference in material permittivity and roughness as well as the material thickness since outdoor materials are typically thicker than those used indoors as shown in the Table 4.2.

Table 4.2 shows penetration losses and material thickness for typical indoor and outdoor building materials. In this study, a penetration loss of over 40 dB was reported for materials found in outdoors such as tinted glass while brick showed a penetration loss of around 28 dB. In indoor environments, the penetration losses are less severe, especially, for materials such clear glass, and walls which showed minimal penetration losses between 3.6 and 6.8 dB. Tinted glass in indoors also showed a high penetration loss of about 24.5 dB which is about 3.5 dB less than what was observed outdoors. In general, it is worth noting that reflection coefficients and penetration losses are typically higher in outdoor environments compared with indoors.

The same authors [4] also made measurements at 60 GHz and 72 GHz and noted similar trends as observed at 28 GHz. In some cases, the penetration loss increased with frequency.

Other studies of mmWave at 30 GHz to 50 GHz reported that for some materials, penetration losses may differ depending on the polarization

of the mmWave signals. For example, the authors reported a mmWave signal that came in contact with solid wood showed a penetration loss difference of about 1.77 dB/cm between a vertical-to-vertical (V-V) and horizontal-to-horizontal (H-H) polarized mmWave [8].

For mmWave signals going from indoors to outdoors, some studies have shown a penetration loss of about 74 dB due to the inability of the mmWave to penetrate building materials for a mmWave signal traveling from inside to outdoors. As a result, we can conclude that mmWave signals generated in an indoor environment will be contained within a building, consequently enabling frequency reuse in indoor and outdoor environments with minimal interference leakage. In addition, similar high penetration loss has been reported for mmWave signals going from outdoors to indoors. Therefore, in most cases, indoor mmWave coverage will not be achieved from outdoor base stations. This indicates a need for heterogeneous networks, repeaters and relays in order to ensure indoor-to-outdoor coverage [4].

4.1.2.2 Foliage Loss

Close to ground level mmWave links are very likely to also encounter the presence of foliage and more broadly, vegetation clutter. The latter is characterized by an assemblage of trees in woods and forests that come in different types, sizes, and distribution. Through the presence of branches, canopy, twigs and a variety of other structure types, this creates problems with characterizing their impacts upon propagation. However, plant and tree foliage are strictly identified by their leaves, and so are easier to characterize due to their limited attributes. Additionally, the envisioned commercial deployment and use of mmWave links are typically restricted to urban and sub-urban environments where stand-alone landscaping trees or lines of trees of same kind, are more prevalent.

The key to understanding why mmWave propagation is impacted more by foliage compared to sub-6 GHz frequency band signals is by characterizing the extent of the Fresnel zones around the obstruction between the transmitter and receiver [4]. These are circles drawn around the object, and each outer circle represents an increase in half wavelength of the path to be travelled additionally by the signal, as shown in Fig. 4.1. If the space identified with the first Fresnel zone is not completely blocked, diffraction loss around that object will be minimal. Inversely, if the first Fresnel zone is blocked, then propagation of the signal will be heavily impacted and will have to rely upon diffraction. With additional zones being blocked, diffraction losses will mount. Obviously then, the much smaller wavelengths associated with mmWave signals are very likely to be cause for encountering full blockage from within the first Fresnel zone, and therefore, full outage to the received signal. Knowing this, it is quite easy to understand why even smaller tree leaves can cause great losses, not to mention the much larger vegetation sources represented by bushes and tree branches. This is further aggravated by short time fading intervals from tree foliage swaying and moving due to winds which may vary the amount of first Fresnel zone that is blocked.

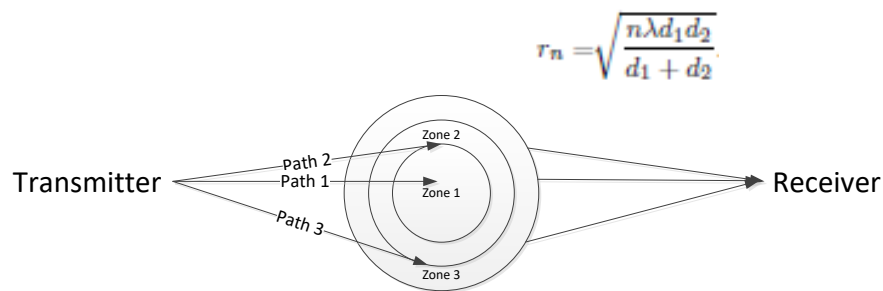


Fig. 4.1. Example of a diffraction object blocking LOS path between transmitter and receiver [4].

Path 2 is $\lambda/2$ longer than path 1.

Path 3 is $\lambda/2$ longer than path 2.

Although foliage causes severe attenuation to mmWave frequency signals, it also creates opportunities for multipath propagation in the form of scattering, backscattering and reflection. In a study completed [9] in an urban environment with peer-to-peer configuration that is common in wireless transmission with beamforming, but by applying highly directional beams and utilizing rotating transmitters and receivers, the specific object contributing to strong signal received through reflection, was identified. Other studies [10] completed in a 38 GHz outdoor channel led to the finding that wet foliage served as a source of multipath reflection.

The following is a brief compilation of mmWave vs lower frequency attenuation levels due to foliage presence and general trends associated with changing frequency.

- **29 GHz – Fading due to moving foliage can be up to 10 dB, while for 5 GHz it is around 2 dB**
- **57.6 GHz – At short distances of up to 5 m of foliage, attenuation was 40 dB greater than that in 9.6 GHz. For foliage length between 20-80 m or 4-14 trees with heavy foliage, 50-80 dB of additional attenuation occurs [4].**
- **With frequency increases up to 28.8 GHz, measured data [9] reveals a substantial foliage loss that tapers off from then on and up to 57.6 GHz, with only incremental correction losses.**

- Tests[9] also reveal signal attenuation in mmWave frequencies that vary depending upon a propagation path restricted solely by vegetation that is the trunk region of pecan trees with defoliated canopy, versus that of foliage from tree canopies that are fully leafed. 28.8 and 57.6 GHz signals were measured to have attenuation rates holding steady with the number of trees in the signal path. On the contrary with the latter scenario, there is an abrupt loss in attenuation rate after 30m or over the space of three separated trees. The vegetation or attenuation loss is between 1.3 and 3 dB/m for this initial distance, but quickly drops to a meagre 0.05 dB/m thereafter. Beam broadening with distance and the aggregated effects of scattering are reason for this reduced loss.

4.1.2.3 Body and Hand Losses

The presence of humans has a significant impact on the propagation characteristics of mmWave signals as humans tend to act as significant obstacles, reflectors and scatterers. This significant impact can be attributed to the size of the mmWave wavelength compared with the human body, which appears quite large compared with mmWave signals. In addition, when a mmWave signal encounters the human body, due to the dielectric composition of the body (especially the skin), there is minimal penetration, but significant reflection and scattering, leading to high losses. On the other hand, a small fraction of the mmWave signals diffract around the human body, allowing some of the energy to be recaptured, therefore, reducing the body blockage [11].

Body or hand loss is typically measured by taking the difference in the received power with humans present and absent. Using this approach, measurements taken at 15, 21.5, 60, or 73 GHz using horn antennas reported body losses in the range of 25 to 40 dB for a single person blocking the mmWave signal [5] [11]. MmWave studies have shown that the extent of this blockage was in general not dependent on the number of humans blocking the mmWaves, but rather on transmitter and receiver antenna type, array size and configuration [5] [11]. This claim was substantiated by studies performed by Raghavan et al, where the authors reported a mean body loss of ~8.5 dB for measurements taken at 28 GHz on UEs with phase array antennas in an environment with mobile humans. The authors explained that the differences in the recorded body losses compared with those from studies based on horn antennas was due to the beamwidth difference between the phase antenna arrays and the horn antennas used in those measurements [11].

In addition to the antenna type and configuration, hand losses that one may experience while holding a mobile device depend largely on the hand grip (firm or loose) and hand size. For example, Raghavan et al reported that for the firm hand grip scenario, a mean loss of ~ 15 dB was reported for measurements with a UE having a phased antenna array. For scenarios with loose hand grip and multiple air gaps between the fingers, a reduced blockage loss is expected (< 15 dB) due to the energy captured from blocked or partially blocked antennas [11].

When there are human body or hand movements in the presence of mmWave signals, the blockage becomes dynamic. Typical body loss time scales measured in pedestrian scenarios are reported to be around 100 milliseconds or more [11]. In an environment with increased mobility, the time scales are expected to be lower than 100 milliseconds. Likewise, in case the environment is static, one will expect even higher time scales than those reported in pedestrian scenarios. The time-variation of the blockage is an important

measure to capture, as it has significant impact on the robustness of the human body or hand blockage mitigation mechanisms, such as beamforming solutions. For example, in pedestrian scenarios, beamforming algorithms such as beam switching need to be triggered at smaller time scales than 100 milliseconds to effectively mitigate the impact of the human body or hand blockage [11].

4.1.3 Scattering

The high free space pathloss or signal attenuation at mmWave frequencies necessitates proximity and line-of-sight (LOS) paths for establishing wireless links between the transmitter and the receiver. Other propagation mechanisms proven effective at lower frequencies, such as diffraction, instead incur substantial loss in strength at frequencies within mmWave bands. And as already discussed, large scale fading in the form of shadowing (or blocking) will more adversely impact propagation in non-LOS paths. Under such circumstances, the impact of small-scale fading upon mmWave propagation from reflection and scattering will be far more pronounced and establish as the dominating multi-path components.

Due to the small wavelength of mmWave signals, even the slightest variation in the top layer boundary of a surface creates a scattering effect. In the context of wave propagation, such surfaces typically act as reflectors. However, with an increase in roughness, a parallel set of rays will now be reflected with altered and varying angles of reflection. Objects with size larger than the propagating wavelength under discussion here, will cause reflection. On the other hand, surface irregularity, a by far more common attribute, reduces the effective wavelength to create scattering. As a result, surfaces with comparable wavelengths are common sources of scattering or diffuse reflection in mmWave channels.

To understand more clearly, a perfect surface can be perceived as a string of adjacent points, where the lines normal to each point, are in parallel. With increasing roughness, there will be greater variation in those normal lines, making them less parallel. Hence, even if propagating waves arrived in parallel, they would end up being dispersed in entirely different directions (different angles of reflections). This makes diffuse scattering a significant source of received power.

The effect of scattering heavily influences mmWave channel modeling based upon ray tracing concepts. Clusters or sources of reflection and scattering are defined as alternative sources of energy. Scattering sub-events are integral part of such channels, and they can be modeled around various representative patterns with the intent of deriving coefficients to capture the effect of the rough surface area of a scattering cross section and the impact of the ensuing power dispersion.

On the receiver end, scattering manifests as multi-path propagation. The spatial spread of all such arriving components is characterized by the angle spread, or more specifically, the angle of arrival (AoA). Together with the channel sparsity associated with outdoor mmWave propagation that could limit the total number of main directions of arrival, signal multiplexing at the transmitter end could be contemplated while low overhead or low complexity channel estimation and equalization techniques be adopted at the receiver.

Different channel conditions create greater or fewer multipath components over varying angle spread. Transmitters closer to ground level for instance in Manhattan, NY, would typically generate greater scattering. Such an environment warrants greater transmit antenna pattern beamwidth to exploit all scattering sources, but with the corresponding loss of gain, would necessitate limited transmitter-receiver separation distances

to overcome pathloss. Inversely, high gain antennas with directional patterns at receivers are useful in generating beams that can be adaptively steered to detect multipath components sourced off multiple scattering surfaces.

Building material permittivity (ϵ) or dielectric properties vary considerably as well, particularly given the range of material types that make up the outer surfaces or object types present indoors. Generally, in NLOS environments, increases in permittivity result in more effective multipath components with greater received signal strengths. This is primarily influenced by material's electromagnetic properties and can be quantified by Absorption loss and Reflection Coefficients (and polarization). With varying frequency within the mmWave spectrum, the permittivity varies too, but the relationship is not similar for all materials. Therefore, to be able to determine the residual power of scattering in ray tracing-based modelling, it is critical to fully understand the range of building material permittivity.

The ubiquitous presence of objects larger than the wavelength in the mmWave propagation environment contributes towards creating many sources of scattering when compared to lower frequencies. In the outdoor environment, the side of walls and lamp posts prominently present themselves as origins, and in NLOS conditions play a key role as the primary means of reception. Here, the ability to scatter an electric field in the direction of the receiver (quantified by its Radar Cross Section or RCS)[4]and the surface roughness, determine scattering limits. While smooth surfaces on lamp posts or metallic objects present themselves more sharply and strongly to higher frequency signals and induces more scattering, other apparently similar objects instead appear to be less perfectly so due to the presence of varying degrees of surface roughness. This reduces the

RCS. Outdoor materials with rough surfaces such as brick walls or tree barks also contribute towards significant scattering of radiated energy, merely due to their exaggerated surface area relative to the wavelength.

Scattering is a common indoor occurrence in the mmWave frequency band as well. Furniture, fixtures, and humans are key sources, with varying degrees of influence. Scattering off furniture adversely impacts received signal strength in LOS conditions, but has an inverse effect in NLOS conditions due to reduced RMS delay spread which could magnify any reflected component. And scattering off human body appear to aggravate the impacts due to larger delay spread [4].

4.1.4 Atmospheric Loss

Absorption losses occur when radio frequency waves traveling through the atmosphere are absorbed by gas molecules via electric- and magnetic-dipole absorption processes, that couple the RF photon to internal degrees of freedom of the gas molecule. The resulting losses have frequency dependences determined by the resonant frequencies of the specific molecular species that are involved.

For the mmWave frequency range, the dominant sources of atmospheric loss arise from oxygen (O_2) and water vapor (H_2O). Fig. 4.2 shows their representative attenuation contributions for the indicated conditions. At a specific location, the magnitude of the loss will vary, depending upon the local density of oxygen and water vapor. In general, the densities of oxygen and water vapor depend upon the local temperature, atmospheric pressure, and humidity. The resulting total absorption loss for air will thus include the sum of the attenuation factors for O_2 and H_2O , as is shown in Fig. 4.3.

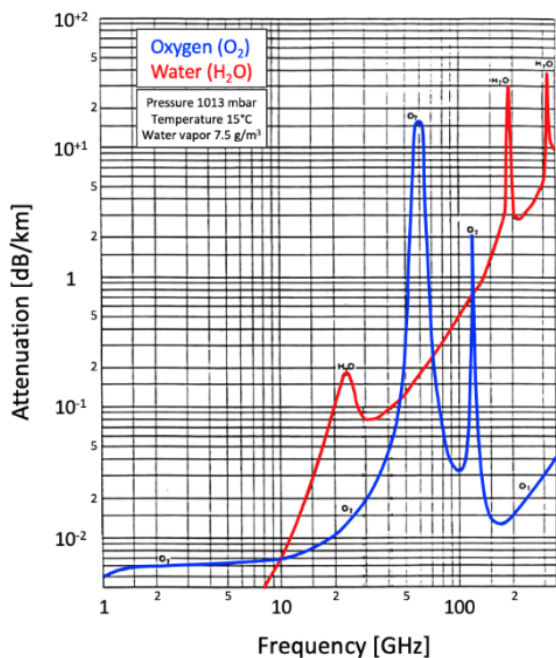


Fig. 4.2: Contributions to the RF attenuation (loss measured in dB/km) due to molecular oxygen (blue) and water vapor (red) as a function of radio frequency (shown from 1 to 350 GHz) for the following atmospheric conditions: 1013 mbar pressure, 15°C (59°F) temperature, and 7.5g/m³ water vapor content (roughly 60% humidity). [12]

The data show multiple peaks arising from the underlying molecular resonances, superimposed on a broad upward-sloping background primarily coming from water vapor. The mmWave peaks are centered roughly near 23 GHz (H₂O), 60 GHz (O₂), 115 GHz (O₂), 180 GHz (H₂O) and 315 GHz (H₂O).

These atmospheric absorptions can result in measurable attenuation of the radio signal, leading to reduced propagation range. For example, the 60 GHz peak is particularly strong – roughly 13 dB/km at sea level and 20°C. This helps explain why satellite providers and other incumbents previously avoided this frequency, and which also contributed to its designation as unlicensed spectrum. The peaks at ~180 and ~315 GHz are also strong, with attenuations of several dB/km.

The spectral regions between these absorption peaks provide “windows” where

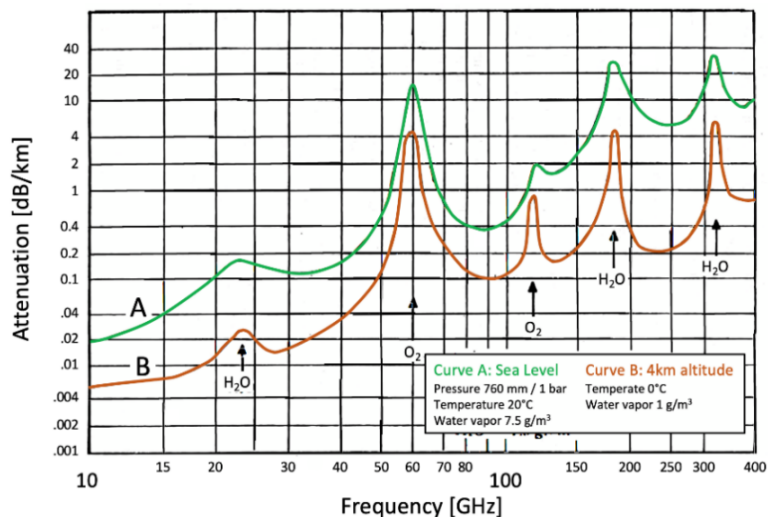


Fig. 4.3: Atmospheric attenuation (units = dB/km) for air as a function of radio frequency (shown from 10 to 400 GHz) for two different conditions - one at sea level (green) and another at an altitude of 4km (brown). [13]

longer range propagation more readily occurs. The resulting transmission windows are roughly centered near 35 GHz, 94 GHz, 140 GHz and 220 GHz.

4.1.5 mmWave Propagation and Channel Models

It should be clear that mmWave propagation is impacted by many factors: distance, blockage (shadow fading), various penetration losses, and atmospheric losses. Furthermore, the presence of intervening and surrounding objects (or clutter) result in additional reflection and diffraction of the RF waves. As the mm wavelengths are small (i.e., <1 cm), in order to accurately calculate all the contributions would require highly accurate knowledge of all clutter - both surface shape, all boundaries/edges, as well as the real and imaginary parts of the RF conductivity - on the length scale of millimeters. Even if cloud-scale computation facilities are available, the largest

challenge is getting sufficiently accurate input data about the scenario and clutter.

Consequently, RF network design generally resorts to use of propagation models which try to approximate the resultant behavior within a desired accuracy, i.e., within a defined fade margin. Such models often provide different parameterization or functional form for various defined scenarios, such as those listed in Table 4.3. The added challenges brought on by mmWave propagation add to the variety and complexity of the models.

Table 4.3. Various scenarios for pathloss models. See 3GPP TR 38.901 for additional details [14].

Scenario Type	Description	Additional Descriptors
UMa	Urban Macrocell	LOS & NLOS
UMi - Street Canyon	Urban Microcell - “Street Canyon”	LOS & NLOS
InH - Office	Indoor Hotspot - Office	LOS & NLOS
InF	Indoor Factory	LOS & NLOS DH: dense clutter & high basestation height DL: dense clutter & low basestation height SH: sparse clutter & high basestation height SL: sparse clutter & high basestation height LOS only HH: high transmit & receive heights

The models do not include the gains of the transmit and receive antennas, they only address propagation pathloss. In actual usage for RF network design, such models may be augmented by available clutter data for the specific region under evaluation.

The 3GPP document TR 38.901 “Study on channel model for frequencies from 0.5 to 100 GHz” [14] provides an extensive list of pathloss models that extend deep into the mmWave regime. Table 9.1 in the Appendix illustrates several pathloss models taken from Table 7.4.1-1 of TR 38.901, for readers not faint of heart.

Another area where accurate mmWave propagation models are required is for developing channel models for use in link-level simulations of receiver performance. This is a comparatively advanced topic, and we encourage the interested reader to consult section 7.7 of TR 38.901 for descriptions of those models.

There is one very important contribution to such channels models, which is generated by motion of the transmitter, receiver, and/or their surrounding environment (for reflected or diffracted waves) via the Doppler shift. Here we’ll describe the Doppler shift in simpler terms, but in more general terms it depends on the time evolution of the channel and is defined as the derivative of the channel’s phase over time.

The Doppler shift is the change in frequency of a wave as seen by a receiver that is moving relative to the transmitting source. The Doppler shift can be positive (higher frequency) if the distance traveled is decreasing (i.e., Tx and Rx are effectively getting closer), conversely the shift can be negative if the Tx and Rx are effectively moving away from each other. The magnitude of the Doppler frequency shift Δf is:

$$\Delta f = f_o \square (\Delta v/c)$$

where:

Δv = relative velocity of the transmitter and receiver (or for the case of reflections, the time derivative of the propagation pathlength)

f_o = the carrier frequency

c = speed of light in air ($\cong 3 \times 10^8$ m/sec)

Because of the high frequency of mmWaves, their Doppler shift is similarly elevated relative to what is encountered at lower frequencies. Table 4.4 provides some example Doppler shifts for a few representative velocities and carrier frequencies.

Table 4.4. Example Doppler shifts for a range of relative velocities and carrier frequencies.

Relative velocity Dv (m/sec)	Doppler shift ($f_o = 30\text{GHz}$)	Doppler shift ($f_o = 40\text{GHz}$)	Doppler shift ($f_o = 60\text{GHz}$)
1 m/s (~2 mph)	100 Hz	133 Hz	200 Hz
15 m/sec (~34 mph)	1.5 kHz	2 kHz	3 kHz
40 m/sec (~90 mph)	4 kHz	5.3 kHz	8 kHz
90 m/sec (~200 mph)	9 kHz	12 kHz	18 kHz

Clearly, this is the reason the subchannel spacing is increased for 3GPP's Frequency Region 2 (FR2), which includes mmWave.

4.2 Opportunities in Millimeter Wave

4.2.1 Larger Bandwidth

Wireless spectrum is of course a finite resource, and sub-6 GHz spectrum has historically been used for multiple applications besides mobile broadband communications – including radio, broadcast television, radar, etc. When this is coupled with the explosion of mobile broadband data, this frequency regime has become increasingly crowded. While other sub-6 GHz spectrum resources will be made available in the US (notably the C-band and the 6 GHz unlicensed band), the sub-6 GHz (soon to be sub-7 GHz) frequency resources are becoming more and more strained.

LTE of course was standardized only for frequencies below 6 GHz, and the bands (both FDD and TDD) tend to have relatively small amounts of spectrum. For instance, Band 66, used by all major US carriers as a primary LTE band, has a total of 90 MHz each paired downlink and uplink spectrum. A single operator likely does not operate more than 20-30 MHz of downlink spectrum in this band. The maximum carrier size in LTE is 20 MHz; carrier aggregation is necessary to use larger contiguous allocations to achieve greater cell and user throughputs.

By contrast, the mmWave regime spans a far broader range in absolute frequency (30-300 GHz) than sub-6 GHz, and by comparison it is less crowded and less intensively used by the existing occupants. Several mmWave bands have already been standardized, providing a tremendous amount of spectrum for mobile

broadband. As shown in Table 4.5, both n257, the global 28 GHz band, and n260, the global 39 GHz band each have 3 GHz of spectrum standardized.

Table 4.5: Standardized mmWave bands and bandwidth (source: 3GPP TR 38.104 V16.4).

NR operating band	Uplink (UL) and Downlink (DL) operating band		Duplex mode
	BS transmit/receive	UE transmit/receive	
	$F_{UL,low} - F_{UL,high}$	$F_{DL,low} - F_{DL,high}$	
n257	26500 MHz – 29500 MHz		TDD
n258	24250 MHz – 27500 MHz		TDD
n259	39500 MHz – 43500 MHz		TDD
n260	37000 MHz – 40000 MHz		TDD
n261	27500 MHz – 28350 MHz		TDD

Not all of this spectrum may be available for mobile broadband in a given country (for instance, in the U.S. only 850 MHz of 28 GHz spectrum is available, standardized as n261), and multiple operators may hold licenses for parts of the spectrum in a given market. That said, it is not uncommon for a U.S. operator to hold 800 MHz or more of contiguous mmWave spectrum in a given band. More spectrum equals more capacity, higher peak throughputs, and opportunities for new use cases that were not possible with the limited spectrum in the sub-6 GHz range.

To that end, much larger carrier sizes have been standardized for mmWave: 50 MHz, 100 MHz, 200 MHz and 400 MHz. 50 and 100 MHz are already widely supported in the mmWave ecosystem, while support is slow to build for 200 MHz (and 400 MHz support is for the time being optional). Note also that as is the case for the sub-6 GHz NR bands, each of the bands has carrier sizes standardized by subcarrier spacing (SCS), with 400 MHz only possible with 120 kHz SCS, as shown in Table 4.6.

These bigger carrier sizes make it easier to aggregate large allocations of contiguous spectrum, as there is significant effort in the standardization and signaling overhead of fewer, larger contiguous carriers versus more smaller carriers. A larger mmWave carrier will also have more spectrum (in time) available for the uplink, which may be heavily taxed in very downlink-heavy configurations that seem to be typical for mmWave.

There are however tradeoffs to be considered when deciding to deploy larger carriers or smaller across contiguous spectrum. For instance, spreading the Tx power both from the cell site (5G NodeB or gNodeB, a name carried over from UMTS) and the device (User Equipment, or UE) across a 200 MHz carrier will effectively reduce the power spectral density of that carrier, thereby inhibiting its coverage, when compared to a smaller carrier.

Table 4.6: Standardized carrier sizes per mmWave band.

NR band / SCS / BS channel bandwidth					
NR Band	SCS kHz	BS channel bandwidth			
		50 MHz	100 MHz	200 MHz	400 MHz
n257	60	Yes	Yes	Yes	
	120	Yes	Yes	Yes	Yes
n258	60	Yes	Yes	Yes	
	120	Yes	Yes	Yes	Yes
n259	60	Yes	Yes	Yes	
	120	Yes	Yes	Yes	Yes
n260	60	Yes	Yes	Yes	
	120	Yes	Yes	Yes	Yes
n261	60	Yes	Yes	Yes	
	120	Yes	Yes	Yes	Yes

4.2.2 Larger Antenna Array in Small Form Factor

mmWave frequency signals with extremely short wavelengths create opportunities to design antenna arrays that are several times greater than the wavelength itself, while remaining physically small. This brings about critical advantages to such antenna systems where cost reduction is realized through inexpensive fabrication technology, and manufacturing scale is achieved from compact integration. The smaller size also creates flexibility with design considerations and maximizes the overall power efficiency. The resulting antenna arrays can achieve higher gains of up to 29 dBi (with a total of 256 cross-polarized elements) to help overcome increased propagation and radio hardware impairment losses. Their adaptive capabilities enhance performance as well.

While the physically smaller sized antenna elements allow opportunities to build electrically large array antennas (large number of total elements between 256 and 1024) to achieve critical performance factors such as far field gain, they can then be etched into an on-chip metal during a CMOS IC production process. Alternatively, the antenna array can also be fabricated into a

packaging technology [4] which already hosts other radio front end components, and then mounted to the printed circuit board (PCB) substrate housing the transceiver itself, as shown in Fig. 4.4. Such approaches help avoid the need to connect a separate antenna array through cables and connectors to other radio components, where the integration process with a PCB would entail several steps and add to the manufacturing cost of the product. Power losses also decrease. An array with equal number of half wavelength total length cross polarized dipole elements stacked vertically and horizontally, and with half λ separation, would be almost twelve times less in either length or height when constructed for 28 GHz frequency as compared to one for 2.4 GHz.

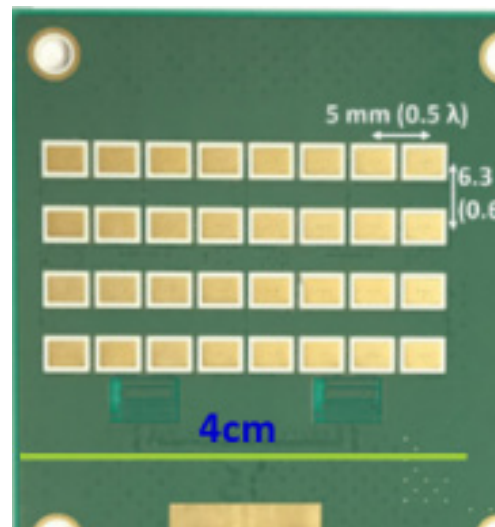


Fig. 4.4: A 28 GHz antenna array side of a printed circuit board spanning only 4 cm in length with eight elements [15].

Additional beamforming gain realized through greater array gain in mmWave frequencies, as compared to sub-6 GHz, allows beam shaping that is more conducive to MU-MIMO operation. Spatial separation is less compromised now between two same-cell users, making their radio channels more orthogonal. The high dimensional array also captures a greater spatial degree of

freedom, allowing the system to further overcome propagation losses off both the azimuth and elevation planes. Antennas designed with higher directivity, but small enough to be part of the end user device, are more capable of negating the effects from Doppler spread due to better spatial filtering ability. This will increase channel coherence time, allowing opportunities to improve DL channel estimation [16].

4.2.3 Shorter TTI and Reduced Latency

One of the key technical characteristics of OFDM/OFDMA is its orthogonality between adjacent subcarriers. This orthogonality comes from the choice that the subcarrier spacing (SCS) and symbol duration (d_s) satisfy the condition that $SCS = m/d_s$ where m is a positive integer (1, 2, ...). The specific values for SCS and d_s for an OFDM-based technology such as 5G NR are then based upon other considerations such as multipath, Doppler, and latency. Those underlying factors are discussed in their respective sections of this white paper, and the associated tradeoffs between them are typically predicated upon the mobility and propagation environment under consideration. In this section, we note that reduced air interface latency can be a natural benefit for the mmWave regime.

Unlike the “one size fits all” approach of LTE, with fixed subcarrier spacing of 15 kHz, 5G NR has subcarrier spacings to accommodate the wide range of frequencies, from below 800 MHz to 39 GHz and above. 5G NR has defined a range of SCSs as multiples of 15 kHz, expressed by the formula 15×2^n , where n is an integer between 0 and 4. All mmWave bands defined to date are standardized for SCSs of 60 and 120 kHz (with 240 kHz only used for the synchronization signal block, or SSB); commercial deployments seem to largely be using 120 kHz. These larger SCSs are necessary for mmWave to combat inter-symbol interference and phase noise (as discussed in section 7.4.2).

As the subcarrier size and spacing increases, the symbol duration decreases. A 15 kHz subcarrier has a symbol duration of 66.7 μ s ($1/15000$ Hz); a 120 kHz subcarrier has a symbol duration an eighth as long, or only 8.3 μ s. As is the case with LTE, NR has a basic frame duration of 10 ms, divided into 10 subframes of 1 ms each. However, NR further divides the subframe into one or more slots, each with 14 OFDM symbols (just like an LTE subframe). For 15 kHz SCS, slot duration is 1 ms for the 14 OFDM symbols along with the cyclic prefix between the symbols; i.e. there is 1 slot per ms. For 120 kHz SCS, the slot duration is again 1/8th of 15 kHz SCS – 0.125 ms, and there are four slots per subframe. The slot in 5G NR is the basic unit of transmission, just like the subframe is in LTE.

This shorter slot for mmWave at higher SCS represents a much shorter time transmission interval (TTI) for mmWave on 5G NR. This TTI imposes a basic system latency on 5G NR at a given subcarrier spacing. Fig. 4.5 shows an abstracted scheduling diagram for an uplink transmission. The UE has data it wishes to send; it cannot do so autonomously, so it has to request to the network that it send data. The network responds with a scheduling grant, informing the UE when and how to transmit the data. After the data transmission, the network has to acknowledge whether or not the data was properly received.

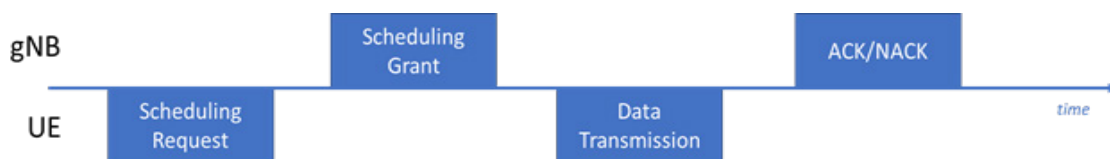


Fig. 4.5. Basic uplink scheduling mechanism.

It should be clear that regardless of the band, a larger SCS will shorten the time between each of these steps, thereby reducing latency. For instance, if each of the steps above required one slot to complete, a band with 15 kHz SCS would take 4 ms for the process to complete, while a band with 120 kHz SCS would take only 1 ms.

5G NR also introduces the ability to further reduce latency by decoupling the TTI from the SCS [17]. Instead of having to use the entire slot for transmission, a mini slot allows transmission of only several symbols over an entire slot. This can be useful in support of the URLLC applications discussed in Chapter 5.3.

4.2.4 Higher Densification

The mmWave transmission range when compared with transmission range in the sub-6 GHz frequency band is reduced as discussed in subsection 4.1. Even though large antenna arrays can be leveraged to provide beamforming gain to recover some of the losses, the resultant transmission range in mmWave networks is still significantly less than that of the sub-6 GHz networks. As a result, given a coverage area where mmWave coverage is desired, higher density of mmWave cells would be expected in that area compared to the density of sub-6 GHz cells if used to provide coverage for the same area. With a higher cell density, mmWave band can deliver on the higher data rates and capacity promise while providing the needed coverage. It is important to note that mmWave cells are typically deployed for capacity relief in areas such as hotspots.

Higher mmWave densification also comes with certain challenges, such as co-channel interference, increased network mobility and higher deployment cost. Higher densification of mmWave cells has the tendency to increase the co-channel interference in the network; however, due to the use of highly directional antennas typically

used in the mmWave networks, the co-channel interference is significantly mitigated. The higher densification also leads to more intercell mobility; therefore, appropriate intercell mobility algorithms are required to avoid performance degradation for mobile users as they cross cellular boundaries in the mmWave network.

To address the higher cost of mmWave deployments, most mmWave operators in the early phase of their deployment efforts have co-sited mmWave base stations with existing sub-6 GHz base stations, and later increase the mmWave densification by adding more mmWave base stations in areas with coverage holes. In this way, the existing base station sites and backhaul infrastructures can be leveraged, reducing the mmWave deployment cost.

4.2.5 Channel Reciprocity

Frequency bands available for mmWave communication are unpaired, which implies that the same frequency must be used for the DL and UL communications but at different times. Such systems are also called Time Division Duplex (TDD). In such systems, when the DL and UL communications are performed within a certain period time known as the channel coherence time, the UL and DL propagation channel characteristics are highly correlated. This phenomenon is termed channel reciprocity.

Channel reciprocity is important for mmWave communications which typically relies on Massive MIMO systems for achieving beamforming gains. Massive MIMO systems have large number of antennas and hence, a significant amount of resources and cost is incurred in estimating the DL/UL channel state information (CSI), especially, CSI at the transmitter (CSIT) which is required for transmit side beamforming.

By leveraging channel reciprocity in Massive MIMO systems, the measurement and sounding resources required for channel estimation are greatly reduced. This is because once CSI in one direction is measured, the CSI in the other direction can be inferred. For example, when DL reference signals (DL RS) are transmitted from the network, the mobile device can estimate the DL CSI and then derive the UL CSI which is in turn used for UL transmit beamforming. Similarly, based on the UL sounding reference signals (SRS) transmitted from the mobile device to the network, the UL CSI can be measured and then the DL CSI can be inferred from UL CSI. The CSIT acquisition leveraging channel reciprocity is illustrated in Fig. 4.6.

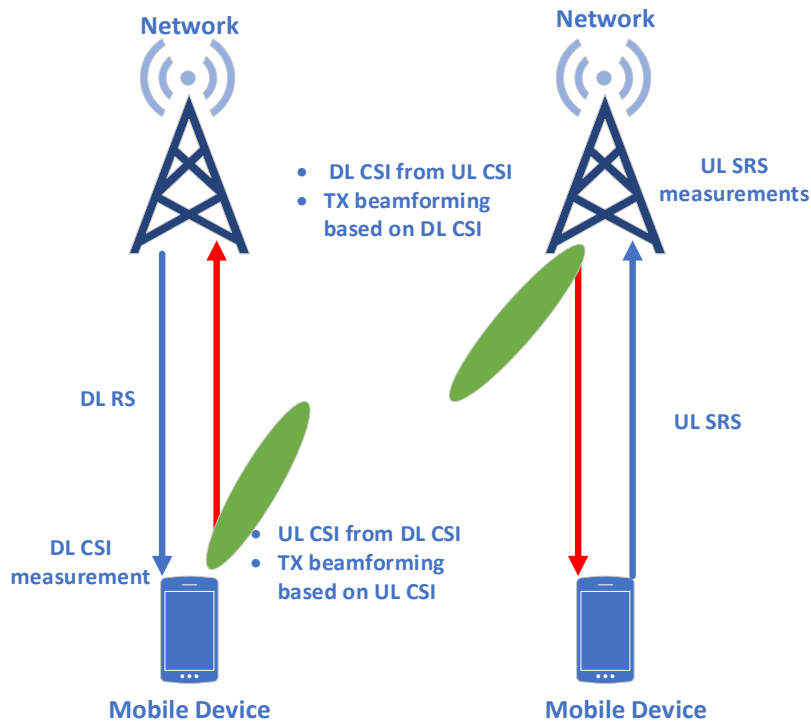
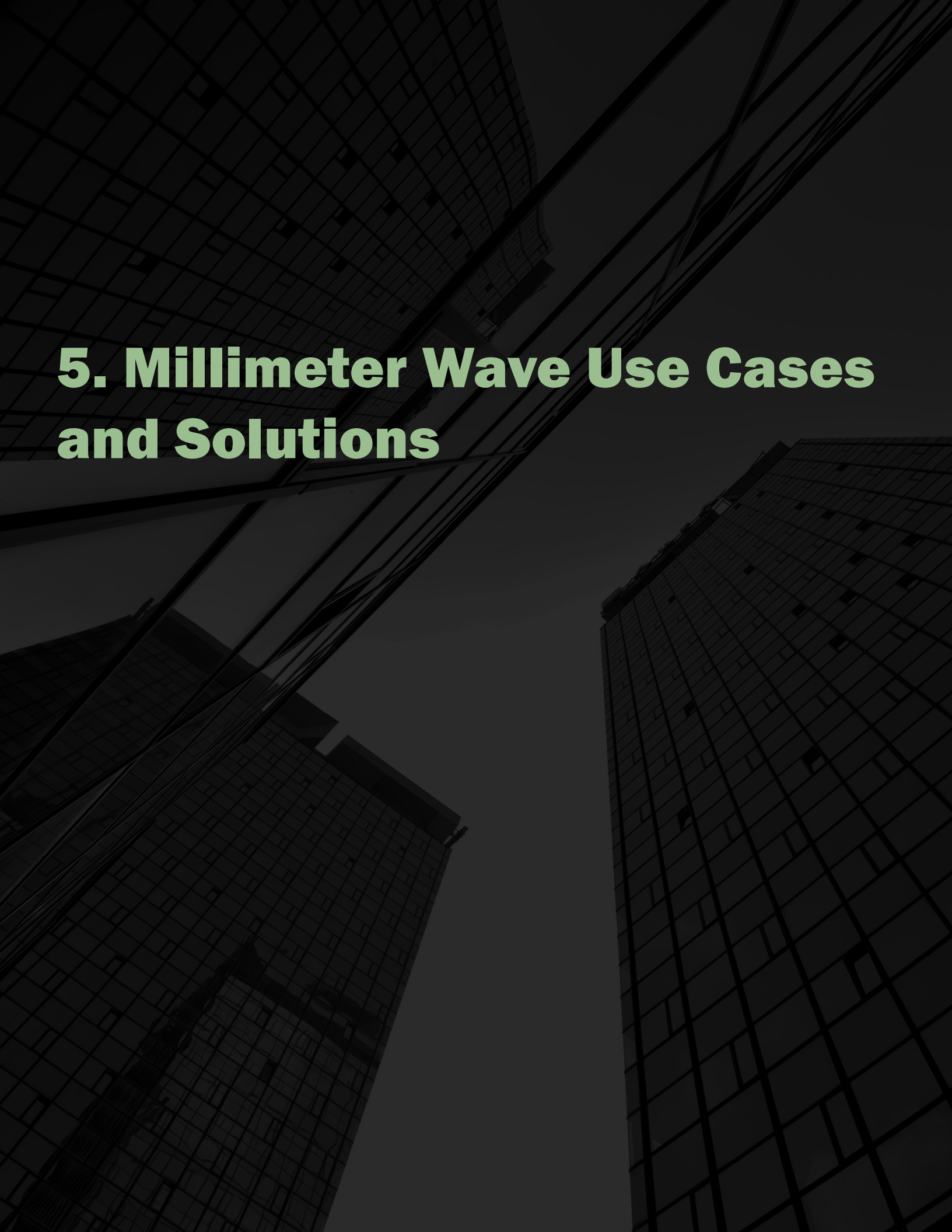


Fig. 4.6: CSIT Acquisition at UE (left) and Network (right).

It is important to note that in order to fully leverage the benefit of channel reciprocity, practical issues such as RF hardware asymmetry at the network and mobile device need to be addressed. RF hardware asymmetry is typically mitigated by employing RF DL and UL calibration at the network and UE.

A low-angle, upward-looking photograph of several skyscrapers with glass facades. The buildings are silhouetted against a dark sky. A prominent grid pattern, resembling a wireframe or a mesh, is overlaid on the image, creating a sense of depth and structure. The grid lines are white and intersect to form a series of squares and rectangles that align with the architectural lines of the buildings.

5. Millimeter Wave Use Cases and Solutions

5 Millimeter Wave Use Cases and Solutions

5.1 Use Case Considerations in mmWave Spectrum

The novelty of 5G is the integration of multiple networks serving diverse sectors, domains and applications, such as multimedia, virtual reality (VR) and augmented reality (AR), machine to machine (M2M) and internet of things (IoT), automotive applications, smart city, etc. The diversity of the 5G applications and their related service requirements in terms of data rate, latency, reliability, and other parameters leads to the necessity for operators to provide a diverse set of 5G networks.

Among the various innovations enabling 5G, one of main necessities and realities is the use of mmWave spectrum be coupled with network densification and massive MIMO to serve as an ultra-high speed access and backhaul systems. A key ingredient for 5G is to enable applications in mmWave spectrum is mobile edge computing (MEC), which is expected to bring information and processing closer to the mobile users and enable ultra-high speed and low latency communications.

One important characteristic of mmWave spectrum is its potential to support large bandwidths and high data rates that are ideal for increasing the capacity of wireless networks. Although the mmWave bands extend up to 300 GHz, the bands from 24 GHz up to 100 GHz are expected to be used for 5G. The mmWave bands in consideration for 5G up to 100 GHz are capable of supporting channel bandwidths of size 500 MHz or even 1 GHz in some cases without the need to aggregate bands together for higher data throughput.

Given the propagation challenges discussed in Chapter 4, mmWave spectrum is generally best suited for short range transmissions, and small cells are a practical means to deliver communication in this band. Small cell ranges are typically no more than 10 to 200 m under NLOS conditions, which are much shorter than the range of sub-6 GHz macrocells, which can be multiple kilometers.

Supporting mobile operation is one of the major challenges in using mmWave for 5G. At very high frequencies, even small variations in the environment can seriously diminish the channel performance. Usage of larger number of antenna elements and RF chains into cost effective phase-array RFICs is considered to be a key mechanism to address this challenge. There has been significant progress in the miniaturization of phase-array antenna systems for low-power, cost effective 5G mmWave devices. The use of beam-steering and beam-tracking techniques leverages massive MIMO antenna arrays to address this issue by creating highly directional beams where the transmitted energy is focused to improve system performance on both uplink and downlink.

Also, some of the latest advancements enhances the possibility to communicate in NLOS conditions using advanced antenna processing by capturing reflected signals and supplementing the LOS signal increasing channel capacity. This in most cases makes it practical to deploy mmWave on existing cell sites for higher channel throughputs for inter-site distances are relatively small – say within 150 meters.

5.2 5G mmWave Deployment Scenarios

In addition to operating across multiple bands, including mmWave, 5G NR will support multi-RAT connectivity, where a device can access

a network with multiple radio access technologies, either simultaneously or separately, including 5G, LTE Advanced, and non-3GPP radio technologies. This helps to address many of the challenges in mmWave by ensuring robustness in countering fading and providing a reliable “always on” 5G capability.

Dual connectivity mode is another deployment scenario where a user device connects to the 5G Network with a macrocell used as an anchor in sub 6 GHz band integrated with a non-located mmWave small cell as an underlay to provide a wider RAN architecture. The anchor macrocell provides a larger coverage and handles control plane procedures including acquisition, paging and mobility where the mmWave small cells provides localized high capacity user-plane services.

5G mmWave Small cells as an underlay are deployed for the following two target cases.

5.2.1 Coverage Extension at the Edge

In this case, small cells are deployed at the edge of a macrocell to extend the coverage of the 5G network. In this scenario, the coverage of the small cell can have a partial overlap with the coverage of the overlaid macrocell as shown in Fig. 5.1a. This configuration is essentially targeted to enhance user perceived experience with respect to service availability. This configuration is applicable to deployments in both indoor and outdoor where coverage at the cell edge requires higher quality of service (QoS) and enhanced data throughput.

5.2.2 Capacity Enhancement

In this case, small cells are deployed within the coverage of an overlaid macrocell to improve data throughput of the overall network. The coverage of the small cell overlaps the coverage of the macrocell as shown in Fig. 5.1b. This configuration is targeted to boost the overall capacity of the network and provide a higher capacity for a hotspot within the coverage of an anchor macrocell.

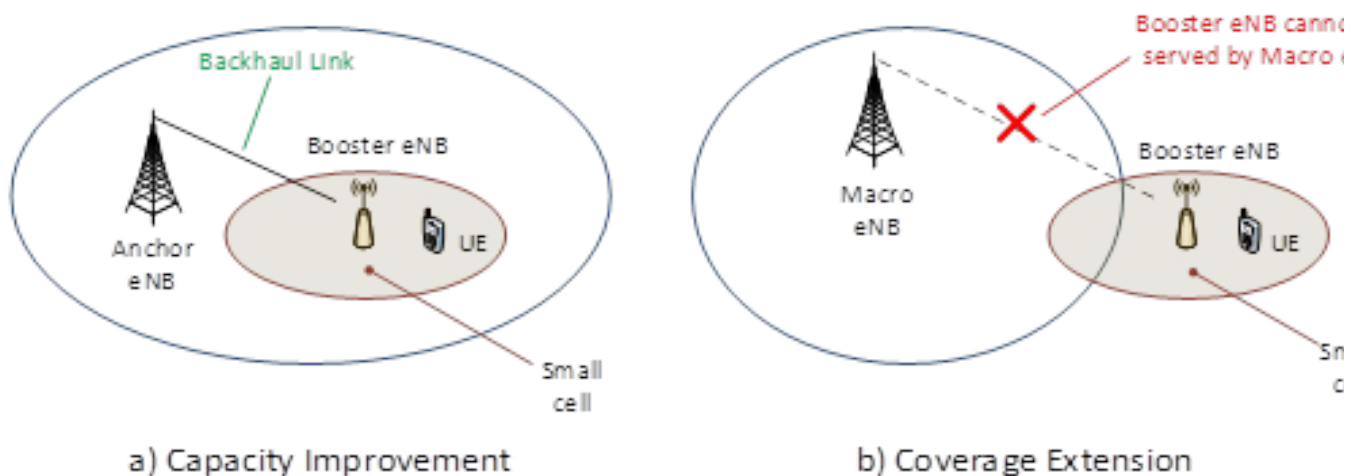


Fig. 5.1: 5G mmWave small cell underlay for capacity and coverage enhancements.

5G networks in mmWave are mainly targeted for urban environments to provide high data rate services. These solutions can be used in coverage extension scenarios by exploiting tracking capabilities and adaptive beamforming. The following use cases are generally identified as favourable to the adoption of 5G in mmWave bands.

5.3 5G mmWave Use Cases

Applications and use cases have been targeted to be addressed by 5G are broadly grouped into three categories:

- **Enhanced Mobile Broadband**
- **The Massive Internet of Things**
- **Ultra-Reliable Low Latency Applications**

The following sections describe the various use cases that 5G mmWave can serve.

5.3.1 Enhanced Mobile Broadband

This group of use cases is characterized by broadband data access in crowded locations, office areas, and high-speed public transport systems. The target is to provide maximum user experience by providing connectivity both indoors and outdoors while delivering high QoS broadband even in challenging network conditions. Multi-user interaction, AR, and context recognition are essential features for this category of use cases. Here are some of the sub-use cases in this category.

5.3.1.1 Hotspots

This use case relates to providing enhanced broadband access in densely populated areas such as high-rise building complexes, urban city centers, crowded areas, etc. Moderate mobility and high data rates will be required.

5.3.1.2 General Broadband Everywhere

This use case relates to providing a consistent user experience, guaranteeing user speeds of 50+ Mbps everywhere towards a mobile and a connected society. The user data has to be delivered consistently across the coverage area. High mobility will be required.

5.3.1.3 Public Transport

This use case is about providing broadband access in public transport systems such as high speed trains. It must provide a robust communication link and high quality Internet for information, entertainment, interaction or work with the ability to support high mobility.

5.3.1.4 Smart Offices

This use case is characterized by heavy indoor data use with low mobility requirements. This is a use case scenario where hundreds of users require ultra-high capacity to serve bandwidth-intensive applications.

5.3.1.5 Special Events

This use case requires providing very high connection density in scenarios such as stadiums, concerts and large gatherings where tens or even hundreds of thousands of users are served at high data rate and low latency.

5.3.1.6 Connected Vehicles

The subcategory of use cases involving mobile communications related to Connected Vehicles is an important driver for 5G. This category of use cases entails supporting advanced safety applications mitigating road accidents, improving traffic efficiency, and improved access for emergency vehicles. These applications require a concerted framework with features supporting ultra-low latency for warning signals, higher data rates to share sensor data and information between vehicles and infrastructure, high mobility, high reliability and scalability of features. Vehicle-to-everything (V2X) communication as defined in 3GPP consists of four types of use cases: vehicle-to-vehicle (V2V), vehicle-to-infrastructure (V2I), vehicle-to-network (V2N) and vehicle-to-pedestrian (V2P).

5.3.1.6.1 Vehicle-to-Vehicle and Vehicle-to-Pedestrian

V2V and V2P communications are between vehicles, or between vehicles and vulnerable road users (e.g., pedestrians, cyclists) to provide information about location, velocity and direction to avoid accidents.

5.3.1.6.2 Vehicle-to-Infrastructure

V2I includes communications between vehicles and traffic control devices in the road vicinity. V2I transmission is between a vehicle and a roadside unit (RSU). An RSU is used to extend the range of a message received from a vehicle by acting as a forwarding node.

5.3.1.6.3 Vehicle-to-Network

V2N transmission is between a vehicle and a V2X application server to provide connected services to a vehicle.

5.3.1.7 Enhanced Multimedia

This subcategory of use cases targets providing a high-quality media experience everywhere to meet the growing demands of consumer media consumption. The targeted users are the end viewer, pay TV operators, broadcasters, new content owners, content aggregators, and OTT providers. Recent developments of 4K and 8K video resolution, 3D video, expanded use of HDTV, streaming audio & video services, and interactive video on the go over a growing number of video-capable devices are key driving factors for this family of use cases. The higher data capacity, faster data rates, and enhanced broadcast and multicast features will serve these use cases and realize the media vision for a seamless mobile TV experience. Some of the use cases follow.

5.3.1.7.1 Broadcast Services

These services distribute content in both real time and non-real time across a wide

distribution area and are typically dominated by the downlink with the uplink providing a feedback channel for interactive services. Sub-use cases consist of:

- **Delivering news and information in audio and video to customers in specific geographic areas.**
- **Delivering local services within 1 to 20 km that include scenarios such stadium events, advertisements, fairs, conventions and emergency notifications.**
- **Delivering services in a larger distribution within 1 to 100 km that includes scenarios such as communicating traffic jams, disaster emergency warnings, etc.**
- **Delivering services at a national level as a complement to broadcast radio or television with additional benefits for the automotive industry.**

5.3.1.7.2 On Demand and Live TV

This use case is based on scaled up delivery of high-resolution content via live TV or on demand video using enhanced data capacity and data rates.

5.3.1.7.3 Mobile TV

Defined by delivery of video streaming and entertainment media to smart phones, tablets and other devices in high mobility environments such as trains, cars, and buses.

5.3.2 Massive Internet of Things

The category of use cases in Massive Internet of Things addresses the emerging Low Power Wide Area (LPWA) needs for low cost devices, extended coverage, and long battery life. The use cases are expected to make up a large part of the new types of services that 5G systems will address by connecting the massive number of devices such as sensors, actuators, cameras, etc.

This family of use cases are expected to be pervasive in urban, suburban and rural areas providing metering, lighting management in buildings and cities, environmental monitoring (pollution, temperature, noise etc.) and traffic control, among many other applications.

These services are expected to require the ability to support a very high density of devices with different characteristics in a common communication framework. The Massive IoT use case category includes applications used in a wide spectrum of industries across society, including both human-to-machine interaction and machine-to-machine interaction, as shown in Fig. 5.2.

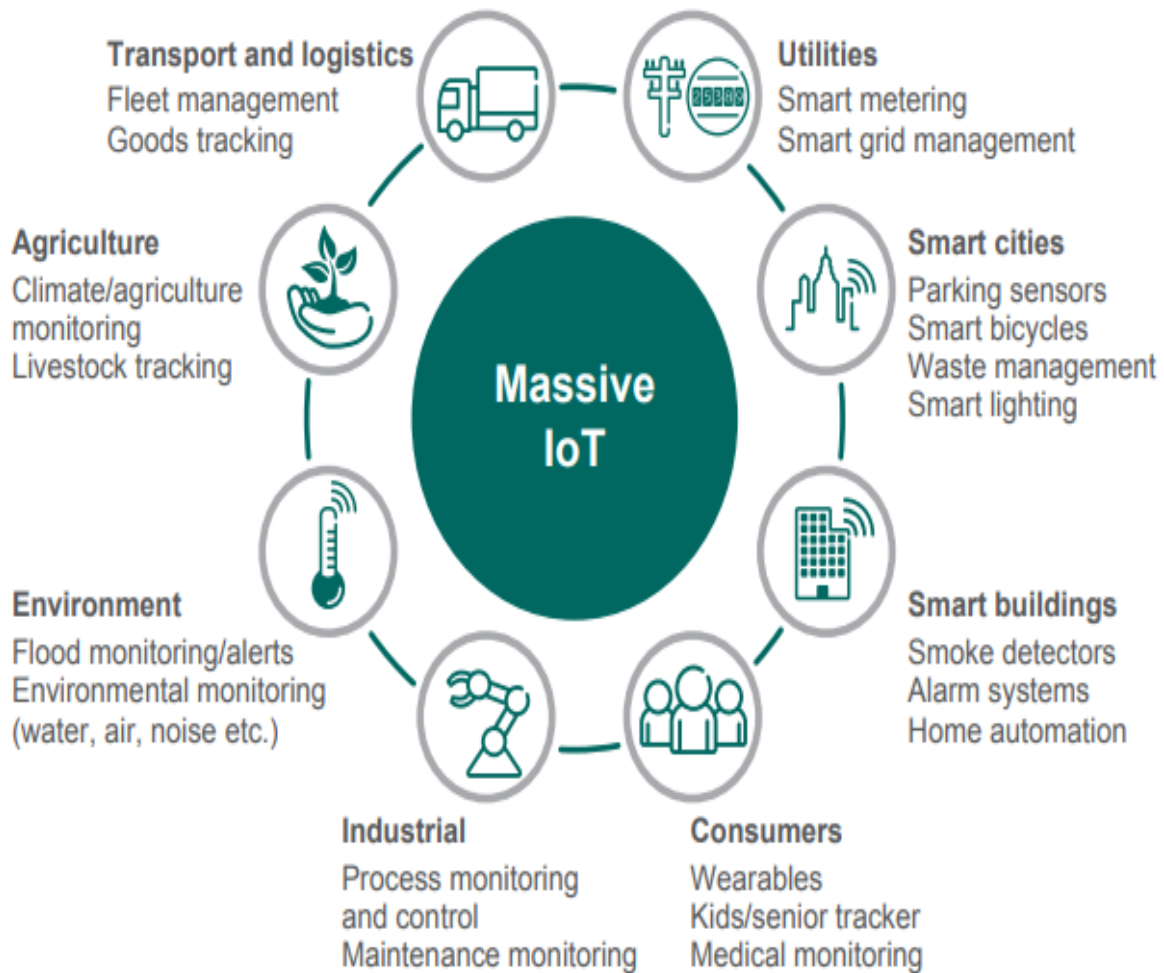


Fig. 5.2: Massive IoT Use Cases Enabled by 5G Technologies [18].

5.3.3 Ultra-Reliable Low Latency Applications

These use cases are the critical IoT applications that will have very high demands on reliability, availability and low latency with lower demands on the volume of data, but significantly higher business value. These use cases also fall into the category of mission-critical machine type communication (MTC).

The mission critical MTC is envisioned to enable real-time control and automation of dynamic processes in various fields, such as industrial process automation and manufacturing, energy distribution, and intelligent transport systems.

These applications and use cases require communication with very high reliability and availability, as well as very low end-to-end latency going down to the millisecond level. These use cases and applications feature interactions across all categories, human-to-human, human-to-machine, and machine-to-machine. Sub-use cases in this category are discussed below.

5.3.3.1 Process Automation

These use cases are centered around information integration and enabling process automation useful in the oil and gas, chemicals, energy and water industries. The application here covers the pumps, compressors, mixers, monitors of temperature, pressure, flow controllers, etc.

5.3.3.2 Automated Factories

These use cases involve communication transfers enabling time-critical factory automation that are required in many industries across a wide spectrum that includes metals, semiconductors, pharmaceuticals, electrical assembly, food and beverage, etc. The applications for the use cases fall into functions related to material handling, filing, labeling, palletizing, packaging, welding, stamping, cutting, metal forming, soldering, sorting, printing presses, web drawing, picking and placing, etc.

5.3.3.3 Tactile Interaction

These use cases involve interaction between humans and systems where humans wirelessly control real and virtual objects and the interaction requires a tactile control signal with audio or visual feedback. Robotic controls and interaction include several scenarios with many applications in manufacturing, remote medical care and autonomous cars. Tactile interaction requires real-time reactions in the order of a few milliseconds.

5.3.3.4 Emergency, Disasters and Public Safety

These use cases require robust and reliable communications in case of natural disasters such as earthquakes, tsunamis, floods, hurricanes, etc. The use cases may require accurate position location and quick communication exchanges between users and systems. Energy efficiency in user battery consumption and network communications are critical in these use cases. The public safety organizations require enhanced and secured communications with real time video and the ability to send high quality pictures.

5.3.3.5 Urgent Health Care/ Remote Surgery

These use cases are envisioned around applications that will conduct remote diagnosis and treatment. There is a need for remote patient monitoring and communications with devices measuring vital signs such as ECG, pulse, blood glucose, blood pressure, temperature, etc. The remote treatment and response based on monitored data can be life critical for a patient, requiring immediate, automatic or semi-automatic response.

Remote surgery applications are envisioned in a mobile scenario in ambulances, disaster situations, and remote areas requires providing precise control and feedback communication mechanisms for surgeons in terms of low latency and high reliability and security.

5.4 Fixed Wireless Access

Fixed wireless access applications (FWA) are examples of early 5G use cases, taking advantage of the combination of existing fiber footprints and 5G technology to provide localized network access. Fixed networks with 5G are planned to complement fiber to provide high speed

data rates without the costly provisioning of fiber all the way to the premises.

5.5 Backhaul

5.5.1 Integrated Access and Backhaul

Cellular networks are typically built out with macrocells. Coverage or capacity problems require densification. This results in ballooning costs, both in terms of deployment as well as ongoing operational cost, needed for high capacity fixed backhaul links. Fiber backhaul also limits the network topology to a fixed deployment, whereas a dynamic and reconfigurable network infrastructure is better suited to fulfill the data capacity demand, which varies in time and space. For example, emerging applications such as IoT, XR and autonomous systems impose stringent requirements on communications and computation infrastructures to enable the delivery of seamless experiences to end users in real time. System requirements can be quantified in terms of computational capacity, radio capacity, latency, and reliability. To circumvent the typical large delay of cloud computation, mobile edge computing (MEC) brings local computation resources closer to end users. The user experience, however, won't be enjoyable if the data transport between devices and MEC servers is not a reliable, high-rate, and virtually zero-delay connection. Hence, the radio network has to be enhanced alongside MEC solutions to fulfill the new requirements for the emerging use cases.

Integrated access and backhaul (IAB) was introduced by 3GPP to help mitigate both CapEx and OpEx of deploying and operating dense cellular networks. IAB is built upon open RAN (O-RAN) architecture. The O-RAN Alliance works to evolve the next generation Radio Access Network (RAN) infrastructure. Empowered by principles of intelligence and openness, the O-RAN architecture is the foundation for building the virtualized RAN on open hardware, with embedded AI-powered radio control. One of the challenges tackled by O-RAN is the realization of dynamic and dense networks of small cells with wireless backhaul using machine learning.

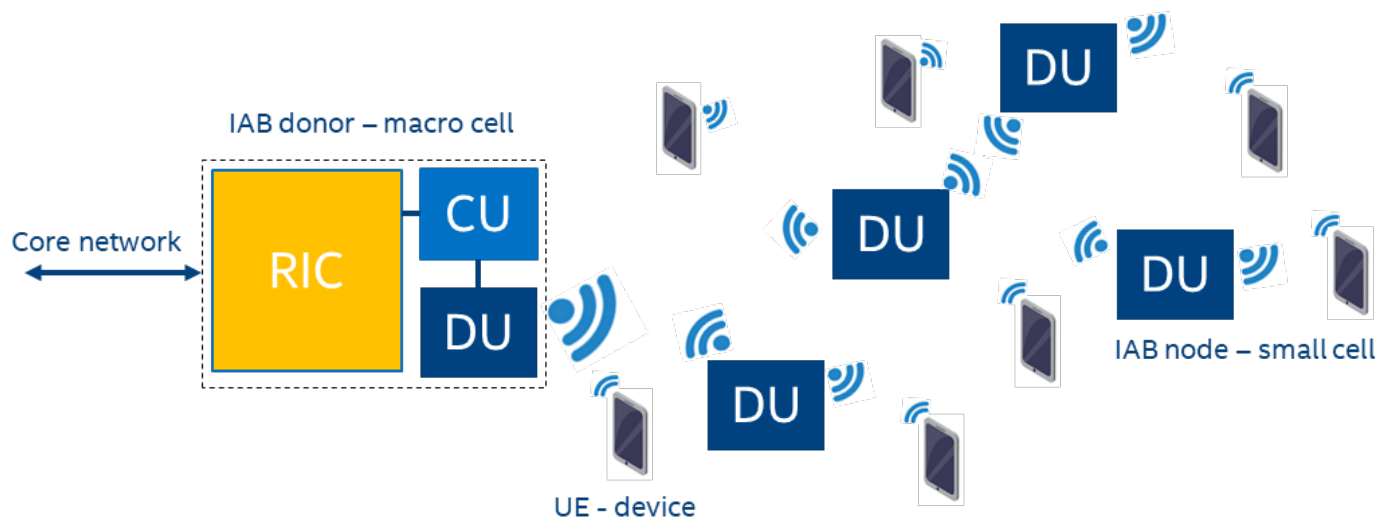


Fig. 5.3: An IAB network with macrocell (IAB donor) and several wireless backhauled small cells (IAB nodes).

Fig. 5.3 shows a typical IAB network, which is as an extension of O-RAN architecture. a macrocell IAB donor serves one or more small cells (IAB nodes). The IAB donor is a central unit (CU), which manages a network of IAB nodes or distributed units (DU). The CU's network management capability is AI empowered

by the radio intelligence controller (RIC). The backhaul links of IAB nodes are wireless and can form a tree or mesh topology. Therefore, IAB nodes can extend coverage of the network through multiple relay hops. In addition, multiple routes might be available between an IAB donor and a specific IAB node. The CU-DU split of the radio protocol stack and the RIC are defined according to open-RAN architecture.

The CU at the IAB donor monitors and manages the operation of the entire network in 10+ ms time scale. Real time scheduling decisions with a 1 ms granularity will happen locally at each DU. A DU can both serve UEs within its coverage area, and additionally act as a backhaul link for other DUs. Topology of the network is completely flexible, and it is left to CU to manage and optimize the topology according to the traffic demand.

Millimeter wave bands are very suitable to utilize for high-rate wireless backhaul links in an IAB network. In Rel-16 of 3GPP, IAB nodes are not mobile, which means that beam tracking and beam blockage are not much of a concern for fixed IAB node backhaul links. The standard allows any combination of sub-6 and mmWave bands for backhaul and access links. Therefore, both in-band and out-of-band IAB is supported by the standard. From practical point of view as mentioned before, mmWave is the best option to realize wireless backhaul links within an IAB network.

5.5.2 Dedicated Backhaul

To date, traditional microwave radios operating in 6-38 GHz frequency bands have been attractive options for aggregated cellular backhaul, particularly for long hauls. But limited bandwidth offered in these bands limits the scope for delivering gigabit backhaul services in these bands. Table 5.1 shows maximum channel bandwidth for different bands used for microwave backhaul [19].

Table 5.1: Maximum channel bandwidth in traditional microwave bands.

Band	Duplex spacing	Old max channel width	New max channel width	ECC recommendation
11 GHz	530 MHz	56 MHz	1123 MHz	REC 12-06 E
	490 MHz	56 MHz	112 MHz	
18 GHz	1010 MHz	110 MHz	220 MHz	REC 12-03 E
23 GHz	1008 MHz	112 MHz	224 MHz	T/R 13-02
28 GHz	1008 MHz	112 MHz	224 MHz	T/R 13-02
32 GHz	812 MHz	112 MHz	224 MHz	REC (01)02
38 GHz	1260 MHz	112 MHz	224 MHz	T/R 12-01 E

Also, the rollout of 5G is progressing very fast globally. 5G requires more capacity in all network domains and always requires long hauls due to limited range in mmWave bands. Millimeter wave technology delivers multi-gigabit wireless throughput in places where fiber is not either not available or is not an economical option.

In 5G RAN network, as shown in Fig. 5.4, fronthaul is the connection between radio and digital units, which uses the evolved Common Public Radio Interface (eCPRI) interface. This interface require high throughput and lower latency compared to other interfaces in transport network as shown in Table 5.2 [20]. Wireless backhaul, midhaul and fronthaul solutions need to achieve not only up to 20 Gbps capacity for short fronthaul links, but also a combination of 4-8 Gbps, with high availability for macrocell 5G connectivity.

Table 5.2: Typical throughput requirement for 5G transport.

BW (MHz)	Frequency band	MIMO layers	Backhaul	Midhaul	Fronthaul
				F1-Split 2	Split 7.2 Compressed
50	2.5 GHz	8/4 (DL/UL)	2 Gbps	2.01 Gbps	11.3/3.5 Gbps
100	3.5 GHz	8/8 (DL/UL)	4 Gbps	4.02 Gbps	22.7/7 Gbps
400	28 GHz	4/2(DL/UL)	6 Gbps	6.44 Gbps	5/10.2 Gbps



Fig. 5.4: End to end transport terminology in 5G.

Two mmWave bands that have attracted lots of interest for 5G backhaul applications are 60 GHz (V band) and 70/80 GHz (E band). MmWave radios operating in E band have become the fastest point-to-point radio solution in the market. Radio transmission products offering full-duplex data rates of more than 10 Gbps, and availability levels of 99.999%, and over distances close to 1 mile or more are available.

5.5.2.1 V band

60 GHz is an unlicensed band used for point-point and point-to-multipoint backhaul and wireless access applications. Allocation of V band frequencies varies across countries. In the United States., V band is characterized by a continuous block of 14 GHz (57-71 GHz). In Europe, it consists of 9 MHz (57-66 GHz). This band has also been very attractive for many component suppliers that are producing high volume 60 GHz parts to support the WiGig standard. When these commodity parts can be reused for small cell backhaul systems, it can result in very cost effective solutions. Electronically steerable antennas used in V band, have many benefits that can be leveraged to reduce Total Cost of Ownership. 60 GHz also allows for small antennas (six inch or 15 cm) in most countries, which is ideal, for low profile street- level small cell deployments, and is also open for many uses beyond telecom. Because it is unlicensed, there is no process to acquire part of the spectrum for exclusive use in a certain geographical area—a potential concern for some operators, as they may face interference. While this currently is not an issue due to light use of the band, the beam widths are very narrow and oxygen absorption limits the interference range. Some features of V band radios are as follows:

- **PtMP capability**
- **Operation across the entire 57-71 GHz (V band). This is particularly of importance, since the upper channel (Ch. 6) can provide much lower oxygen loss and hence wider coverage.**
- **Air interface technology: 802.11ad (WiGig)**
- **Channel bandwidth of up to 2.2 GHz and throughput of up to 10 Gbps**
- **Antenna: Phase array with gain of 34 dBi and EIRP of 40-49 dBm**
- **Latency: < 50 µsec**
- **Self antenna aligning capability**

5.5.2.2 E-Band (71-76/81-86 GHz)

This band is available in most countries, also making it very suitable for high density and high capacity wireless backhaul applications. The oxygen absorption in the E-Band is much lower compared to the V-band, but it faces higher fade due to rain. This can be engineered into the link though. The E band is a lightly licensed band in most countries, and is restricted to backhaul applications. The fees are typically quite low, especially on a per-MHz basis, so it is very economical for backhaul deployments. What's more, because it is more regulated, it does not face any of the interference concerns that may rise in the V-Band spectrum. E-Band also permits small antennas suitable for street level deployments, with the exception of the United States, where there is currently 43 dBi minimum antenna gain limitation, although the FCC is publicly considering changing this regulation through their recent NPRM process.

Throughput as high as 40 Gbps over a 1.4 km link with latency less than 100 μ s have been reported in E band. The demonstration used two 2 GHz channels, i.e., a total bandwidth of 4 GHz, with 128 Quadrature Amplitude Modulation (QAM) and two polarizations per antenna (i.e., four antennas). The high data rate is achieved by the combination of cross-polarization interference cancelling technology (XPIC) and 10 Gbps in a 2 GHz wide channel, thereby generating a 20 Gbps data stream that in combination with a second 2 GHz channel and link aggregation realizes a 40 Gbps full duplex channel.

5.6 Distributed Antenna Systems

DAS systems are well-established solutions to solve both indoor and outdoor coverage problems. The motivations for and types of DAS systems are detailed in the Appendix in Chapter 9.3.

5.6.1 DAS for mmWave

Architecture similar to legacy sub-6 GHz DAS systems can be used to operate in mmWave. For remote units below 6 GHz, the DAS antennas are normally simple hemispheric pattern radiators. Obviously, this will not work for mmWave antennas that are directional type. The short wavelength at mmWave make larger arrays possible with small footprint. An active array (6x6 patch array) is quite feasible for mmWave. In mmWave, there is also a need for beam steering and beamforming, which can be implemented with antenna array. In mmWave, beamforming with a number of antennas is used to overcome the pathloss. The concept of hybrid beamforming system for mmWave has found some traction. The use of hybrid analog/digital processing strategy to reduce hardware cost and computational complexity over the full digital beamforming. Fully digital control systems traditionally require many digital/analog signal and frequency converters. This generally increases power consumption, capacity and cost for the entire system.

NEC [21] has recently announced the development of millimeter-wave distributed antennas for the efficient use of 5G mmWave spectrum (28 GHz band). Demonstration experiments were conducted with this technology in 2019, where the capability of high-speed, large-capacity communications with stable propagation channel quality were confirmed. In the experiment, NEC applied digital beamforming, which had been developed in the sub-6 GHz and millimeter bands, to 28 GHz band antennas. By combining and multiplying the space of radio waves, NEC achieved high-speed, high-capacity communication, but also stabilized the propagation path.

5.7 Repeaters

A repeater is a low-cost device designed to help coverage issues in wireless communication systems. It consists of a donor antenna, which in the downlink direction receives a signal from a donor sector, and then amplifies and retransmits the signal through its service antenna. Repeaters are primarily used to reduce pathloss without providing an increase in network capacity. Implementing repeaters can be an efficient and cost-effective method of increasing the received signal strength for mobiles in an area without having to place additional sites. As simple diagram is presented in Fig. 5.5 [22].

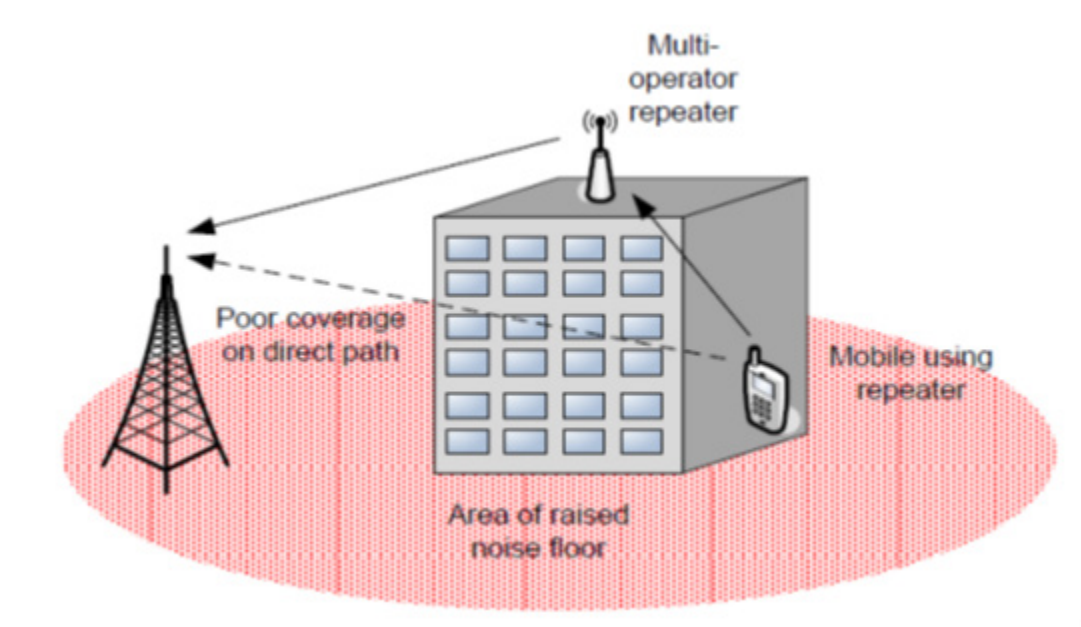


Fig. 5.5. Repeater.

However, repeaters will transmit not only the signal but wideband noise. This is because, like any electronic device, there is thermal noise inherent in its components. This can effectively limit the effectiveness of repeaters. Generally, repeaters add noise and amplify noise in the uplink, which can limit their effectiveness, however a good design and properly placed repeater can reduce noise levels within a network and enhance the overall capacity. Cascaded repeaters are of particular concern. If repeater A is used to provide coverage to repeater B, then on the uplink the noise out of repeater B is further amplified and added to by repeater A, creating a much higher noise level than one repeater type.

Table 5.3 tabulates some major key points comparing mmWave and sub 6 GHz frequency bands. As seen, the major issue of building a mobile network is coverage and the need for massive number of base nodes. The use of repeater seems to be a good fit for systems operating in mmWave to offset high pathloss.

Table 5.3. Sub-6 GHz and mmWave differences.

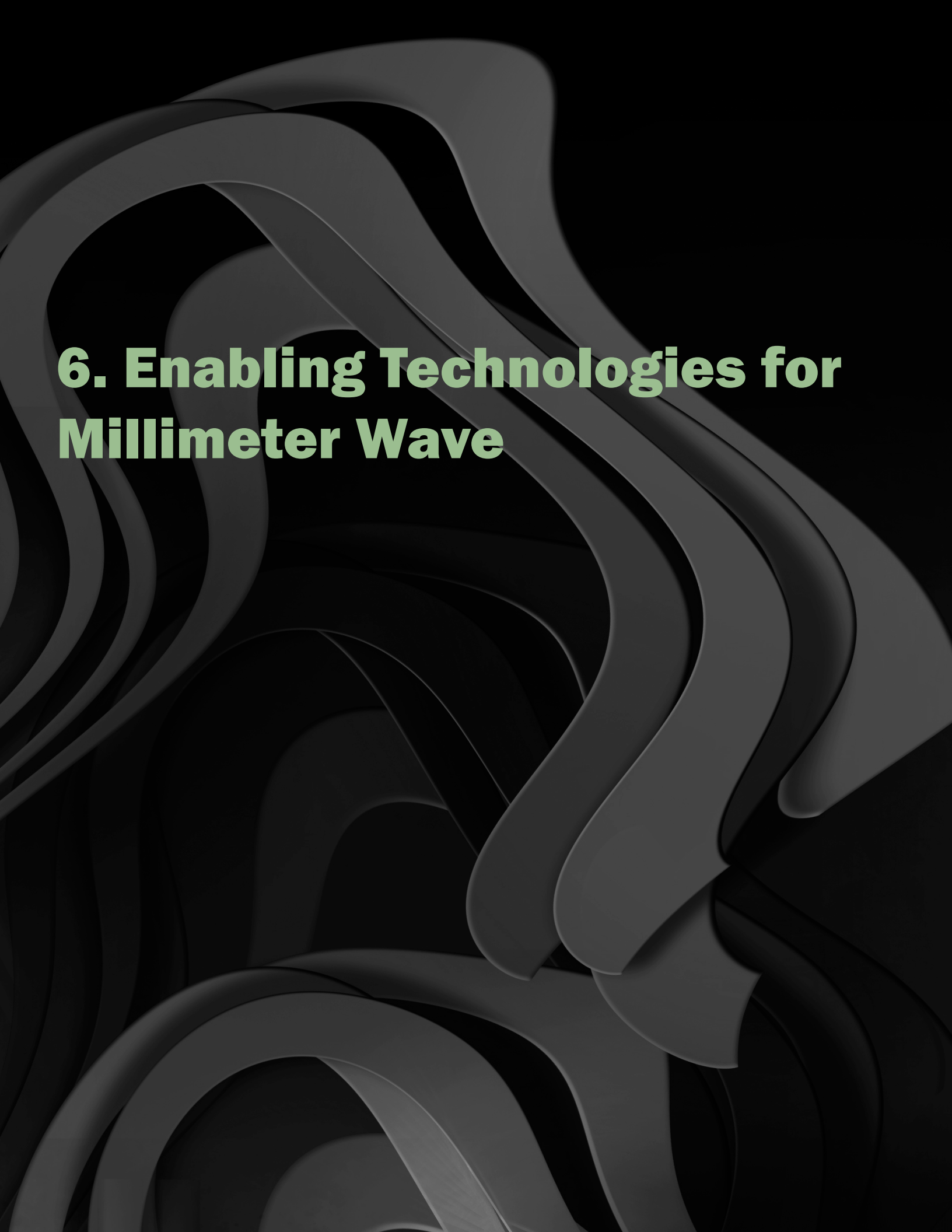
	Sub-6 GHz bands	mmWave band
Pathloss	Low	High
Radio Channel	Rich multi path	LOS and nLOS
Indoor penetration	Average	Much worse
Channel size	Small- medium	Wide
Cell size	Mid to Large	Low
Major challenge	Capacity	Coverage

This use of beamforming for mmWave repeaters would provide more immunity to interference commonly encountered in sub 6 GHz repeaters. Moreover, direction of the donor and target are known and beamforming can be implemented with much less complexity compared with sub 6 GHz band. Phased array antennas is a common method being used for beamforming.

A much simpler and lower cost approach called Holographic Beam Former (HBF) is also commercially available now [23] [24]. HBF requires only a single, simple, biased control component like a varactor diode at each element. The HBF transforms an incoming RF signal into a dynamic, rapidly steerable beam by manipulating the bias state of the control components. A picture of such device is produced in Fig. 5.6.



Fig. 5.6. Examples of outdoor (left) and indoor (right) mmWave repeaters.



6. Enabling Technologies for Millimeter Wave

6 Enabling Technologies for Millimeter Wave

6.1 RAN Architecture

The Radio Access Network has evolved since the beginning of commercial wireless networks (1st generation analog cellular). In early generations, the antenna was the only component installed on top of the tower. All other RAN functions including radio and baseband processing were performed in an equipment called the Base Transceiver Station (BTS), normally installed in a shelter on the ground. The radio signal from the antenna was connected to BTS via long coaxial cables, resulting in significant RF signal loss particularly with higher frequencies.

In the current phase of wireless networks (2G through 4G), radio and baseband functions are separated. In a macrocell deployment, a cluster of antennas forming three or more sectors are used to create full 360-degree coverage. Each sector is equipped with a high gain directional antenna and a Remote Radio Head (RRH) which handles the RF chain, Analog-to-Digital converters (ADC), Digital-to-Analog Converters (DAC) and up/down converters. The RRHs are typically mounted up on the tower connected to the antenna(s) with short RF jumper cables. Starting in 4G, the RRH typically features MIMO configurations with 2×2 , 4×4 , 8×8 or even higher antenna counts for Massive MIMO. The Baseband Unit (BBU) handles baseband processing and the backhaul interface. One BBU, typically installed on the ground, is connected to multiple RRHs depending upon the number of sectors supported by the base station. The protocol interface connecting RRH and BBU is known as the Common Public Radio Interface, or CPRI. The combined infrastructure (antennas, RRHs and BBU) is termed as eNodeB in 4G (Evolved NodeB).

In the case of short-range base stations (small cells), antenna types may vary from low-gain omnidirectional antennas to directional patch antennas with higher gain for a single-sector. In the case of patch antennas, the RRH and BBU functions are integrated into a single unit.

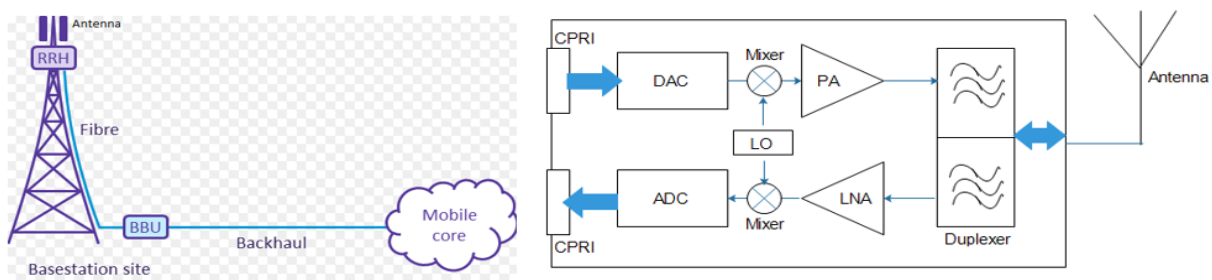


Fig. 6.1: Sub 6 GHz RRH [22].

6.1.1 RAN Architecture for 5G

Radio access networks have evolved significantly since their origins to the point at which today's RANs support multiple-input, multiple-output (MIMO) antennas, wider spectrum bandwidths, multi-band carrier aggregation, with many enhancements for 5G and beyond. Modern RAN architectures separate the user plane from the control plane into different network elements. This separation of the control plane and data plane is an essential aspect of the flexible 5G RAN, as it aligns with Software Defined Network (SDN) and Network Function Virtualization (NFV) techniques such as service chaining. Fig. 6.2 provides an overview

of different possible RAN split options for the gNodeB [23] which includes the separation of a distributed unit (DU) and centralized Unit (CU). For the CU, it also can be decomposed into user plane (CU-UP) and control plane (CU-CP), where the E1 interface connects the two.

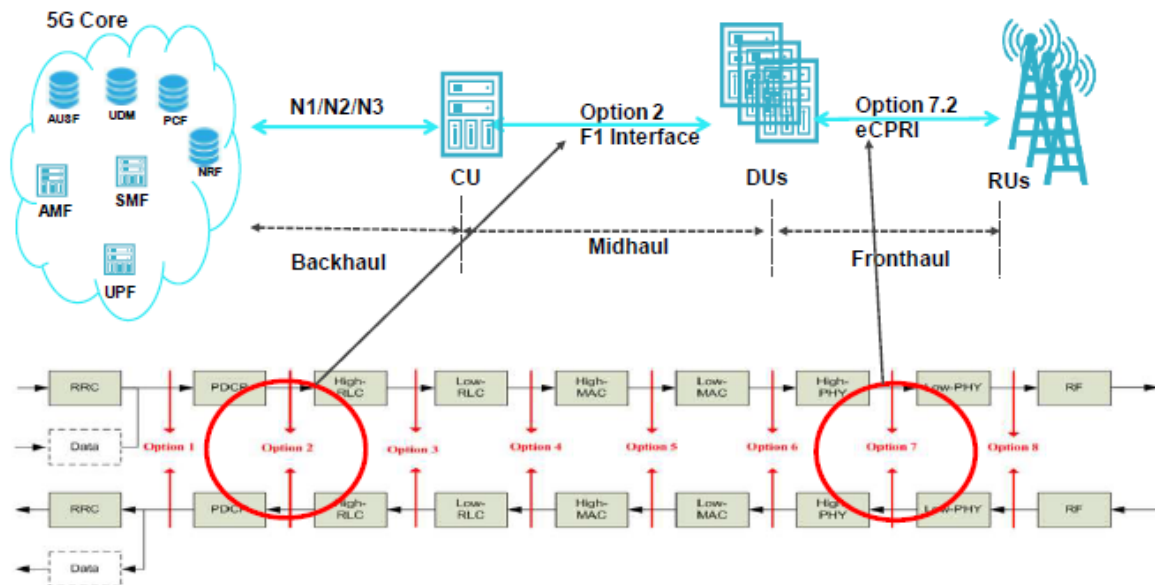


Fig. 6.2: RAN split options and RAN network elements [23].

- **Option 1 (RRC/PCDP 1A-like split) distributed architecture similar to all-in-one small cell**
- **Option 2 (PDCP/RLC Split 3C-like split)**
- **Option 3 (High RLC/Low RLC split, Intra RLC split)**
- **Option 4 (RLC-MAC split)**
- **Option 5 (Intra MAC split)**
- **Option 6 (MAC-PHY split)**
- **Option 7 (Intra PHY split)**
- **Option 8 (PHY-RF split), similar to CPRI interface as defined in 4G**

This decomposition and isolation of functions, along with the well-defined interfaces between them, allowing operators to disaggregate software from hardware. The choice of how to split New Radio (NR) functions in the architecture depends on factors related to radio network deployment scenarios, constraints and intended supported services.

The lower layer fronthaul split connects the Radio Unit (RU) with the DU and is characterized by:

- **low latency on the order of 100 msec**
- **the ability for the DU to serve multiple RUs**
- **RU-DU distance that can be 20 km or more**
- **Throughput requirement that depends on the bandwidth, MIMO configuration and split point between the DU and the RU.**

When eCPRI is implemented in 5G fronthaul, it splits into multiple paths where beamforming is achieved by controlling the phase of each path. This enables a single beam to be steered per data path, so in theory only one user at a time can be served.

Analog beamforming is the simplest architecture but limited in performance due to lack of multi beam and MIMO support. Hybrid beamforming offers a compromise. It is a beamforming architecture with a much lower number of digital transceivers than the total of number of antenna elements. Hybrid beamforming essentially combines digital pre-coding and analog beamforming to create several beams simultaneously in space, and hence ability to serve more than one user in a time slot and single MIMO support.

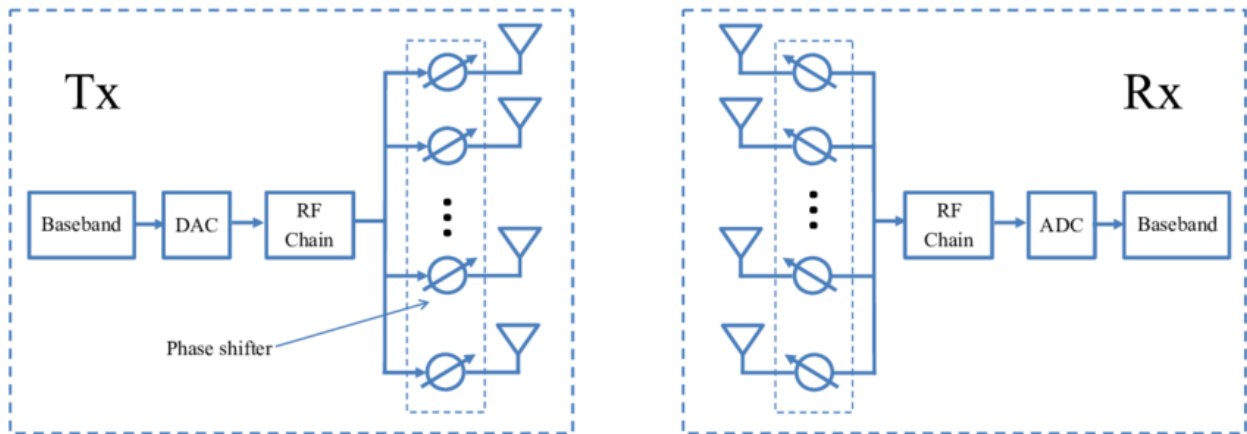


Fig. 6.3: Analog beamformer diagram [24].

A simple diagram of hybrid beamforming architecture is shown in Fig. 6.4. The RF chain is associated with a subset of antenna elements and represents the number of antenna port configurations. For instance, a 2x2 system supports two RF chains and 4x4 system is associated with 4 RF chains. The reduced number of RF chains including DAC reduces the power consumption significantly while providing a sufficient number of beams into different directions of toward a single user for MIMO support.

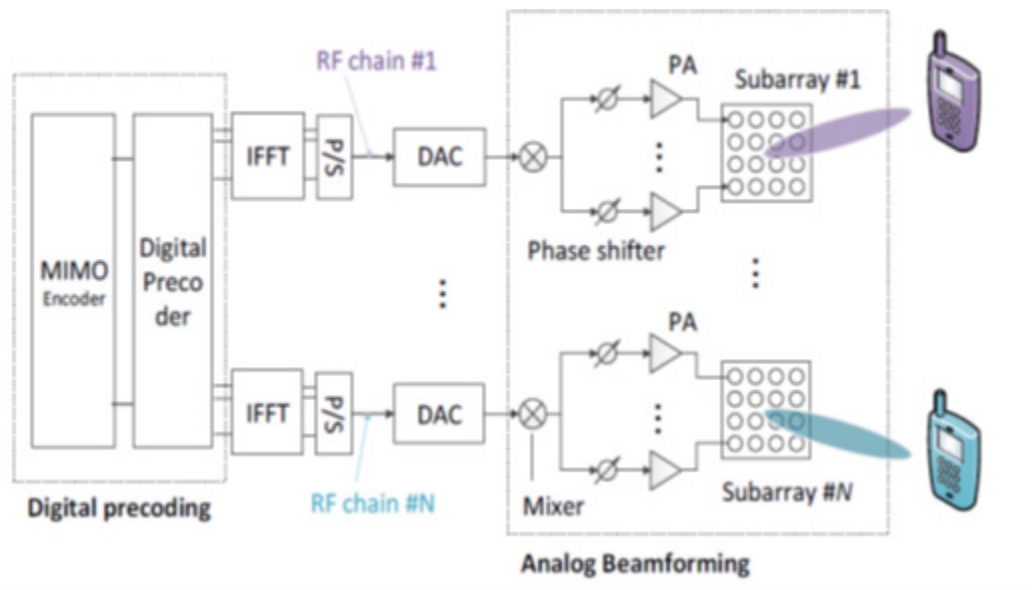


Fig. 6.4. Hybrid beamforming structure [25].

6.2 Antennas

6.2.1 Macrocell base stations

The antenna is an invaluable segment of any wireless network. 5G Americas has published several whitepapers on evolution of antenna for 4G and 5G systems [26]. Early 2G and 3G systems operated with two receive antennas spaced at least a lambda spacing to optimize the uplink receive diversity performance.

4G LTE introduced the concept of Multiple Input, Multiple Output (MIMO) and beamforming transmission to boost spectral efficiency and throughput. In its most basic form, the antenna for a 2x2 MIMO system is similar to antennas used in 2G systems. The higher order MIMO (4x4) or beamforming (8x8) requires more antennas. In 4x4 MIMO system, the 4 antenna ports are comprised of 2 cross polarized antenna columns spaced at least by 1 lambda. In 8x8 MIMO/beamforming system, the 8 antenna ports are comprised of 4 cross polarized antenna columns with spacing of 0.5 or 0.65 lambda spacing. In both cases, each antenna port is represented by one column per polarization comprised of 10-12 elements. All antenna systems discussed so far are called passive antenna, where antenna and radio modules are separate units interconnected by a short or long coaxial cable. Fig. 6.5 shows different generations of macro base station antenna systems for sub 6 GHz [27].

The active antenna systems where antenna and radio modules are integrated is a new trend for base station architecture in 6 GHz band. It is already in operation by several operators around the world. The active antenna systems typically have much higher number of antenna ports (32 or 64) and are being called massive MIMO. In such systems, single user and multi-user MIMO are being used to exploit further enhanced spectral efficiency.

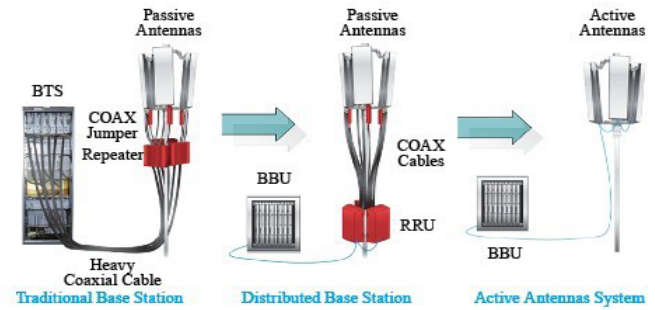


Fig. 6.5. Evolution of base station architecture.

The antenna module used in massive MIMO systems are phased array antennas that are also a very attractive choice for mmWave. The small wavelength at mmWave frequencies implies that the antenna elements will be closely spaced, which results in using large number of elements within a reasonable size. At mmWave, the number of antenna elements at the base station can vary from 64 to more than 1000. Coverage-enhancing solutions are essential in mmWave. A high number of antenna elements would provide wider coverage from a single radio and antenna through beamforming/steering.

Fig. 6.6 shows a typical antenna made up of rows and columns of individual dual polarized antenna elements with each element connected to radio chains. In sub 6 GHz, multiple antenna elements are interconnected to form a subarray connected to radio chains.

Directivity is the measure of how concentrated the antenna gain is in a given direction relative to an isotropic radiator. It follows a $10 \cdot \log(N)$ relationship, where N is the number of elements in the array. Gain, however, takes into account directivity as well as ohmic and scan losses [28]. So, in general, array gain equals $10 \cdot \log(N)$, plus the embedded element gain (G_e), minus the ohmic and scan losses:

$$\text{Array gain} = 10 \cdot \log(N) + G_e - L_{OHMIC} - L_{SCAN}$$

G_e is the embedded element gain, which is the gain of a single radiator embedded in the array. If the radiating elements are spaced $\lambda/2$ apart in both the azimuth and elevation directions, then the area of each element is $\lambda^2/4$. Since antenna gain is $4\pi/\lambda^2 * A_e$, where A_e is the effective area of the antenna, then the G_e equals π or 5 dBi.

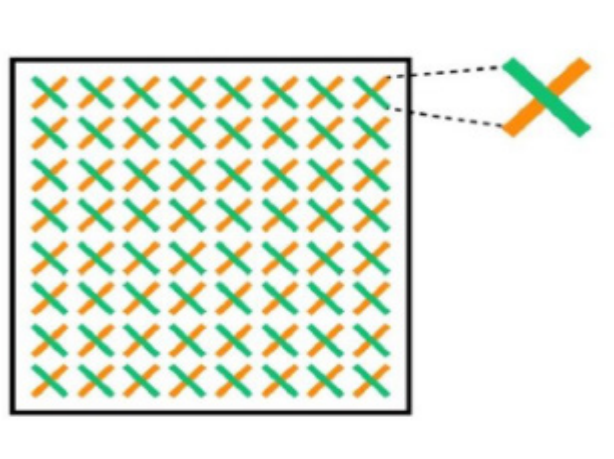


Fig. 6.6: Typical phased array antenna (8x8) [26].

6.2.2 Antennas for Smartphones

The small physical size of antennas at mmWave frequencies makes the use of chip-integrated arrays – often containing 4-8 elements a feasible option. These antennas have a high gain and support multiple beams, thus addressing the design goals of providing a high-quality data link in all directions around the phone. Achieving high UE EIRP with acceptable power consumption requires high antenna gain and the ability to steer the beam in desired direction to maintain the link [29]:

- **Physics dictate antenna size and spacing**
- **The number of antenna element in the array determines gain and EIRP**
- **Beamforming allows more antenna gain**

To achieve this a group of 4-8 antenna elements are arranged in an array and phased to concentrate radiation in a relatively narrow beam (gain= $G+10\log(N)$, where N is number of elements and G is the element gain). This gain applies in both uplink and down link. Fig. 6.7 shows a typical diagram for such antennas.

There are challenges of integrating the antenna in the device behind a cover, which at mmWave frequencies has a significant effect on the radiating performance of the antenna. Techniques used for Radom design in the aerospace industry find application here. Antennas can be efficiently integrated behind plastic or glass covers by engineering the cover geometry to act locally as a lens or even behind metal covers by including electromagnetic windows, perhaps based on Frequency Selective Surfaces (FSS) design principles. Another option made possible by the small physical size of antennas at mmWave frequencies is the integration of slot-based designs in the metal rim of phone [30].

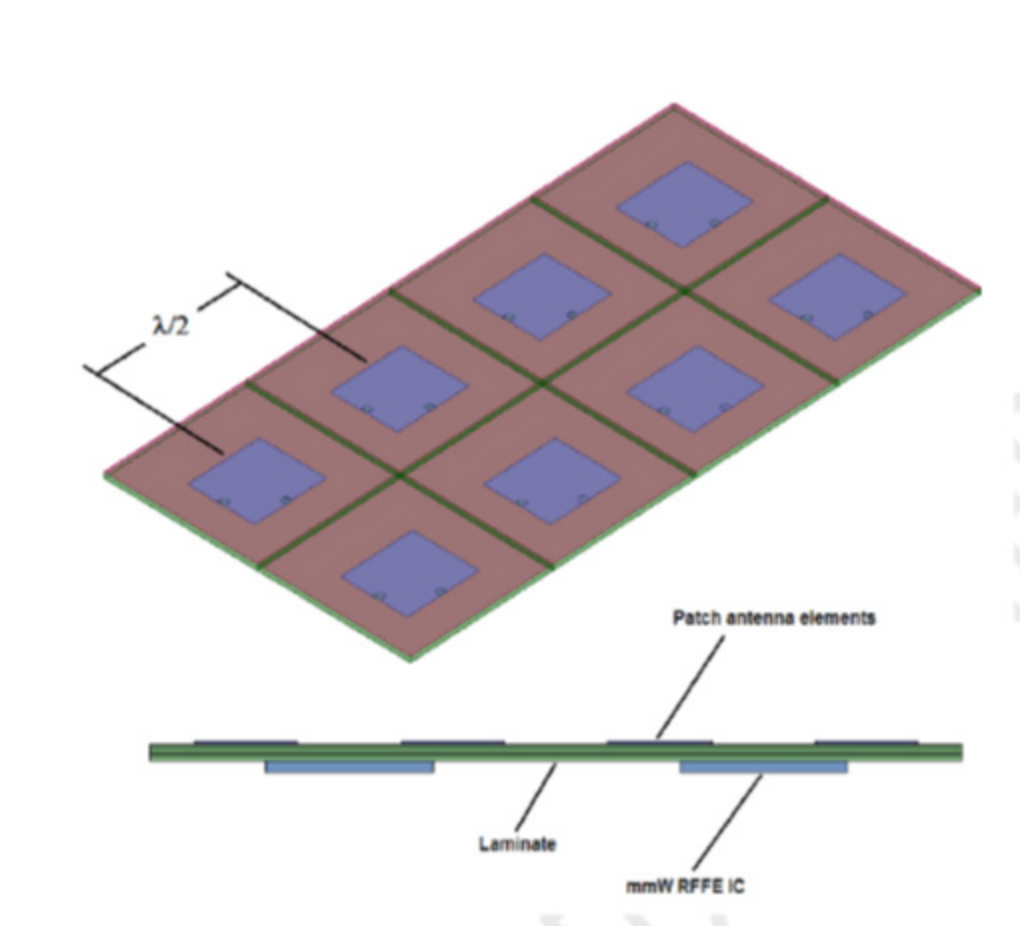


Fig. 6.7. Typical antenna design for mmWave smartphone.

6.3 Beamforming

The small wavelength of mmWave frequencies allows us to pack many antennas in a small area. Transmitting a signal through many antennas with specific phase offsets provides beamforming gain by coherently combining the electromagnetic signal radiated from each transmitter antenna. Similarly, the coherent combination of in-phase received signals from multiple antennas produces a signal-to-noise ratio (SNR) gain when the receive antennas have uncorrelated noise. The realized beamforming gain at both transmitter and receiver makes the communications channel directional, which reduces inter- and intra-cell interference as shown in Fig. 6.8. Transmit and receive beamforming power gain, coupled with reduced interference, boosts signal-to-interference-plus-noise ratio (SINR), bringing higher data rates, more cellular capacity, and extended cell coverage. The realized gain in SINR is especially useful for mmWave communication systems, given the high penetration and propagation losses at mmWave frequencies discussed in section 4.1. Furthermore, multiple beams at the transmitter can be used to multiplex parallel data streams to communicate with spatially separated multiple users (MU-MIMO). Multiple beams at the receiver can bring diversity gain, increasing reliability via redundant data streams.

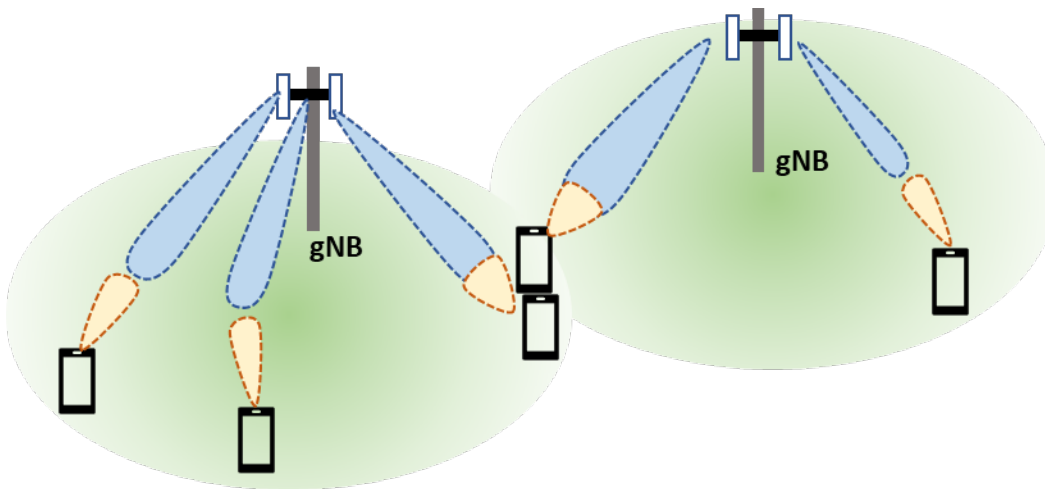


Fig. 6.8. mmWave beamforming with reduced inter-cell and intra-cell interference.

To realize efficient beamforming, each antenna requires an amplitude controller, phase shifter or time delay element. A specific configuration of these elements, coupled with the antenna array geometry, determines the beamforming radiation pattern. Either open-loop or closed-loop beamforming estimates can be used to perform beamforming. Closed-loop techniques consider that the channel estimated between each transmitter and receiver antenna is known, allowing the best beamforming configuration to be obtained from the estimated channel matrix. Open loop techniques utilize a pre-established codebook for beamforming at both the transmitter and receiver. The best beamforming configuration from the codebook is selected according to the received signal strength without explicitly estimating the channel.

Depending on the choice of phase shifter types in the analog or digital domains, several beamforming architectures have been considered. Three common beamforming architectures for mmWave communications are: i) analog phase array (APA) ii) hybrid phase array (HPA), and iii) fully digital architecture (FDA). These architectures are briefly introduced in Chapter 6.1.1. Although FDA is popular choice for sub-6 GHz massive MIMO communications, it is less suitable for mmWave due to the channel sparsity, high propagation loss etc. HPA and APA are the preferred architectures for mmWave frequencies when performance and cost tradeoffs are considered. FDA is considered as a next generation architecture for mmWave, with pending advancements in circuit technologies [31].

6.3.1 Analog

Analog phased array (APA) is considered as a solution to reduce hardware costs for analog to digital converters (ADCs). This architecture places phase shifters in the analog domain at radio frequency (RF), analog baseband (IF) or in local oscillator (LO) paths.

Analog RF beamforming is one of the most commonly used architectures, since it requires a single mixer/LO component. However, it suffers from a high noise figure if the phase shifters are passive, or high-power consumption if the phase shifters are active. RF beamforming also provides spatial blocker rejection before the mixer and IF circuit, which relaxes the linearity constraints of downstream receiver circuit components. Conversely, analog IF and LO beamforming both require multiple mixers and LO distribution circuits but can employ low power phase shifters.

Analog beamforming with any of the three architectures given above requires only one pair of ADCs and digital-to-analog converters (DAC). It combines the signal at the output of receive antennas in the analog domain using phase shifters prior to digitizing with ADCs for receiver processing. Or it applies phase shifting at the input of each transmit antenna after converting a single digital data stream to the analog domain, as shown in Fig. 6.9.

Since analog beamforming supports only single stream transmission, it can serve users only in a single beam direction at a time. Communication with spatially separated users can be achieved by beam switching to different directions in time. Analog combining at the receiver has advantage of rejecting both directional in-band (inter- and intra-cell) interference as well as out-of-band interference, which also reduces the requirement on the ADC bit resolution, and therefore lowers ADC power consumption.

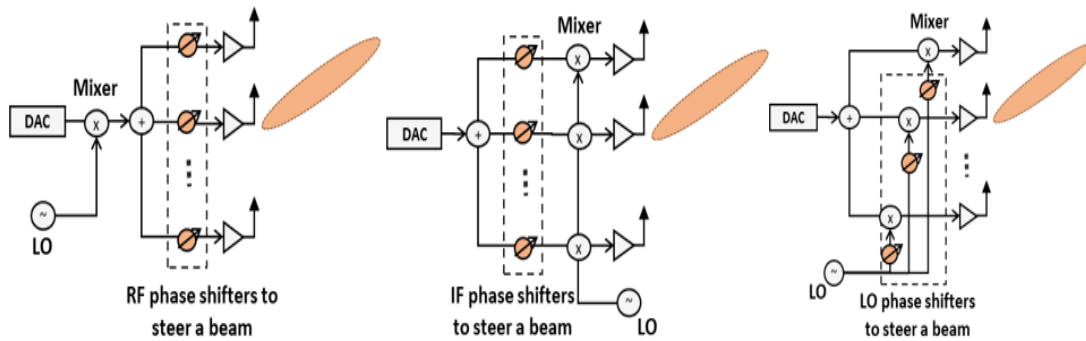


Fig. 6.9. Analog beamforming architectures: i) RF beamforming (left), ii) IF beamforming (middle), iii) LO beamforming (right).

However, mmWave communication relies heavily on highly directional transmissions to overcome the large pathloss. The use of directional transmissions with analog beamforming significantly complicates beam search and tracking capability, as discussed in Chapter 6.3. For example, angular beam search with a single beam at a time can slow down the initial access, given the potentially large beam search space. In addition, relying on connection to a single beam at the receiver can result in frequent connection failures due to beam blockages, reducing the overall reliability of the system. In the data plane, beamforming with a single stream is a very inefficient use of the channel in a non-line of sight environment.

6.3.2 Hybrid

Hybrid phased array (HPA) architectures which use multiple pairs of ADCs/DACs (RF chain) are also considered to support multi-user/multi-stream transmission. The number of RF chains are usually much smaller than the number of antennas and can be as low as the required number of data streams.

There are two common HPA architectures in terms of connection types between RF chains and antenna elements: fully connected HPA and sub-array connected HPA, as shown in Fig. 6.10. In a fully connected HPA, each RF chain is connected to all antenna elements through separate phase shifters. Therefore, the number of phase shifters scales with the number of RF chains and the number of antenna elements. The fully connected HPA provides maximum beamforming gain with the narrowest beamwidth by using all antenna elements. Therefore, it provides higher received signal power and lower inter-beam/user interference.

In sub-connected HPA, each RF chain is connected to disjoint and co-located sets of antenna elements, therefore having a more practical and simpler architecture. In this architecture, the number of phase shifters

is limited by the number of antennas; therefore, this architecture is more power efficient and popular than fully connected HPA. However, since each RF chain is connected to a smaller number of antenna elements, the beamforming gain is lower and the beamwidth is wider. This results in lower receive signal power and more inter-user/beam interference. Both architectures can be implemented with RF, IF or LO analog phase shifting, as described in Chapter 6.2.1.

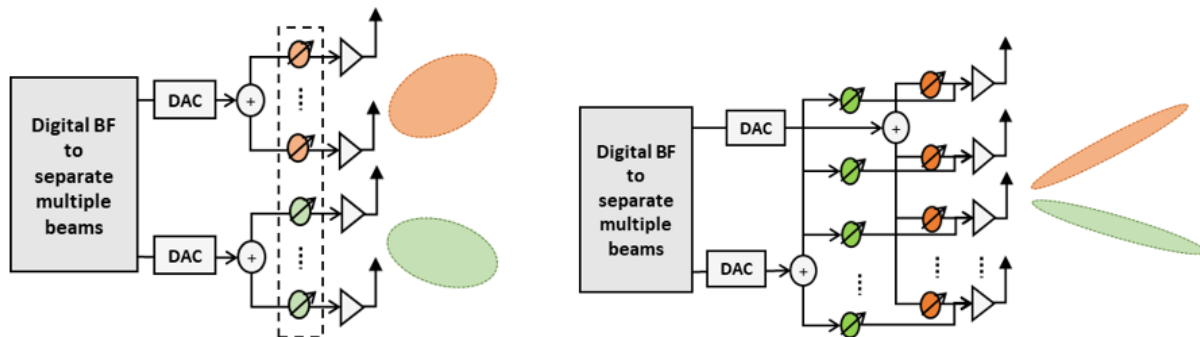


Fig. 6.10. Hybrid beamforming architecture with two RF-chains: i) sub-array connected HPA, ii) fully connected HPA.

HPA utilizes both digital beamforming with multiple RF chains and analog beamforming with analog phase shifters (thus “hybrid”). The digital beamforming can be used further reduce the inter-beam interference. The main benefit of HPA is to enable multi-beam transmission to support multi-user communication using the same time and frequency resources. In addition, the digital beamforming part of HPA can be useful for improving beamforming gain in non-line-of-sight channels for better coverage. At the receiver, HPA can enable dual/multi-connectivity with multiple base stations, which can increase the reliability of the mmWave communications system. Compared to analog beamforming, HPA can provide faster initial access, since a transceiver with HPA can create multiple beams in different directions at the same time. This functionality is critical especially when control channels are also beamformed to improve mmWave cell coverage. In a mobile environment, multiple beams can be used to track beam direction, either through digital beamforming and/or by constantly monitoring the best beam direction with the available RF chains.

Although HPA provides better performance than analog beamforming, its performance is still limited by number of RF chains. In a high user density mobile environment, the overhead of beam acquisition can be still very large. The beam tracking of HPA is also limited to the direction of the beams, while other directions remains blind to the transceiver. In addition, as discussed above the most popular and power efficient sub-array HPA type has lower beamforming gain and higher sidelobes, which might not be desirable in certain interference-limited scenarios.

6.3.3 Digital

Fully digital architecture (FDA) where each antenna element has a separate pair of RF chains as shown in Fig. 6.11 has become increasingly popular. Theoretically, at the transmitter FDA can support as many users as there are antennas. Like HPA, it can provide the highest beamforming gain and the least inter-user interference. Therefore, FDA allows the implementation of MU-MIMO with more layers. It also has ability to send a pilot sequence for beam search in all directions at the same time, which can significantly reduce initial access and beam tracking latency. In addition, FDA has ability to adapt beamforming to channel, due to flexible digital processing and phase allocation, and therefore provides the best beamforming gain in a non-line-of-sight channel. At the receiver, FDA can constantly monitor all directions at the same time for the

possible best beam connections, and hence provides the most robust mmWave communications in the mobile environment.

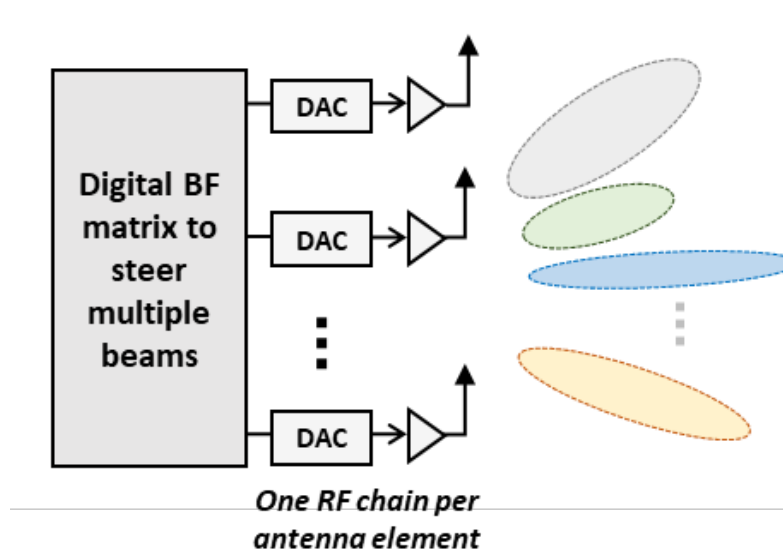


Fig. 6.11. Digital beamforming architecture.

Although FDA can provide optimal performance, it has the highest power consumption at ADCs/DACs for a given bit resolution and sampling rate. Similarly, power dissipation at the input/output (I/O) interface between Radio Frequency Integrate Circuits (RFICs) and baseband processors increases linearly with the number of RF chains. FDA also has highest power consumption at the baseband processor, since the complexity of channel estimation and multiple-input multiple-output (MIMO) processing increases linearly with the number of RF chains. In addition, it has lower signal-to noise ratio (SNR) per RF chain, which leads to high channel estimation error per antenna element when conventional channel estimation methods are considered (e.g. least square (LS) or minimum mean square error (MMSE)).

Since power dissipation at ADCs/DACs scales linearly with sampling rate, and exponentially with the number of bits per sample, it may not be desirable to operate the system with high resolution ADCs/DACs. Recently, FDA with low resolution processing has attracted significant interest [31]. To facilitate reduced power consumption at I/O interfaces, time domain compressions such as common packet radio interface (CPRI) [1] and spatial domain compression/precoding methods have been considered. The spatial compression in time domain exploits the received signal correlation to reduce the number of received signal inputs to baseband integrated circuit (BBIC). If the compression matrix is identified blindly, without any requirements for training or time/frequency recovery, the beam tracking latency can be reduced as well. Continuously adapting the spatial compression matrix to capture most of the receive power can lead to better beamforming than fixed codebook-based beamforming. Therefore, the use of compression for blind and relatively faster beam tracking and management, without any baseband processing, can be useful for FDA. Since the total number of inputs to the baseband processor is reduced by compression and precoding, the complexity of MIMO processing algorithms remains similar to HPA.

Table 6.1. Beamforming architecture comparison.

	Analog phase array (APA)	Hybrid phase array (HPA)	Fully digital array (FDA)	Benefit
Power dissipation	Single pair of ADC/DAC (RF-chain) The phase shifters are as many as number of antennas.	Several pairs of ADC/DAC The number of phase shifters can be more than the number of antennas for fully connected hybrid array	Each antenna requires a pair of ADC/DAC Large number of I/O interfaces between BBIC and RFIC	Longer battery life for user device, and low-cost base stations
Beam tracking	Slow	Improved beam tracking latency but limited by number of RF chains	The best possible beam tracking latency	Better quality of connection with high speed nodes
Initial access latency	Very high	Beam search can be parallelized with each RF-chains	The lowest latency by searching beams in all directions at the same time	Fast initial access and/or better coverage with directional UEs
Multi connectivity /multi-beam reception for device	Not possible	Possible with multiple panels but at the expense of coverage reduction and lack of fast multi-beam tracking capability	Multi-beam tracking and connectivity while maintaining quality of every beam	Diversity and reliability improvement and blockage mitigation. Soft and fast handover.
Multi-user support for base station	Multi-user communication is supported with beam switching. (Single user per TTI)	Simultaneous multi-user communication is supported for spatially separated users	Flexibility of multi-user support while maintaining beam qualities.	Coverage and throughput improvement.
Use case	Fixed wireless access	Multi-user MIMO communication in moderate user density and mobility environment such as smartphones	Multi-user MIMO communication in very dense and mobile environment such as cars and drones, and V2V communications	

6.4 Beam Acquisition and Tracking

As just discussed, the high pathloss of mmWave bands requires high beamforming gain to have a reasonable SNR and decent user experience. These beams need to be aligned between the cell site and UE at all times to maintain the communication link, as shown in Fig. 6.12. Such beam alignment is a challenge in changing mobile environments where blockage is always a possibility, as discussed in Chapter 4.1. The human body, brick walls, and glass are all obstacles that may cause blockage as the user moves through space. This severe loss cannot be compensated by increasing transmission power or beamforming gain. Instead, the mmWave transmitter needs to find alternative paths or spatial channels.

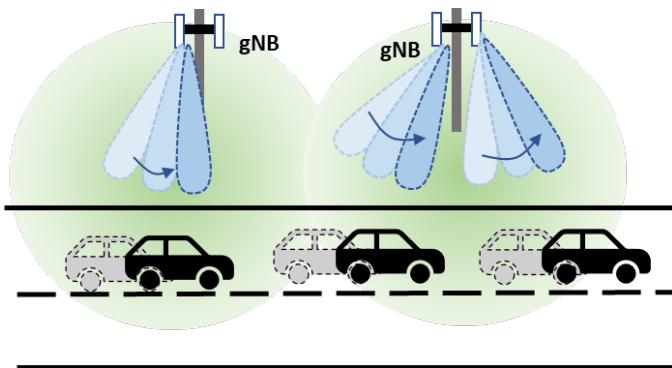


Fig. 6.12. Beam tracking at the base station to maintain the communication link between base station and car.

With APA and HPA beamforming solutions, the direction of the beams is adjusted by periodically sweeping the channel according to the movement and rotation of the mobile station. However, frequent beam sweeping increases overhead and reduces throughput. FDA solutions can transmit and receive signals in all directions at once since its antenna elements are omnidirectional, and FDA can virtually form directional and narrow beams covering the whole space at the same time. FDA transmitters and receivers can dynamically identify the new beam direction and find the best beamforming vector without increasing the

latency. At the receiver, FDA can use blind beam tracking, which constantly monitors the best beam directions from data symbols without requiring pilots while data path is communicating with the current data beam.

One of the challenges of mmWave systems is beam acquisition for mutual beam detection at both the base station and the user. The 5G NR standard supports periodic transmission of synchronization signals with directional transmission and directional receiver beam sweeping. Assuming both transmit and receive nodes are directional with N beams, respectively, the exhaustive search over possible beam combinations leaves us with total possibilities. Therefore, the latency of the initial access is $N^2 \times T_{\text{beam}}$ sec for APA/HPA, where T_{beam} is beam sweeping period. However, for FDA with wide beamwidth antenna patterns, a receiving device can find the best beam direction in one shot. All possible receive directions are examined, and the best beam can be virtually determined in zero-time (ignoring the processing latency), when processing the digitally stored signal. Therefore, an FDA system initial access latency is reduced to only T_{beam} sec.

As a performance comparison, let's assume the typical time duration to sweep every beam direction is T_{beam} . Assuming $N = 64$ and $M = 16$, and an exhaustive beam search, the total time to continuously search for the best beam pair is around 5s for an APA or HPA device. For an FDA device, the acquisition time is limited to 320ms, regardless of number of beams at the fully digital receiving device. In other words, the acquisition time drops by a factor of 16.

6.5 Standardization of Enabling Technologies For mmWave

6.5.1 3GPP NR FR2

The standardization of 5G NR for mmWave began with an “early drop” of 3GPP Rel-15 in December 2017. The initial drop of Rel-15 only addressed standardization of the RAN, and required LTE to operate a 5G network, as discussed further in Chapter 7.1.1. The initial Rel-15.0 specification defined the basic operating characteristics for 5G NR of the sub-6 GHz bands that have been used for LTE and prior generation technologies, defined as Frequency Range 1 (FR1) but also for higher frequencies between 24 and 52.6 GHz, defined as Frequency Range 2 (FR2) – what we have been referring to in this document as mmWave.

The first three standardized FR2 bands in Rel-15 were n257 (global 28 GHz), n258 (24 GHz) and n261 (39 GHz). Channel bandwidths, subcarrier spacing, guard band sizes, PRB allocations, channel numbering, modulation and coding schemes and all other primary aspects were defined in these early specifications. Also, Rel-15 introduced the framework for beam-based operations, which as we have seen are intrinsic to enabling mmWave to work for mobile broadband.

Later Rel-15 development expanded to begin standardization of “standalone” 5G with work on the next generation 5G core network. The specifications have continued to evolve since this time as shown in Fig. 6.13, enhancing use cases beyond eMBB with Rel-16 having completed at the 3GPP RAN #88 plenary which ended in early July 2020. Rel-17 study items/work items underway.

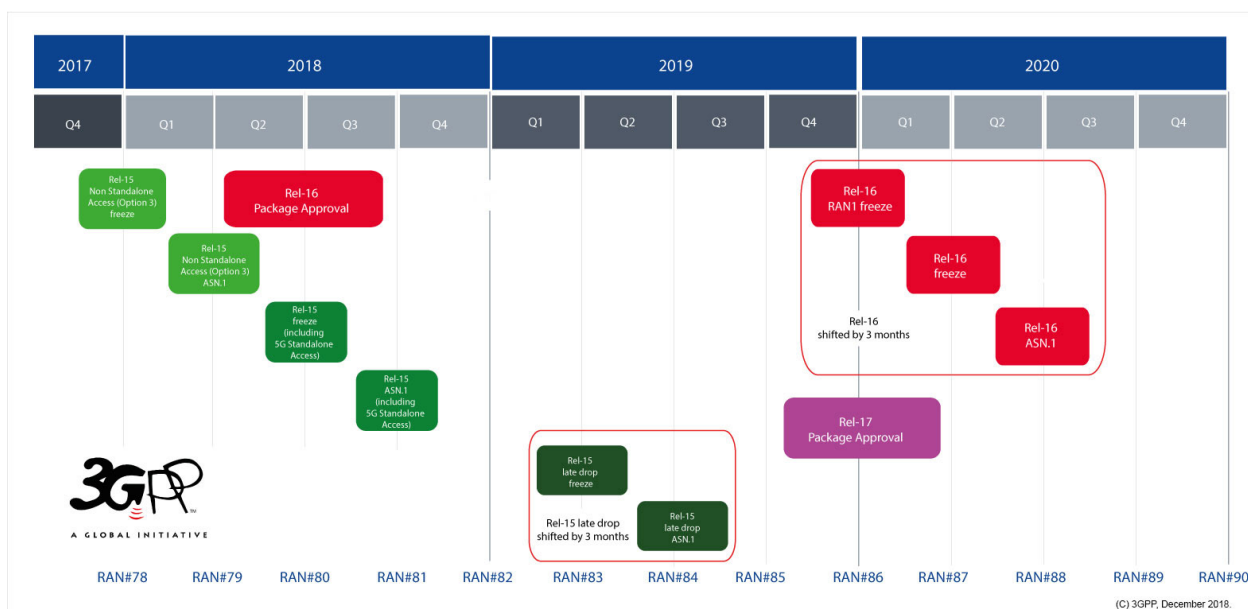


Fig. 6.13. High-level 3GPP timeline (source: www.3gpp.org).

As is the case everywhere, the global COVID-19 crisis that started early in 2020 necessitated the shifting of 3GPP working groups and plenaries from 4-6 in-person meetings a year to online meeting meetings only. This somewhat slowed development of Rel-16 and Rel-17.

6.5.1.1 3GPP NR FR2 Beam Management

In 3GPP Rel-15, 3GPP NR introduced basic beam management procedures including beam refinement procedure and PCell beam failure recovery (BFR). The beam refinement procedure can be classified as DL based and UL based. The DL based beam refinement is illustrated in Fig. 6.14, and can be divided into three hierarchical phases: the P1, P2 and P3 procedures. In the P1 procedure, UE P1 receive beam measures multiple candidate gNodeB P1 transmit beams, and the UE reports good gNodeB P1 transmit beam(s) to the gNodeB. Here, the UE P1 beam can be pseudo omni directional beam, and the gNodeB P1 transmit beam can be coarse wide beam, e.g. SSB beam. In the P2 procedure, the gNodeB selects one reported P1 transmit beam, and transmit multiple narrower candidate P2 beams within the selected P1 transmit beam. The UE P1 receive beam measures the multiple transmitted candidate gNodeB P2 transmit beams, and the UE reports good gNodeB P2 transmit beam(s) to the gNodeB. In the P3 procedure, the gNodeB selects one reported P2 transmit beam and repeats it for multiple times, based on which UE performs receive beam sweep across narrower candidate P3 receive beams and identifies the best P3 receive beam. After the hierarchical P1/P2/P3 procedure, the beam pair link is therefore refined with the best matched gNodeB/UE beams.

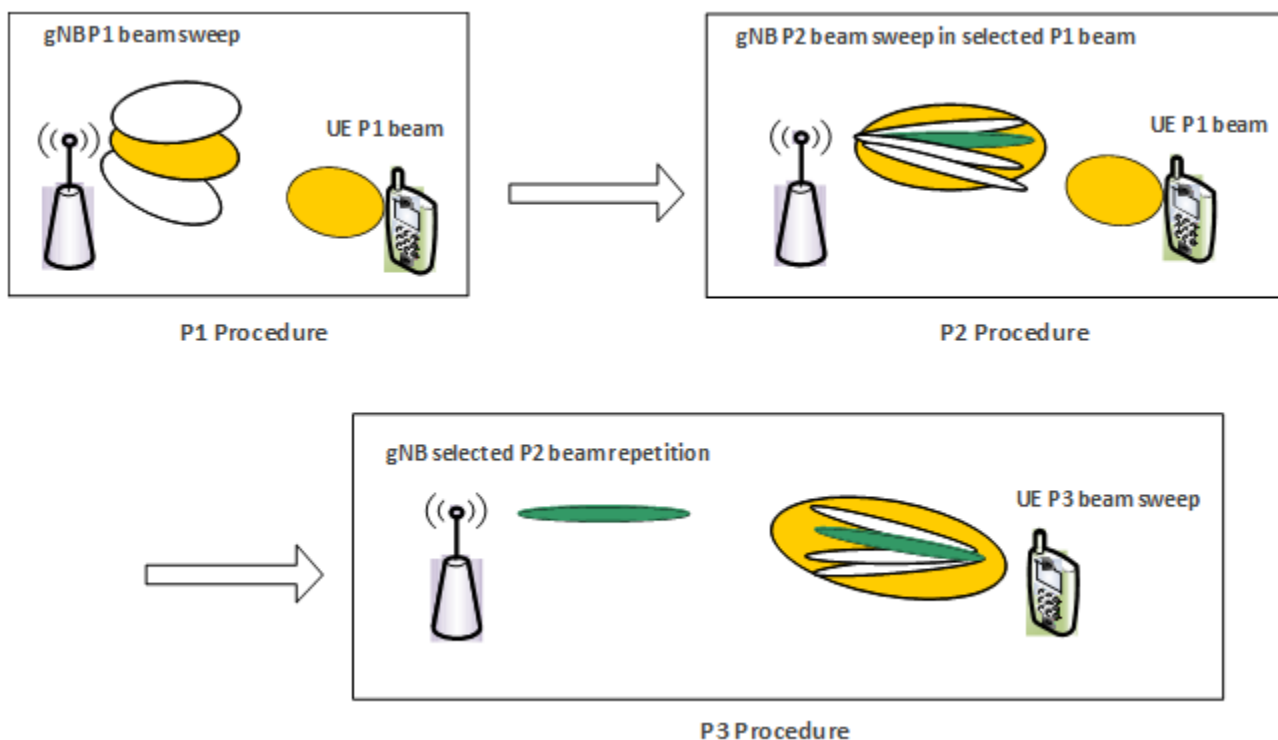


Fig. 6.14. DL-based beam refinement procedure.

In Rel-15, another feature fundamental to FR2 is PCell BFR, where the UE continuously monitors beam failure detection (BFD) reference signals, which are associated with DL control beams of PCell. If the quality of all BFD RSs is below a threshold, it implies all monitored DL control beams have failed, and the UE can initiate the PCell BFR via contention free-based random access (CFRA) procedure. After sending the CFRA preamble, the UE will monitor the BFR response from the PCell on a search space dedicated to BFR. The BFR response and the following messages will be sent via the new beam identified in the CFRA to further refine the new beam pair link.

In Rel-16, additional enhancements were further introduced to FR2, including SCell BFR, L1-SINR based beam refinement, and enhancements on beam management overhead/latency reduction. One major use case of the SCell BFR is to recover a failed SCell on FR2 while the PCell is on FR1. An example is shown in Fig. 6.15 in case of FR1+FR2 carrier aggregation (CA) with basic steps listed below.

- Step 1: UE detects that all DL control beams have failed for a SCell on FR2
- Step 2: UE sends link recovery request (LRR) on PCell on FR1 via corresponding PUCCH resource
- Step 3: PCell allocates UL grant for UE to report failed SCell index
- Step 4: UE sends the SCell BFR MAC CE to report failed SCell index + potential identified new candidate beam
- Step 5: PCell replies with BFR response, acknowledging the reception of BFR MAC CE

Based on reported failed SCell index, PCell may further carry out more extensive beam training to identify best new beam on SCell

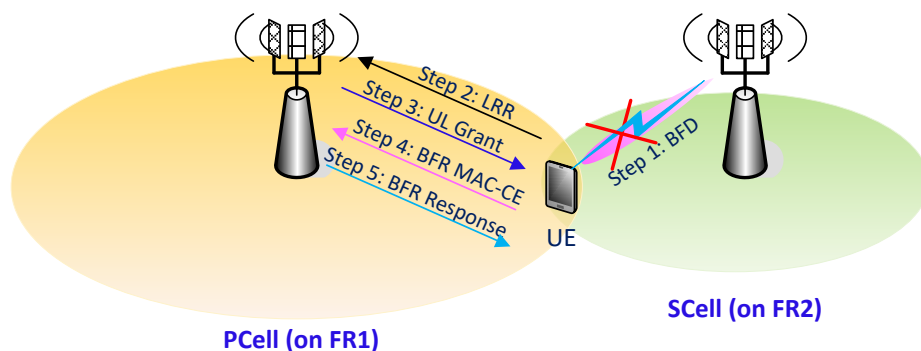


Fig. 6.15. SCell BFR procedure.

In Rel-15, beam selection is based on L1-RSRP, which does not consider the interference. To incorporate the impact of interference in beam selection, L1-SINR is introduced as a beam reporting metric in Rel-16. For each beam report, up to 4 beams can be reported, and absolute SINR value is reported for the 1st reported beam, which has the highest SINR. Differential SINR value is reported per remaining beam, and is computed with respect to the highest SINR. In addition, as listed in Table 6.2, Rel-16 defines five total combinations of channel measurement resource (CMR) and interference measurement resource (IMR) for the L1-SINR measurement resource configuration.

Table 6.2. Possible CMR/IMR Combinations for L1-SINR.

Combination	Channel Management Resource	Interference Management Resource
1	NZP CSI-RS	Same NZP CSI-RS
2	SSB	ZP CSI-RS
3	SSB	NZP CSI-RS
4	NZP CSI-RS	ZP CSI-RS
5	NZP CSI-RS	Another NZP CSI-RS

To further reduce beam management overhead and latency, the MAC CE-based pathloss (PL) reference signal update has been introduced in Rel-16, where the PL RS for PUSCH and aperiodic (AP)/semi-persistent (SP) SRS can be activated/updated via a MAC CE. With this feature, both UL beam and corresponding PL RS can be dynamically updated by MAC CE to avoid the latency due to RRC-based PL RS update.

On the other hand, in FR2, multiple component carriers (CC) typically share the same analog beamformer, especially in intra-band CA case. The beam indication signaling overhead and latency can be reduced by exploiting the property that a common analog beam is shared across multiple CCs. Therefore, Rel-16 introduced the feature of simultaneous DL/UL beam update across CCs, where a single MAC CE can activate a same set of beam IDs for multiple CCs as illustrated in Fig. 6.16. The simultaneous beam update across CCs further includes the following three sub-features:

- **For PDSCH beam update, a set of PDSCH TCI state IDs activated by a MAC CE can be applied to all BWPs in the CCs in an applicable CC list**
- **For PDCCH beam update, a TCI state ID activated by a MAC CE can be applied to all CORESET(s) with same CORESET ID for all BWPs in the CCs in an applicable CC list**
- **For SRS beam update, a SP/AP SRS spatial relation info activated by a MAC CE can be applied to SP/AP SRS resource(s) with same resource ID for all BWPs in the CCs in an applicable CC list**

In each of above sub-features, up to two lists of CCs can be configured by RRC per UE, and the applied list is determined by the indicated CC in the MAC CE.

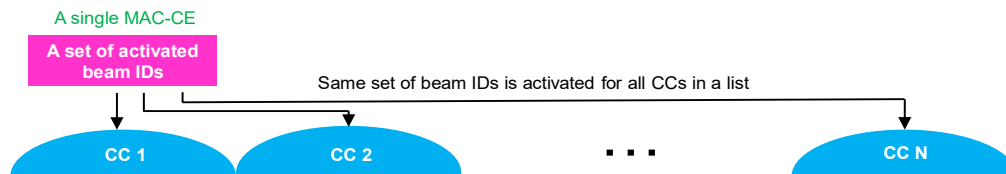


Fig. 6.16. Simultaneous DL/UL beam update across CCs.

To further reduce UL beam switch latency and overhead, the concept of UL default beam is introduced in Rel-16 to allow UL beam to automatically follow a DL beam without additional signaling. For PUCCH/SRS/PUSCH without spatial relation configured, the default spatial relation and PL RS are determined in the following two cases: If CORESET(s) are configured on the CC, the quasi-colocated Type-D (QCL Type-D) RS of the TCI state / QCL assumption of the CORESET with the lowest ID in active BWP serves as the default spatial relation and PL RS; Otherwise, the QCL Type-D RS of the activated PDSCH TCI state with the lowest ID in active DL BWP serves as the default spatial relation and PL RS.

A low-angle, upward-looking photograph of several skyscrapers with glass facades. The buildings are silhouetted against a dark, overcast sky. A prominent grid pattern, resembling a wireframe or a mesh, is overlaid on the image, creating a sense of depth and perspective. The grid lines are most visible in the upper left and right quadrants, converging towards the top of the frame. The overall tone is dark and industrial.

7. Millimeter Wave Operational Aspects

7 Millimeter Wave Operational Aspects

7.1 Multi-Connectivity

Even though mmWave cell sites can function autonomously with the introduction of the 5G core network, operators are unlikely to deploy mmWave sites without connectivity with other band assets. The following will discuss means to connect mmWave with FR1 bands traditionally used for LTE and prior generation technologies.

7.1.1 EN-DC

The first mechanism used to bring mmWave to market was EN-DC. To allow for the timely delivery of 5G devices and services to consumers, the initial release of 3GPP standards for 5G NR in late 2017 did not include specifications for the 5G Next Generation Core Network, which were still under development. Instead, the initial specifications were for so-called “Non-Standalone” mode, where a 5G base station (gNodeB) is connected to both an LTE cell site (eNodeB) operating on one or more FR1 bands/channels and to the LTE core network, or EPC. This is known as Option 3x, one of six initial options (plus several sub-options) that proposed different means of connecting 5G and LTE cell sites and core networks together to bring 5G to market. Additionally, Option 1 was proposed as the baseline LTE-only network, and Option 2 as a 5G-only network.

From these options, the industry coalesced around Option 3x (itself an elaboration upon the initially-proposed Option 3) to quickly introduce 5G while leveraging the existing 4G infrastructure, and Option 2 to introduce an all-5G network (RAN and core) once the Next Generation Core network standardization was complete. All initial 5G mmWave networks deployed globally were done so using Option 3x. Note that the LTE and 5G cell sites may or not be co-located in Option 3x.

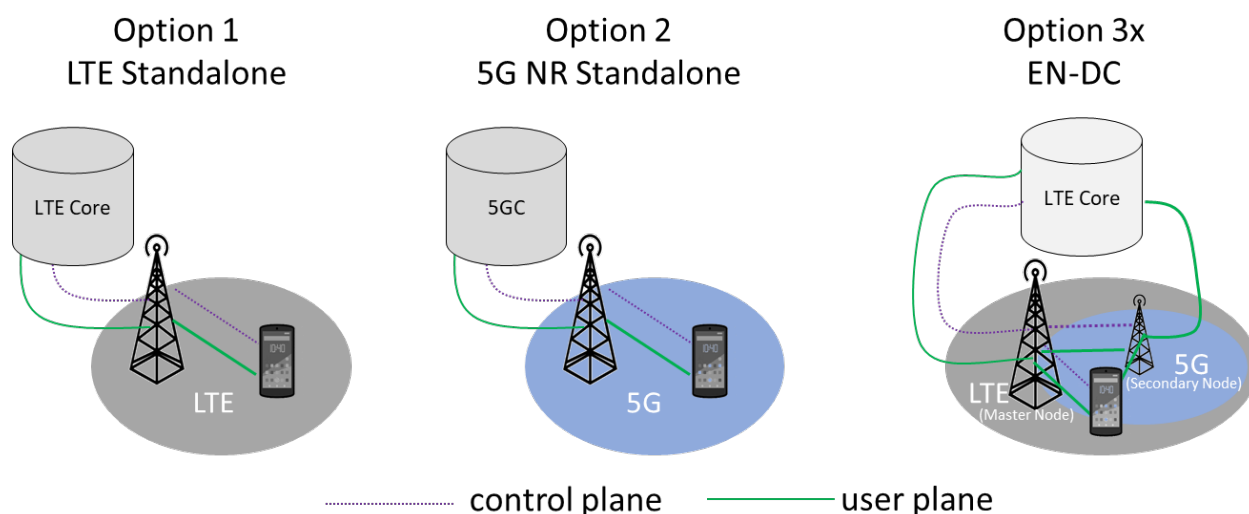


Fig. 7.1. Options 1, 2 and 3x.

Early deployment of Option 3x was a necessity, given the lack of a 5G Core network in the early days. But it also allowed operators to augment the 5G user experience with their significant spectrum resources that were otherwise 100% devoted to serving their LTE subscriber base. A 20 MHz FDD carrier using 256

QAM and 4x4 MIMO has a peak theoretical downlink throughput of almost 400 Mbps, which can significantly enhance a mmWave-only user experience, especially given how the amount of mmWave spectrum may vary from carrier to carrier and market to market. Needless to say, no operator wanted to deploy a 5G network with inferior customer experience than the legacy “4G” LTE networks! As subscriber uptake of 5G devices is slow in the early days (as it is with every new generation technology), Option 3x allows LTE and 5G NR to gracefully coexist while meeting the needs of both types of users.

The dual connectivity concept was first introduced in LTE for heterogenous network environments, where a macrocell overlays one or more non-collocated small cells, and the distance between the cells proved excessive for the latency requirements of carrier aggregation. While it never gained much traction for LTE, dual connectivity is the mechanism by which Option 3x works – specifically EUTRA-5G NR Dual Connectivity, or EN-DC. As shown in Fig. 7.1, in EN-DC the 4G core network (EPC) connects directly to both the eNodeB (Master Node or MN) and gNodeB (Secondary Node, or SN), with all control-plane data being passed to the UE over the S1-C interface between the EPC and MN, but user data being passed to both the MN and SN over the S1-U interface. Additionally, there is direct data and control connectivity between the MN and SN via the X2 interface. This architecture combines Option 3, which has no direct EPC-SN connectivity, with Option 3a, which has no X2 connectivity between the MN and SN, into a more flexible and robust architecture. Both the MN and SN must have both downlink and uplink connectivity to the UE in Option 3x.

The radio bearer, which is the data connection between the cell site and UE, can be routed in three ways:

- **completely over LTE as an MCG bearer (this is the Master Cell Group, which contains the Master Node and any other LTE carriers in carrier aggregation with the MN)**
- **completely over NR as an SCG bearer (Secondary Cell Group, containing the Secondary Node and any other NR carriers in carrier aggregation with the SN)**
- **as an SCG split bearer, where data flows from the EPC to the gNodeB (SCG), and some data is then routed via X2 to the eNodeB (MCG), allowing the UE to receive data from LTE and NR simultaneously, allowing the best end-user experience**

As shown in Fig. 7.2, the split in EN-DC occurs at the PDCP layer in the radio protocol stack. This is appropriate for sites that are non-collocated, or of different foundational technologies (such as LTE and 5G NR), given that coordination lower down the protocol stack requires tight interworking and low latency.

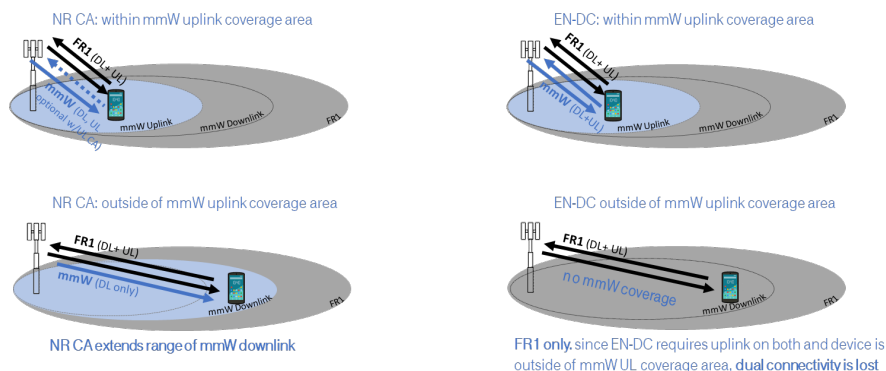


Fig. 7.2. Option 3x SCG split bearer protocol stack.

As of this writing over 4,500 EN-DC combinations with one or more mmWave carriers have been standardized in 3GPP, many in combination with other FR1 5G NR bands.

7.1.2 NR Carrier Aggregation

NR carrier aggregation (NR CA) can also be employed to use mmWave and FR1 resources concurrently. Operators have begun to “refarm” some of their legacy low- and mid-band spectrum resources from LTE to 5G (initially to enable a second generation of 5G devices that supported 5G NR FR1 in EN-DC). Now, the introduction of Dynamic Spectrum Sharing (DSS) provides additional opportunity to operators with less spectrum in bands they wish to use for both LTE and 5G by time-sharing the resource between the two technologies. It is expected that operators will continue to refarm spectrum to NR over time as 5G device penetration increases.

As is the case with EN-DC, FR1-FR2 carrier aggregation can be used to improve user throughput by combining the spectrum resources from both the lower bands and mmWave. Carrier aggregation has two primary differences from dual connectivity. First, the aggregation occurs at the MAC layer as shown in Fig. 7.3, instead of the PDCP layer as is the case for dual connectivity. MAC layer coordination is very responsive, with the ability to activate and deactivate Secondary Cells (SCells) very quickly based upon need.

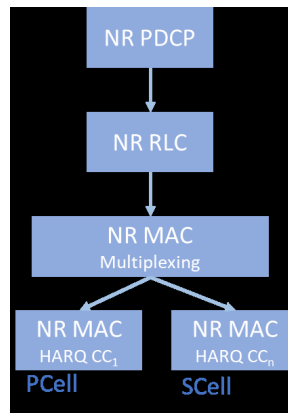


Fig. 7.3. NR carrier aggregation protocol stack.

Second, carrier aggregation requires an uplink only on the Primary Cell (PCell). This is in contrast with dual connectivity, where both the MCG and SCG require an uplink on their primary cells. For a mmWave SCell in carrier aggregation with an FR1 PCell, this means that the mmWave uplink, which is significantly limited and tends to therefore inhibit mmWave coverage. It is possible to effect uplink carrier aggregation in an FR1-FR2 CA combination as well. When the user exceeds the range of the mmWave uplink, that leg is dropped and the uplink will be served exclusively by FR1, while the mmWave downlink can continue to be used; these scenarios are illustrated in Fig. 7.4. As we will see in section 7.2, this can have significant capacity and coverage ramifications.

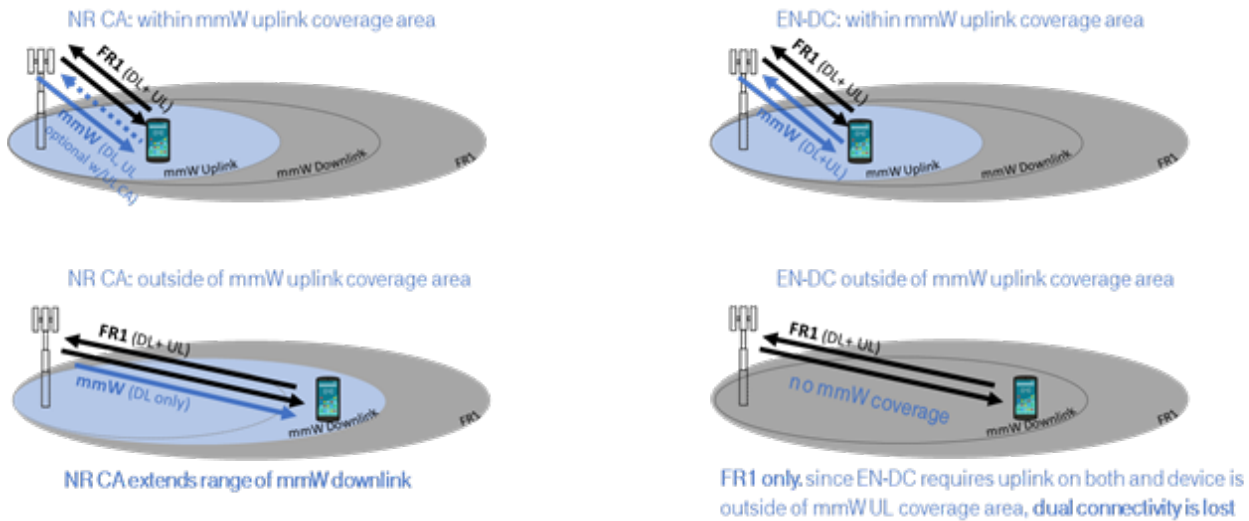


Fig. 7.4. FR1-mmWave range extension with carrier aggregation vs EN-DC.

It is important to note that Options 1 (LTE only), 2 and 3x are not mutually exclusive, and can coexist in the network, and even in the same cell site to serve various users' needs. For instance, legacy LTE users can continue to be served by the low- and mid-band LTE coverage layers; subscribers with first-generation 5G phones operating only on Option 3x can continue to operate in Option 3x; and subscribers with the latest standalone-capable 5G devices can operate in Option 2, with end-to-end 5G connectivity between the UE and 5G core network.

As of this writing, over 210 NR CA FR1-FR2 (mmWave) combinations have been standardized and can be enabled from 3GPP Rel-16 onward (2022 estimate).

7.1.3 NR-DC

A third alternative to use mmWave and FR1 bands concurrently is NR-NR Dual Connectivity, or NR-DC. As is the case with NR CA as discussed in the previous section, this falls under Option 2, as it is an all-5G solution. That said, it shares PDCP-level aggregation over non-ideal backhaul with EN-DC, and like all dual connectivity solutions, requires an uplink on both carriers.

NR-DC may have utility over NR CA in HetNet environments, where the mmWave cell sites are not colocated with the FR1 macrocells, and tight baseband coordination is not possible. But as will be demonstrated in Chapter 7.2, it is likely less preferable than NR carrier aggregation in most scenarios. Far fewer FR1-mmWave NR-DC combinations have been standardized to date that EN-DC or NR CA.

7.1.4 Comparing DC and CA Channel Assignment per Band

Carrier Aggregation and Dual Connectivity are both intended to provide diversity of UL connectivity to compensate coverage difference across bands. This is achieved for PDSCH and PUSCH using either approach; however, DC is still dependent on maintaining reliability of both bands for control and common channels. Lower dependence on UL will make CA far more effective at extending coverage if the necessary coordination can be achieved, as shown in Fig. 7.5.

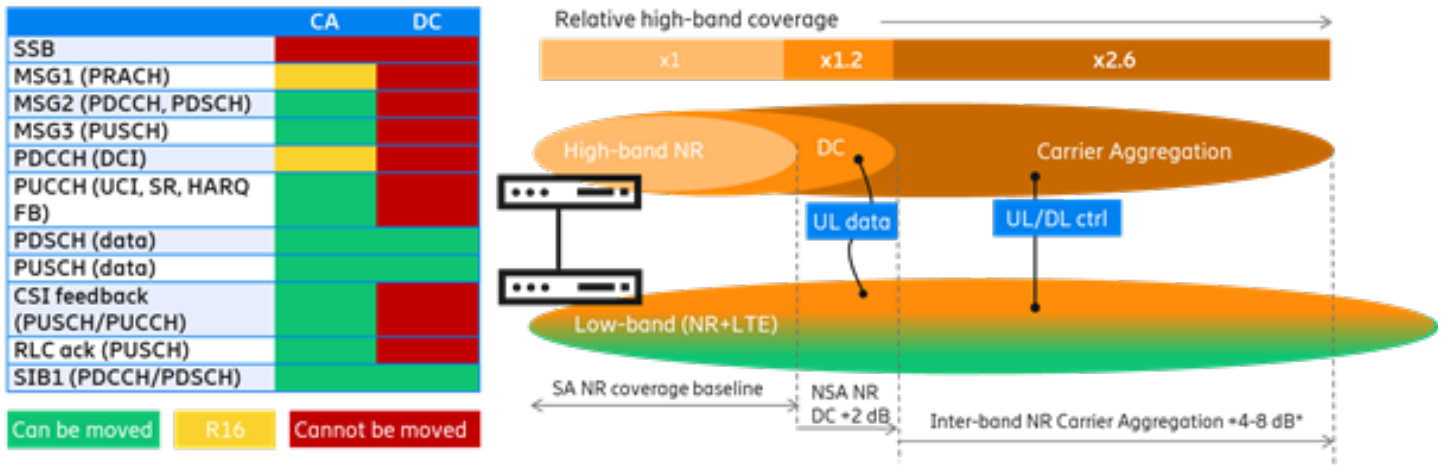


Fig. 7.5. CA vs. DC's ability to reallocate mmWave channels to FR1.

System simulation results comparing layered FR1-FR2 deployments using DC versus CA are discussed in Section 8.3.

7.2 Practical Deployment Challenges

Architectural and physical transport solutions over fiber, IAB and microwave have been covered in earlier sections. This section is focused on logical connections, rather than connections in the physical medium.

A key requirement to achieve load balancing objectives between mmWave and sub-6 GHz bands is very low latency connectivity – preferably below 250 μ s – between FR1 and FR2 BBU resources for coordinated scheduling. For non-colocated FR1-FR2, this can be achieved as shown in Fig. 7.6 through distributed BBU, with very low latency transport between different location; hubbed BBU, with centralization of RAN BBU resources (i.e. C-RAN) for shorter direct interconnect, or more commonly, by a combination of both.

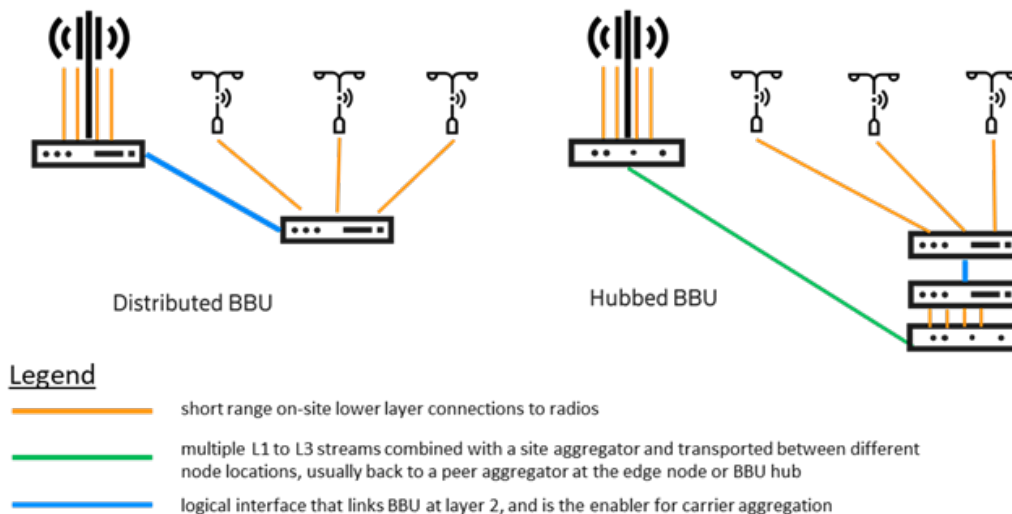


Fig. 7.6. Distributed vs. hubbed BBU architectures.

These baseband resources may be implemented on purpose-built physical hardware or virtualized on general purpose processing platforms with accelerators for L1 processing. The key interface and transport requirements are the same.

Achieving sufficiently low latency between BBUs at different physical locations comes at cost that must be traded against the CA benefit. Inter BBU layer 2 interfaces often assume co-siting with fast physical connection over short distances.

It is feasible to create a customized inter-BBU Layer 2 interface that shares common 10 GigE transport paths that could support carrier aggregation to a UE served by an FR1 macrocell with local BBU as PCell, and an FR2 mmWave small cell with its BBU at a nearby hub. Increasing latency over the inter-BBU 10 GigE link will delay data sent on the SCell, arriving in a later TTI, thereby reducing peak user throughput; however the data will still be delivered, maintaining the capacity offload benefit of using FR2 as the SCell.

This configuration anticipates network evolution to Option 2 standalone with FR1 and FR2 anchored to a common 5G Core (5GC) as per Fig. 7.1 in Section 7.1, and the necessary Rel-16 capable devices to support CA over different carrier numerologies. Earlier EN-DC deployments should anticipate this as the final configuration.

There are also some 3GPP-defined UE requirements that FR1 and FR2 signals must arrive within 30 μ s. This relates to the relative path length differences when sites are time synchronized, and should not be a constraint to practical urban and suburban deployments

To recap:

- **Advanced coordination features described in section 7.2 require low latency connectivity between FR1 and FR2 BBU**

entities that may be at different locations

- **Deployment practicalities may introduce higher latencies than desired, which will reduce peak user throughput, while the capacity benefit is still maintained**

7.3 Hardware Impairments

Physical (PHY) layer algorithms developed for a standardized technology need to take into account critical hardware impairments. For example, the approach to a modulation and coding scheme assignment has to factor in the varying degrees of impairments and tradeoffs associated with their mitigation. A PHY layer design that is challenged to overcome hardware impairments, will not be adequately successful in delivering the generational leap in performance expected of any new set of standards. 5G NR designs therefore build upon approaches and solutions that address performance issues arising out of limitations in the mmWave band spectrum.

Here we discuss several key problem areas and tradeoffs that exist in mmWave when used to support high data rate eMBB use cases. High frequency mmWave signal processing is more likely to suffer from sampling errors, leading to noise rise. Also, the very short signal periods impose stringent time synchronization requirements upon the circuit design and layout, without which it is far more difficult to adequately digitize the analog RF of the mmWave signal.

Phase noise, an artifact of incorrect oscillating frequency, leads to the generation of a different signal from that intended in the frequency domain. This is discussed more broadly as it impacts the mmWave upconversion to the much higher frequency. Finally, power amplifier design criteria for mmWave bands pose constant challenges around selecting the right balance between transmission line technologies, active

devices and circuit material. All of these challenges are captured below in context to the hardware in the transmitter or receiver paths where their presence manifests most adversely.

7.3.1 ADC/DAC Impairments

Today, integrated access and backhaul applications rely upon RF channel bandwidths over several hundreds of MHz to greater than 1 GHz. Also, highest order modulation schemes in the baseband range from 256 QAM and above. To meet the stringent requirements behind such needed real time performance, intensive digital signal processing capability is required. mmWave digital baseband circuits are therefore greatly reliant upon gigabit-sample-per second (GSPS) ADC and DAC designs to support the resulting extremely high data rate transmission applications. They are critical components in transceiver designs for wireless communication systems supporting any 3GPP NR FR2 transmission bandwidth. However, mmWave converter design involve tradeoffs between key requirements such as high-speed performance (sampling rate) and accuracy (resolution) with power consumption and mismatch inefficiencies even when fabricated circuit elements have similar design approaches. Such trade-offs can be sources of additional hardware impairments.

Low clock jitter in high speed convertors is needed to restrict inter-symbol interference (ISI). ISI occurs due to timing mismatches in the sampling of the RF signal that subsequently cause erroneous conversions. The adverse impact of clock jitter increases with signal frequency, leading to degradation in achievable signal-to-noise ratio. Higher frequency mmWave signals need to be sampled sufficiently faster to exceed the Nyquist limit and avoid aliasing-based noise rise. However, attempting to sample signals much higher than 1 GHz and with high dynamic range also leads to excessive power consumption.

To limit quantization error during the digitization of every sample, it is desirable to have a larger number of bits to encode each sample. Greater number of bits leads to higher accuracy or resolution of the digital representation of the analog signal. This is critical as with mmWave signals the difference between the signal period and the timing mismatches in the circuit become indistinguishable, causing errors.

The above issues can be addressed by alternative receiver architectures where either several high resolution but lower speed ADCs operate in parallel or by instead opting for high speed but low resolution ADCs. Either way, undesired artifacts again manifest. While power consumption is better manageable with the first approach, errors arise due to the mismatched ADCs (staggered phase from a single clock) operating in parallel. The input signal which is split and multiplexed to each ADC introduces noise into the receiver chain. Adopting the latter approach especially allows to reduce hardware cost and also power consumption, but will require considerably more complex signal processing algorithms to address elevated non-linear distortions.

Advances in ADC technology will permit the avoidance of interleaving architectures and not require to deal with interleaving spurs. Factory trimmed algorithms and on-chip calibration ensure that each ADC operates without being exposed to mismatch variances.

Focus upon the use of technology disruptors through digital processors has allowed for the advent of high-speed RF DACs. Elimination of gain-phase errors and local oscillator leakage allows for the realization of superior error vector magnitude (EVM) performance with higher order modulation (HOM).

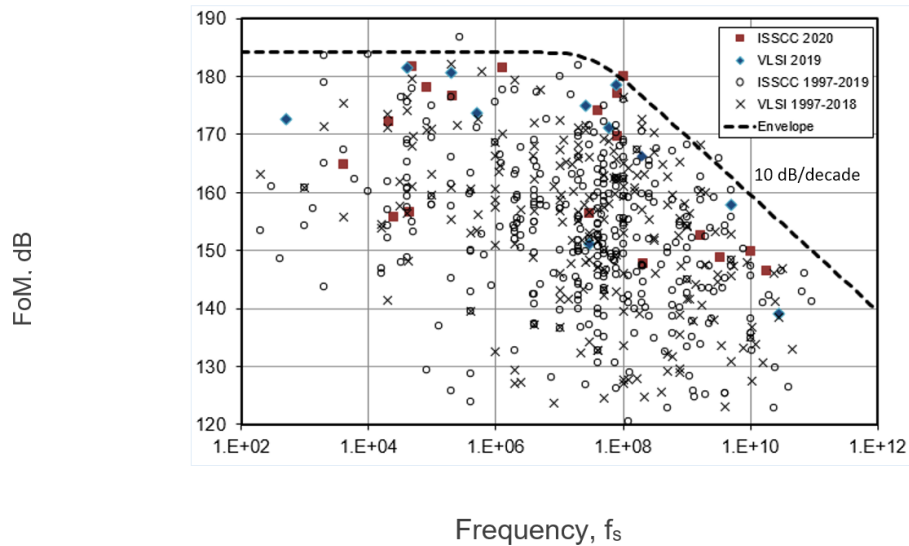


Fig. 7.7: ADC technology supported figures of merit based upon Schreier's formula. [35]

The figure of merit (FoM) values based upon a widely used formula for analyzing performance of ADC technologies are illustrated in Fig. 7.7. The results' envelope indicates to a constant FoM value up to approximately 100 MHz of sampling frequency, f_s (Bandwidth \times 2). Within this range, signal to noise and distortion ratio can be maintained (hold FoM constant) with frequency increase, but at the expense of power consumption. Doubling the frequency leads to twice the power consumption. Beyond 100 MHz, the envelop roll-off is at 10 dB/decade. For every doubling of frequency beyond 100 MHz, power consumption increases four times. Obviously this is more problematic with mmWave bands.

7.3.2 Impairments Due to Phase Noise

A transceiver's analog oscillator used to drive mixers for the critical purposes of up and down conversions, are sources of another impairment identified as Phase Noise. The spectrum of an oscillator would ideally have an impulse at the oscillating frequency only. However, random variations are found to be present around the oscillating frequency, which are attributed to phase noise. These variations are greater at higher carrier frequency mmWave bands, leading to the increased presence of phase noise.

The impact of phase noise is diminished through the selection of a numerology that specifies a larger sub-carrier spacing (SCS), when designing systems operating in the mmWave band. Larger SCS reduces the impact from frequency errors and phase noise. Consequently however, the increased overhead from the cyclic prefix length can be addressed through the selection of a smaller duration value instead (0.6 – 1.19 μ s). This is possible due to the expected smaller cell sizes and considerably greater use of beamforming in the mmWave bands, which reduces the delay spread profile.

Using Phase Lock Loop (PLL) to generate the local oscillator output entails locking the phase of the Voltage Controlled Oscillator (VCO) to a very stable low frequency reference crystal oscillator. In this way, the PLL can achieve the frequency and phase accuracy of the reference oscillator while retaining the VCO's flexibility around tuning. The PLL stabilizes the frequency output, which in turn, reduces the phase noise.

Though the PLL is designed for phase and frequency stability, its capability is limited by the quality of the reference oscillator and other circuit components. Hence, phase noise persists as an intrinsic problem

associated with a variety of challenges and choice of semiconductor technology, due to tradeoffs made around the overall transceiver performance and cost. It typically is present over much of the bandwidth of the sub-carrier spacing, causing sub-carrier constellation blurring. The noise level varies with time but remains relatively fixed for a given frequency. Due to this property, the PTRS (Phase Tracking Reference Signal) signal used in mmWave frequency NR operations for phase noise estimation and compensation is designed to be present more in time domain compared to the frequency domain.

Another source of impairment associated with frequency error however causes constellation rotation on all demodulated sub-carriers. The oscillating frequency generates a signal at a smaller offset from the intended frequency instead. The related phase variation is not random, but continuously increases or decreases. As the frequency offset increases, so does the rate of rotation. This error can be corrected using multiple DMRS (Demodulation Reference Signal) signals as they are pilots within the same symbol, or through a combination of PTRS and DMRS signals, for lower overhead instead.

Typically, for a ten-fold increase in oscillation frequency, a 20 dB degradation occurs in phase noise level, for a specific offset frequency. This limits the highest order modulation scheme. To maintain a phase noise level at a certain offset while increasing the oscillator frequency by a factor of N requires the power to be increased by N^2 . [17]

7.3.3 Power Amplifier Impairments

To meet the required performance criteria associated with new standards, PA design for mmWave systems requires special design techniques with process technology, during implementation. The presence of significantly larger circuit parasitics and the challenges with achieving a high Q value

in passive elements degrade the performance of PA networks, and can ultimately limit the capability of the mmWave transmitter. PA power output is critical as signal level at the receiver depends on the transmitter end PA power gain. However, at mmWave frequencies, the transistor power gain falls due to parasitics. A power combining architecture is one method adopted to increase the RF output power. Moreover, beamforming architectures deploying a large antenna array will lower the power handling burden per PA. Other transmitted signal impairments are caused by the PA's non-linear responses. PA non-linearity creates both in and out of band intermodulation products. Power back-off mechanisms are used to force a PA to operate within its linear region, but in doing so, its power efficiency is lowered. Digital pre-distortion schemes then become a necessity. Also, the PA power efficiency at mmWave frequencies is much lower due to intrinsic loss mechanisms [4]. The Doherty PA [36] improves efficiency, and is effective with signals that have a high PAPR, such as OFDM. However, when implemented on Si substrates for mmWave design, they suffer from transmission line losses. Hence for this band of operation, further improvements are brought about to the Doherty PA utilizing transformer based and active phase shifting designs. GaN, GaN HEMT or GaAsPHEMT semiconductor technologies are chosen for high efficiency and linearity.

7.4 Handset Challenges

Implementing 5G mmWave in handset form factors presents difficult but solvable challenges. Many of these challenges are caused by the propagation nature of mmWave frequencies while others are due to the form factor constraint. The key design challenges include link budget, uniform handset performance, power consumption, mmWave RF design, thermal stability and regulatory compliance. In the following paragraphs,

we present more in-depth discussions into the first three challenges listed above. For the interested reader, more information on many of key challenges can be found in [37].

7.4.1 Link Budget

One of the key challenges with implementing mmWave in handsets is to guarantee a reliable link budget in the uplink direction. This is achieved by ensuring the mmWave smartphone radiates adequate Equivalent Isotropic Radiated Power (EIRP) in order to close the link between the mobile user and the gNodeB. To achieve this required EIRP, the array and beamforming gains from a large antenna array need to be exploited. As shown in Fig. 7.8, the EIRP is impacted by the power and gains from the Power Amplifier (PA) output and antenna array. Therefore, the optimization of the PA output is required taking into accounting the cost, available process technology, device size and PA efficiency. Next, the single antenna element gain needs to be optimized with considerations for the module's x/y/z orientations, multiband support and cost of antenna substrate. Finally, an optimization is required for the shape and number of antennas in the array, factoring in the device size, cost and power consumption.

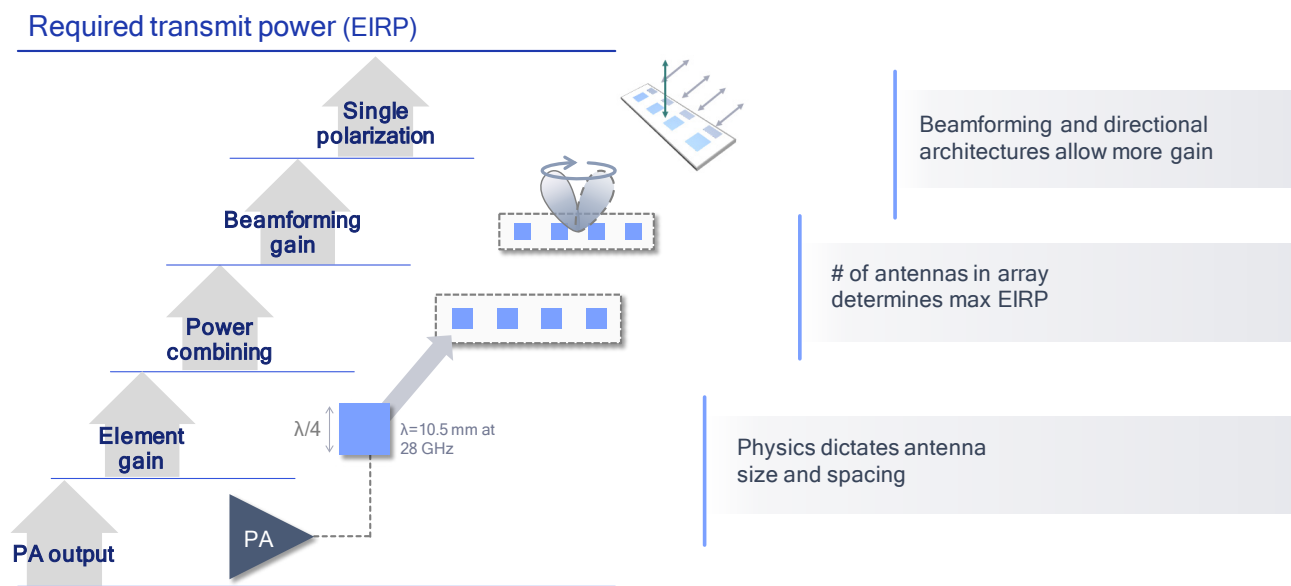


Fig. 7.8: Achieving required UL mmWave EIRP.

7.4.2 Uniform Handset Performance Independent of Device Orientation

For robust performance of mmWave smartphones, it is important to ensure that the performance is independent of the mobile device's orientation. Therefore, ensuring a uniform spherical mmWave coverage around the mobile device is critical. In general, when comparing the spherical mmWave coverage of a sub 6 GHz device to that of a mmWave device, mmWave's coverage is more limited, especially, when beam directivity is used. This is best illustrated by results obtained from a study on mmWave handset spherical coverage [11], [37]. Some of these results are presented in Fig. 7.9. For the non-blocking scenario considered in Fig. 7.9 (figure on the upper left), a mmWave mobile device with a single antenna array module on top of the phone achieved only 36% mmWave spherical coverage. This coverage further reduces to 18% when hand blocking is introduced as shown in the upper right figure in Fig. 7.9. The study reported that the coverage for blocking and non-blocking scenarios is significantly improved to almost spherical coverage by using multiple

strategically placed antenna array modules coupled with smart algorithms to select the best unblocked antenna array. This improvement is shown in the lower two figures of Fig. 7.9. By using three antenna modules mounted on top and on either side of the smartphone, the spherical mmWave coverage improved from 38% to 78% in the non-blocking scenario (lower left figure) and for the blocking scenario, the coverage improved from 18% to 60% (lower right figure). It is reported that these results drove the design for commercially deployed Qualcomm 5G NR mmWave antenna module products [37].

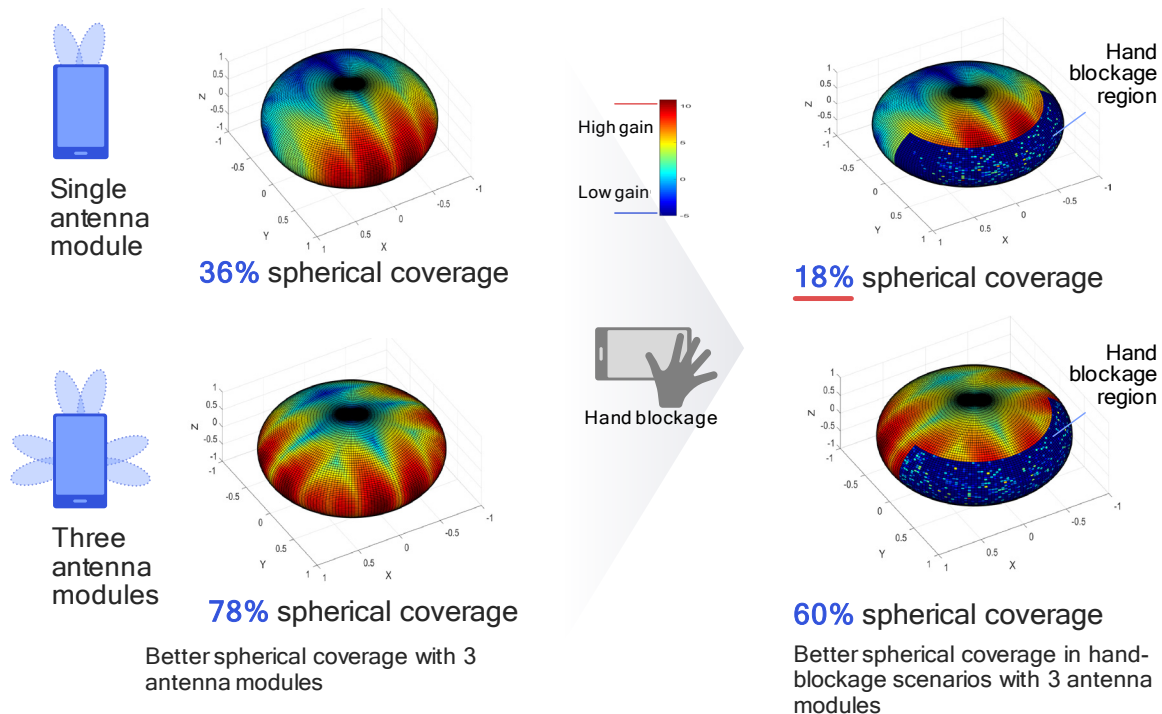


Fig. 7.9: Spherical mmWave coverage in handsets with and without hand blocking.

7.4.3 Power Consumption

Multi-Gbps throughputs on mmWave smartphones require the use of wide bandwidth and large number of antennas, therefore, the power consumption on these devices may be high, especially for applications that require the device to be active for long durations. To address this issue, power saving techniques are required for mmWave handsets. Some commercially deployed mmWave handsets are reported to have already implemented some of the power saving techniques standardized in 3GPP 5G NR Specifications [38]. One of such techniques is the connected-mode discontinuous reception (C-DRX), a procedure that turns off the mobile receiver circuitry periodically when the mobile user is in connected mode with the gNodeB to reduce battery drain. As shown in Fig. 7.10(upper figure), a mobile device in connected mode spends a significant amount of time monitoring control signaling from the network even when no data is transmitted to the device. With C-DRX, the mobile device has more opportunities for sleep as shown in Fig. 7.10(lower figure). This is because in every C-DRX cycle, the device is only expected to monitor control signaling for short durations known as the C-DRX ON duration. While monitoring the control channel in the C-DRX ON duration, if data and/or control signaling is received from the network, the mobile device is expected to keep monitoring the downlink for a duration governed by the inactivity timer. If this timer expires and no data or control signaling is received, the device can enter a sleep state for the rest of the C-DRX cycle.

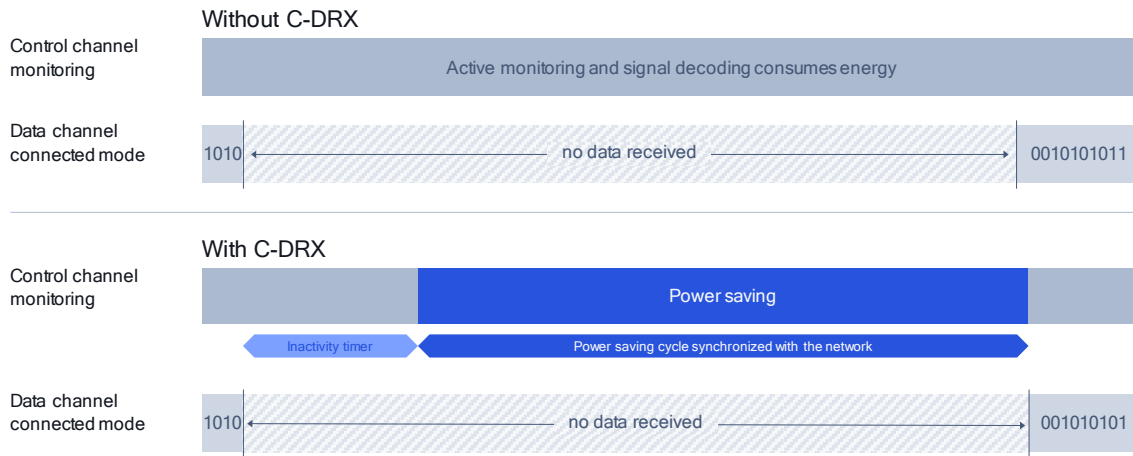
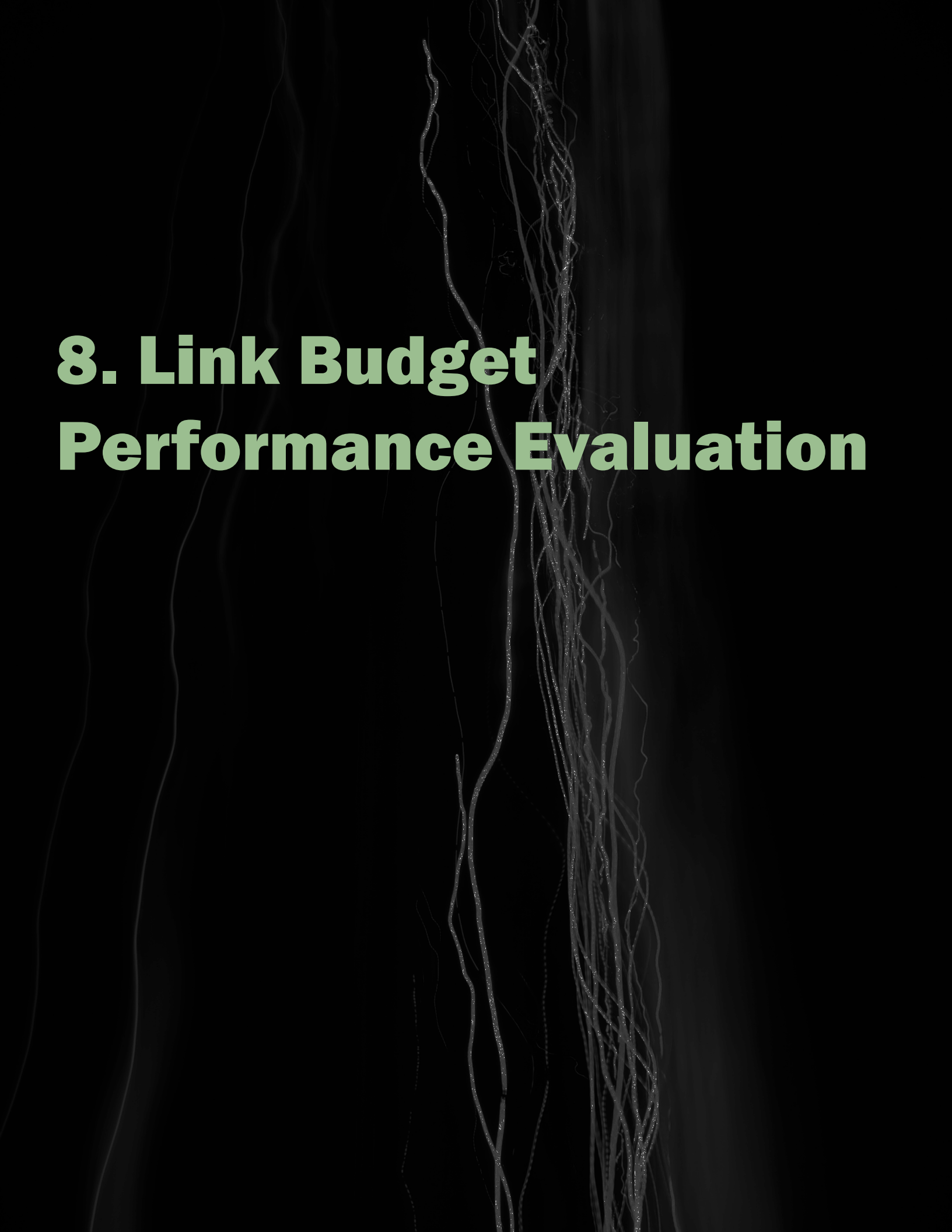


Fig. 7.10: Control and data channel monitoring and decoding with and without C-DRX.

In conclusion, there are some challenges encountered in implementing mmWave mobile handset but many of these challenges are solvable. To address these challenges, the mmWave mobile handset industry stakeholders are developing innovative solutions to ensure the multi-Gbps throughput promise of mmWave is delivered to the end user.



8. Link Budget Performance Evaluation

8 Link Budget and Performance Evaluation

To provide insights into the expected user experience in mmWave networks, we present a detailed coverage prediction and system performance analysis for various 5G NR mmWave network deployments in outdoor and indoor environments. This analysis also characterized the impact of leveraging existing infrastructure by co-siting mmWave gNBs with LTE sites in outdoor environment and Wi-Fi Access Points in indoor environment.

Also, in this section, we present some of the challenges that can be encountered during FR2 deployments, especially in scenarios requiring outdoor-to-indoor coverage. We present an analysis showing that in those scenarios, a layered FR1-FR2 deployment using CA approach is more effective than a layered FR1-FR2 approach with DC.

8.1 Outdoor Deployments

8.1.1 Link Budget

To commence this analysis, we present an example of a high-level 5G NR mmWave UE link budget for 28 GHz downlink and uplink outdoor coverage. This link budget is designed for a target downlink cell edge spectral efficiency of 0.4 bps/Hz and target uplink cell edge spectral efficiency of 0.1 bps/Hz, using a 100 MHz component carrier [39]. The analysis is scalable up to 800 MHz.

Table 8.1. a 5G NR mmWave outdoor downlink link budget.

Effective Transmit Antenna Gain	26.1 dBi
Total EIRP/ 100 MHz	60.2 dBm
Receiver Sensitivity	-82.6 dBm
Total Additional Gains & Losses	11.2 dB
Maximum Allowable Pathloss (MAPL)	131.6 dB

Table 8.2. a 5G NR mmWave outdoor uplink link budget.

Effective Transmit Antenna Gain	6.0 dBi
Total EIRP / 100 MHz	21.0 dBm
Receiver Sensitivity	-99.2 dBm
Total Additional Gains & Losses	-5.3 dB
Maximum Allowable Pathloss (MAPL)	125.5 dB

In the outdoor downlink link budget shown in Table 8.1, a downlink transmit antenna gain of 26.1 dBi and EIRP of 60.2 dBm were used. On the uplink, as shown in Table 8.2, the transmit antenna gain and EIRP used were 6.0 dBi and 21.0 dBm, respectively. These are typical values for gNodeB and user transmit antenna gains and EIRPs in mmWave outdoor networks. This link budget also accounts for additional gains and losses, such as receiver effective antenna gains and losses discussed in Chapter 4.1 such as hand loss, body loss, lognormal shadowing and rain attenuation. In addition, the receiver noise figures for the gNodeB and UE models defined in 3GPP TR 38.901 [14] were used in deriving this outdoor link budget.

8.1.2 Coverage Prediction

8.1.2.1 Significant 5G NR mmWave outdoor coverage with existing LTE sites

Once the 5G NR mmWave link budget was established and maximum allowable pathloss (MAPL) determined for the simulation studies, a commercial LTE network planning tool was used for the simulation studies to predict 5G NR mmWave coverage. The studies were performed on a modified version of the LTE network planning module, in line with 5G NR mmWave requirements based on the network planning tool vendor's guidelines.

To ensure accurate signal propagation estimation for each outdoor location in this study, high-resolution geographical data of the global cities with 2m x 2m resolution was utilized, including 3D building databases. Furthermore, since foliage can potentially create impediments to the propagation of mmWave signals, the 3D geographical data utilized for the simulations also included accurate and up-to-date information about foliage type, depth, height, and other relevant details. This information was then used in the network planning tool to estimate foliage attenuation based upon relevant details, including attenuation-per-meter assumptions.

For the simulation studies for each location, a one-to-one 5G NR mmWave co-siting deployment on existing 4G LTE macro and small cell sites was assumed.

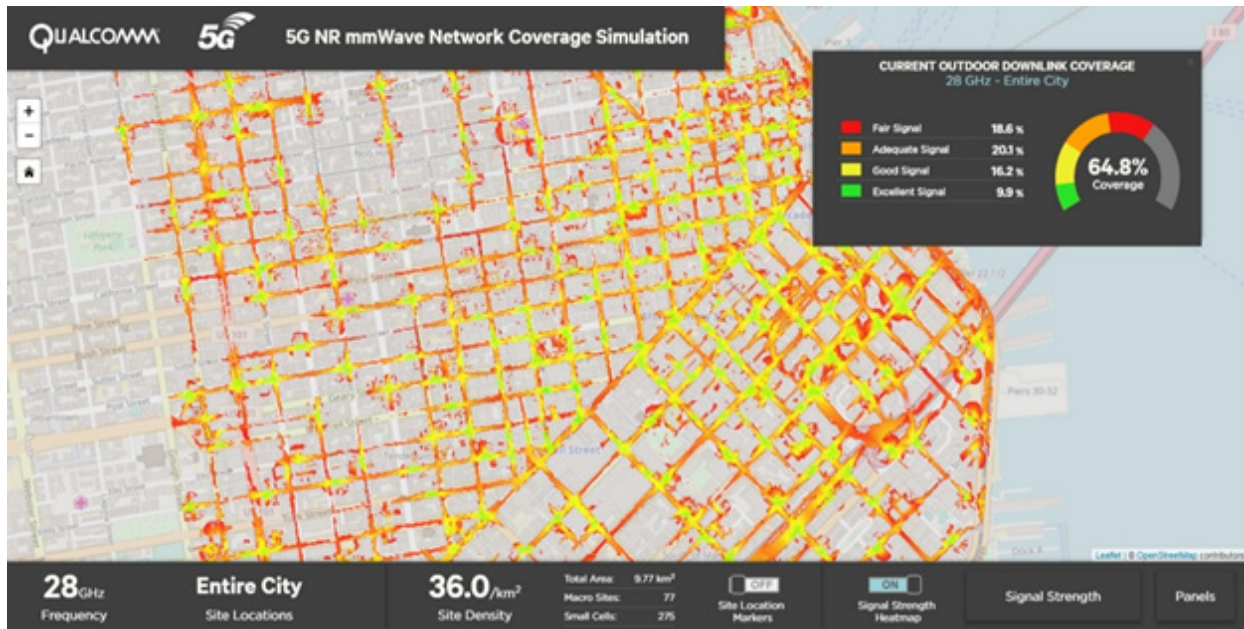
Considering the utilization of well-established network planning techniques, high-resolution geographic terrain, building and foliage data, actual LTE site databases, and the use of 3GPP propagation models defined for dense urban and urban morphologies, there is high confidence that the results are very close to the actual 5G NR mmWave network coverage. Actual measurements were also performed in some of the locations to fine tune the prediction parameters and improve the coverage prediction accuracy. Of course, additional variations in coverage are possible due to temporary blockages, and extensive over-the-air 5G NR mmWave field measurements are to follow.

Fig. 8.1. Coverage prediction methodology.



Using the coverage prediction methodology illustrated in Fig. 8.1, the network coverage simulation studies were conducted for a number of cities, including San Francisco. Fig. 8.2 shows a signal strength heatmap for San Francisco based on these 5G NR mmWave coverage simulation results.

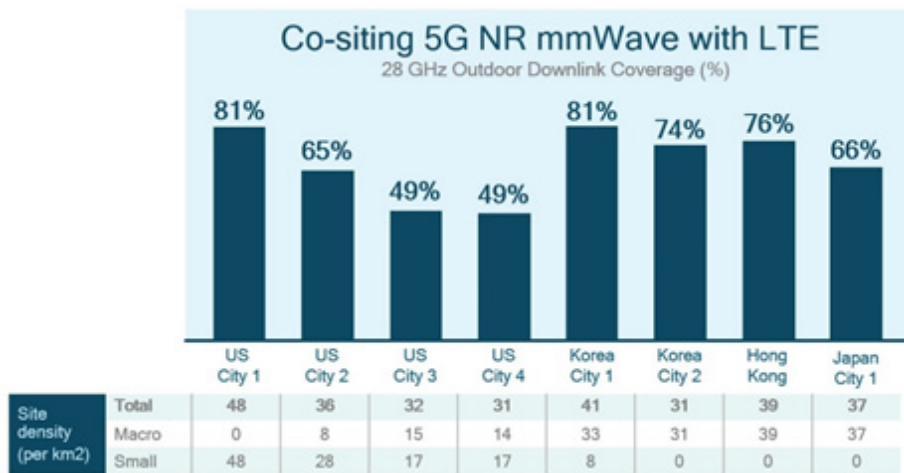
Fig. 8.2: San Francisco 5G NR mmWave coverage heatmap.



The total coverage area for the modeled San Francisco location is 9.77 km², and by co-siting with 77 LTE macro sites and 275 LTE small cells, 65% downlink mmWave coverage was achieved.

Similar studies were carried out across various global cities in dense urban areas with high mobile traffic and approximately ten square kilometers each in area (barring some city-specific variations). The results from these simulation studies for 28 GHz outdoor downlink coverage is summarized in Fig. 8.3. (Note that “US City 2” is San Francisco.)

Fig. 8.3. Qualcomm Research 5G NR mmWave network coverage simulation.



The results show that significant outdoor coverage is possible when co-siting 5G NR mmWave with existing 4G LTE macro and small cell sites. The positive results show that mobile deployments with seamless outdoor coverage in urban areas is certainly feasible with high site density, especially when considering the tight interworking of 5G NR with 4G LTE. The results also show that macrocell density may not be sufficient for decent outdoor coverage, and that use of outdoor small cells is typically needed.

In addition to the impact of high site density, the simulation studies revealed some key aspects of 5G NR mmWave which helped contribute to the positive outdoor coverage results. One key contributing factor to the positive 5G NR mmWave outdoor coverage results is that legacy LTE sites were designed to provide coverage for users requiring out-to-in coverage allowing 5G NR mmWave resources to be focused on providing coverage to outdoor users. Other contributing factors include a higher EIRP for 5G NR mmWave versus 4G LTE small cells (while ensuring compliance with regulatory limits), as well as the use of massive MIMO antenna arrays (256x2 3D antenna array used for simulations) to create highly directional beams that focus transmitted RF energy to overcome the propagation and pathloss challenges in both the uplink and downlink.

Although 5G NR mmWave outdoor-to-indoor coverage is challenging, however, the outdoor mmWave coverage may free up resources in the spectrum bands below 6 GHz or sub-6 GHz for outdoor-to-indoor or outdoor capacity in areas not covered by 5G NR mmWave. More discussion on FR2 deployments in scenarios requiring outdoor-to-indoor coverage follows in Section 8.3.

8.1.2.2 Achieving 95% 5G NR mmWave outdoor coverage with additional sites

In addition to the 5G NR mmWave network coverage simulation studies based on existing LTE sites in global cities, simulation studies were performed to assess the feasibility of achieving greater than 95% coverage, as well as compare 5G NR mmWave outdoor downlink coverage for 28 GHz versus 39 GHz (39 GHz outdoor MAPL ~1.5 dB weaker than 28 GHz). The results of this are summarized in Fig. 8.4. The study utilized a baseline configuration of 73 sites per square kilometer based on a 0.8 km² dense urban area in San Francisco.

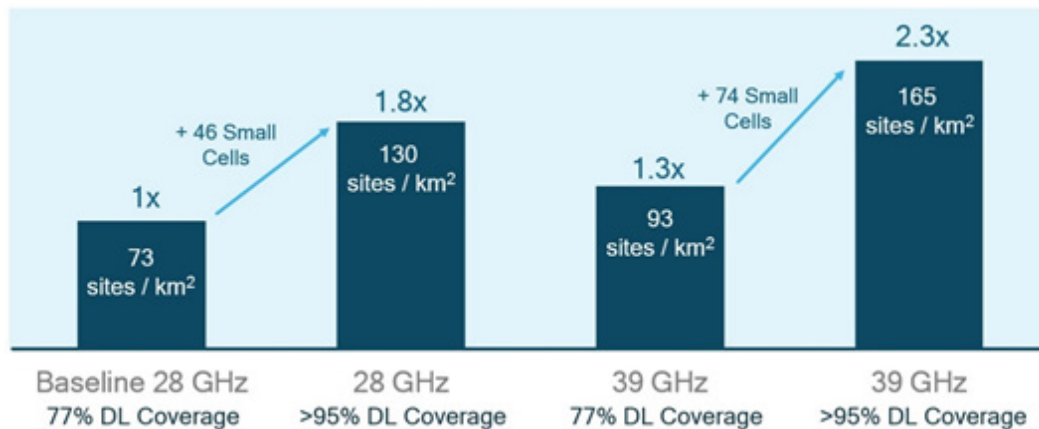


Fig. 8.4. Additional 5G NR mmWave coverage simulation studies.

The results show it is feasible to achieve 95% outdoor downlink coverage for 28 GHz by adding an additional 46 small cells (or increasing the site density by ~75%). Alternatively, the gap in coverage to reach 95% can be covered by utilizing sub-6 GHz bands (either LTE or 5G NR). The results also show that 39 GHz requires ~25% increase in site density to achieve the same outdoor coverage as 28 GHz [40].

8.1.3 User Experience

8.1.3.1 Cell Edge Data Rate based on target spectral efficiency

To estimate the user experience expected in outdoor mmWave deployments, we start by estimating the cell edge data rates using target spectral efficiency of 0.4 bps/Hz for the downlink and 0.1 bps/Hz for the uplink for the San Francisco location. The cell edge data rate for the fair signal is 40 Mbps for 100 MHz bandwidth and 100% TDD DL configuration and 320 Mbps for 800 MHz. For the uplink, 10 Mbps for 100 MHz bandwidth and 100% TDD UL configuration and 80 Mbps for 800 MHz. Meanwhile, the cell edge data rate for an excellent signal based on the same assumptions is 500 Mbps for 100 MHz bandwidth and 4 Gbps for 800 MHz. The downlink and uplink edge data rate for 100 MHz, 400 MHz and 800 MHz bandwidths are shown in Fig. 8.5. and Fig. 8.6 below.

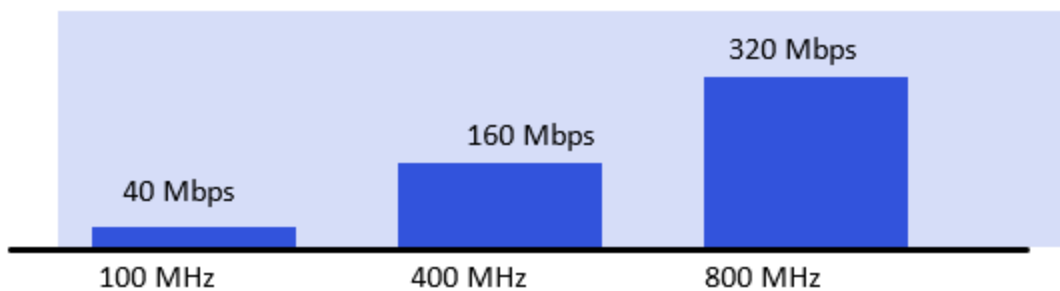


Fig. 8.5 Cell edge data rate based on target 0.4bps/Hz downlink spectral efficiency.

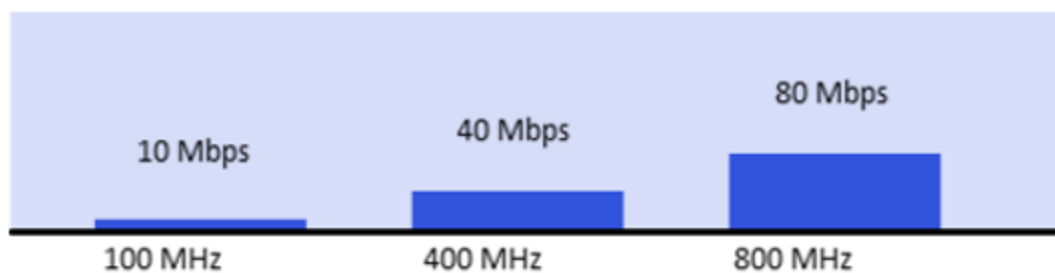


Fig. 8.6. Cell edge data rate based on target 0.1bps/Hz uplink spectral efficiency.

8.1.3.2 User Perceived Throughput

While the data rate based on target spectral efficiency provides an estimate of the expected data rate for a cell edge user, an analysis incorporating the multi-user impact is desirable to gain deeper insights into the user performance in a typical mmWave network. To this end, we modeled a Non-Standalone (NSA) 5G NR network in San Francisco, California, operating in 800 MHz of 28 GHz mmWave spectrum, with an underlying Gigabit LTE network operating across four licensed LTE spectrum bands plus License Assisted Access (LAA) bands. In this network capacity simulation, existing site locations were used where 5G NR cell sites were co-located with 13 existing macro and small cell LTE sites.

Inputs into this mmWave network simulator includes the network layout, randomly selected LTE and 5G NR mmWave user locations within the San Francisco deployment area and the predicted pathloss from the coverage studies. Around 14,000 user devices, of various capabilities, were randomly distributed across

the network with approximately 50 percent of the users indoor and 50 percent of the users outdoor. Each user in the network is associated with a given gNodeB based on considering factors such as pathloss and beamforming transmit and receive gains. The network simulator also modelled small fading using models defined in 3GPP TR 38.901. The user perceived throughput in a multi-user network is predicted considering factors such as the scheduler settings, gNodeB and UE transmit and receive antenna configurations, TDD configurations as well as traffic patterns based on user applications.

A mmWave network simulator illustration is presented in Fig. 8.7 and the key mmWave simulation parameters are summarized in Table 8.3.

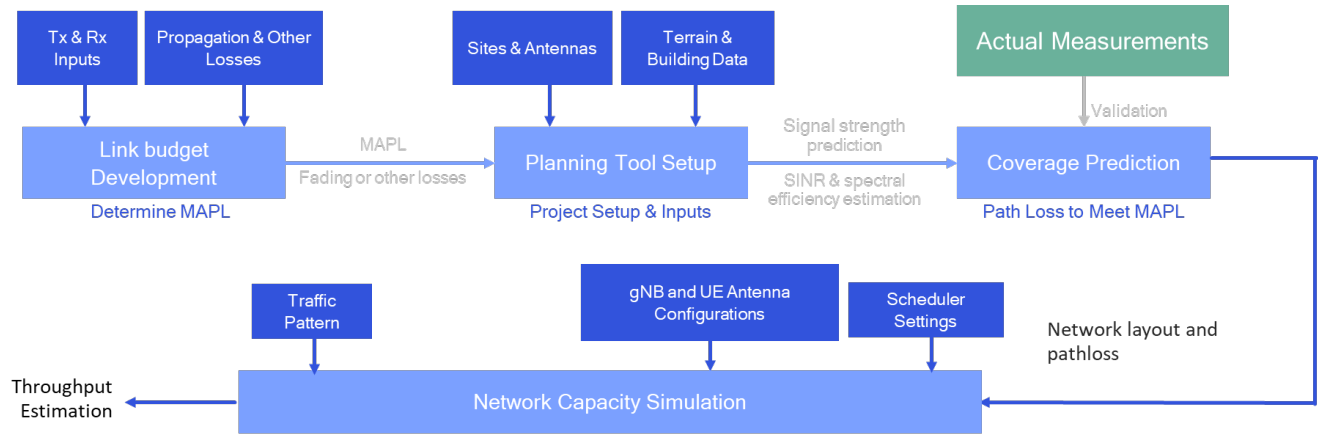


Fig. 8.7. 5G NR mmWave network capacity simulation methodology.

Table 8.3. Key mmWave parameters for San Francisco network simulations.

Parameters	DL	UL
Antenna Configuration	256 Antennas per polarization	4 Antennas per polarization
EIRP	63 dBm	21 dBm
Carrier Frequency	28 GHz	
Bandwidth	800 MHz	
TDD Configuration	100% DL	100% UL
Traffic Pattern	<ul style="list-style-type: none"> • FTP File download/upload (30 % of the simulated users) • Video Streaming/Video Broadcast with frame rate up to 120 Frames/sec (20% of the simulated users) • Web Browsing/Posting (50% of the simulated users) 	

The San Francisco network analysis provided the first glimpse of the impact of the significantly increased capacity afforded by 800 MHz of additional mmWave spectrum on real-world user experience. Key findings included:

- Browsing download speeds increasing from 71 Mbps for the median 4G user to 1.4 Gbps for the median 5G user in mmWave coverage, a gain of approximately 2000 percent
- Approximately 23x faster responsiveness, with median browsing download latency reduced from

115ms to 4.9ms

- File download speeds of more than 186 Mbps for 90 percent of 5G users, compared to 10 Mbps for LTE, a 1,826 percent gain. The median 5G file download speed was 442 Mbps.
- Median streaming video quality increasing from 2K/30 FPS/8-bit color for LTE users to 8K/120 FPS/10-bit color and beyond for 5G users.

The results from the 5G Network Capacity Simulation lend credence to the promise of 5G, with expected real-world performance that is substantially better than what is currently possible with 4G across multiple metrics. The findings also illustrate that these emerging 5G networks will have the capacity and performance to support a whole host of new services and experiences beyond the traditional categories of browsing, downloading, and streaming.

8.2 Indoor Deployments

For indoor venues (e.g., convention centers, event halls, concert, indoor stadiums, etc) and/or enterprise deployments (e.g., office buildings, shop floors, meeting rooms, auditoriums, etc.), 5G NR mmWave can complement existing Wi-Fi deployments with new and enhanced experiences through dense spatial reuse enabled by gNodeB and UE beamforming and vast amounts of spectrum availability:

- Bringing multi Gigabit, low latency and virtually unlimited capacity
- Supporting devices beyond smartphone: tablets, always-connected laptops, XR
- Leveraging existing infrastructure: Wi-Fi or cellular by co-siting small cells so that both power supply and wired backhaul connectivity are already available at these locations, and it is the most efficient way to start any 5G NR mmWave deployments.

In this subsection, we provide examples of coverage prediction and system performance analysis for an indoor enterprise deployment scenario.

8.2.1 Link Budget

In comparison to the outdoor deployment scenario, typical mmWave coverage challenges are not of major concern for indoors because of the following reasons:

- No out-to-in building penetration losses
- Rain and foliage attenuation not a factor
- Signal decay likely not significant for short ranges

Therefore, the link budget utilized for the outdoor coverage simulations was adjusted based on indoor-specific EIRP limits and deployment specific considerations (e.g. 128 or 64 gNodeB antenna configuration are typical indoor environment instead of 256 antennas in gNodeB). In addition, pathloss and indoor wall loss was adjusted inside the network planning tool (Indoor Ray Tracing model) resulting in a MAPL of approximately, 115 dB for indoor downlink coverage and 117 dB for indoor uplink coverage. The details of the link budget for this indoor example is summarized in Table 8.4 and Table 8.5.

Table 8.4. a 5G NR mmWave indoor downlink link budget.

Total EIRP/100 MHz	52	dBm
Receiver Sensitivity	-82.6	dBm
Total Additional Gains and Losses	11.2	dBm
Additional Crowd Loss	8	dB
Maximum Allowable Pathloss (MAPL)	115.4	dB

Table 8.5. a 5G NR mmWave indoor uplink link budget.

Total EIRP/100 MHz	52	dBm
Receiver Sensitivity	-82.6	dBm
Total Additional Gains and Losses	11.2	dBm
Additional Crowd Loss	8	dB
Maximum Allowable Pathloss (MAPL)	115.4	dB

Comparing the indoor link budgets in Table 8.4 and Table 8.5 with the outdoor link budgets in Table 8.1 and Table 8.2, a difference in the MAPL is approximately 16 dB on the DL and 8 dB on the UL. The differences are mainly due to the higher EIRP in outdoors compared with indoors and the differences in the losses in both environments. For the indoor environment, a crowd loss was added to incorporate the impact of the body losses, which is significant in large indoor venues like convention centers.

8.2.2 Coverage Prediction

To assess the feasibility of targeted indoor 5G NR mmWave deployments, a network coverage simulation study was conducted on an indoor New Jersey enterprise location following a similar coverage prediction methodology as the outdoor coverage simulations and leveraging existing small cell and/or Wi-Fi deployments for the gNodeB placements. The simulation study included an analysis of this enterprise location (including walls, support pillars and furniture) to simulate indoor coverage. A pathloss heat map of this enterprise location and the mmWave gNodeB locations are shown in Fig. 8.8.

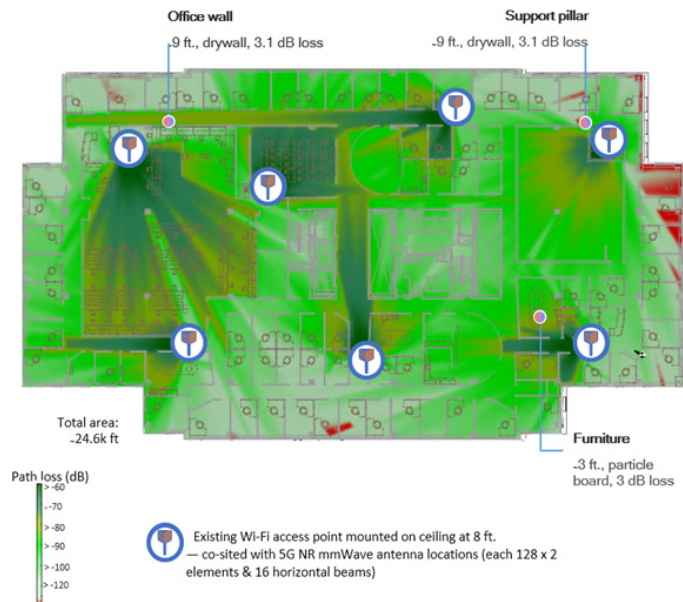


Fig. 8.8. Pathloss heatmap of the New Jersey indoor enterprise location.

By co-siting the mmWave gNodeB with the 7 Wi-Fi Access Points in this enterprise location, we are to achieve a DL coverage of ~98% with 115 dB MAPL and uplink coverage of 99% with 117 dB MAPL. The similar coverage prediction analysis was performed for other indoor venues such as enterprise locations, subway stations, shopping malls and airport concourses [37].

8.2.3 User Experience

8.2.3.1 Cell Edge Data Rate Based on Target Spectral Efficiency

For the New Jersey Enterprise deployment, we consider similar target spectral efficiencies for the downlink and uplink as were considered for the outdoor deployment in subsection 8.1.2.1. The corresponding data rates for a cell edge user with fair signal strength in the downlink and uplink directions are similar to those presented in Fig. 8.5 and Fig. 8.6.

8.2.3.2 User Perceived Throughput

For the New Jersey Enterprise deployment, we used the mmWave network simulation methodology presented in subsection 8.1.2.2 to simulate a Standalone (SA) network with 7 mmWave gNBs and 350 mmWave mobile device. Each user in the network used one of these traffic applications, FTP File download/upload, Video traffic with frame rates of up to 120 Mbps or Web browsing on the DL/Web posting on the UL. The key DL and UL simulation parameters are summarized in Table 8.6.

Table 8.6. Key mmWave parameters for the new jersey enterprise network simulations.

Parameters	DL	UL
gNodeB Antenna Configuration	128 Antennas per polarization	
UE Antenna Configuration	16 Antennas per polarization	
EIRP	52 dBm	21 dBm
Carrier Frequency	28 GHz	
Bandwidth	800 MHz	
TDD Configuration	100% DL	100% UL
Traffic Patterns	<ul style="list-style-type: none"> • File download/upload (30% of the simulated users) • Video Streaming/Broadcast (20% of the simulated users) • Web Browsing/Posting (50% of the simulated users) 	

With the parameters and the traffic applications presented above, the DL and UL 10th, 50th and 90th user perceived throughput estimates for users with video traffic are presented in Fig. 8.9.

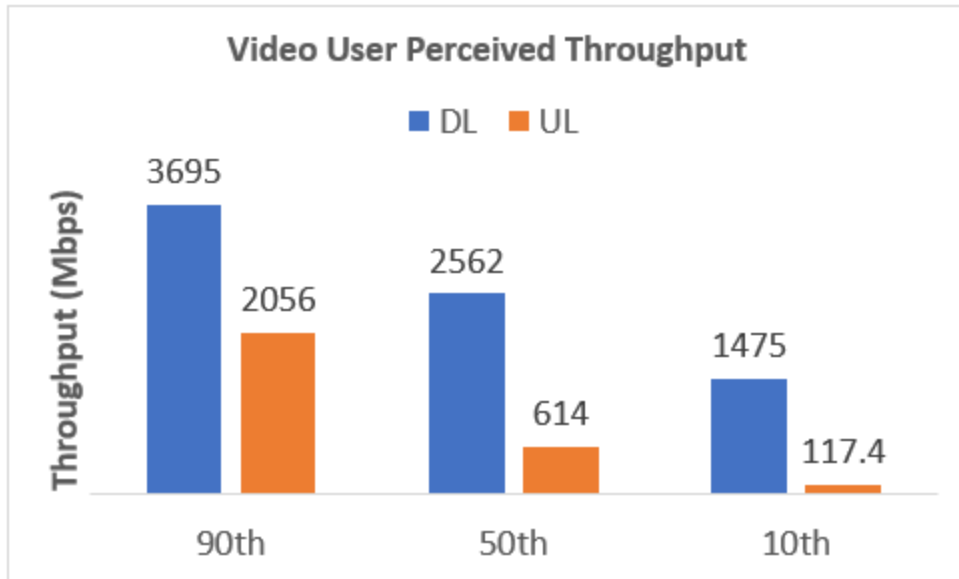


Fig. 8.9. Video streaming user perceived throughput for a new jersey enterprise deployment.

The 90th percentile performance is the typical performance experienced by a cell center user, while the 10th percentile performance depicts the typical user experience of a cell edge user. The results demonstrate that the Gbps promise of 5G NR mmWave network would be experienced by a cell center user with speeds of about 3.7 Gbps and 2.1 Gbps in the DL and UL directions, respectively. Even the typical cell edge user experiences approximately 1.5 Gbps on the DL and over 100 Mbps on the UL.

For FTP application, the user perceived download throughput varies from 594 Mbps to 813 Mbps while the user perceived upload throughput varies from 179 Mbps to 755 Mbps as presented in Fig. 8.10.

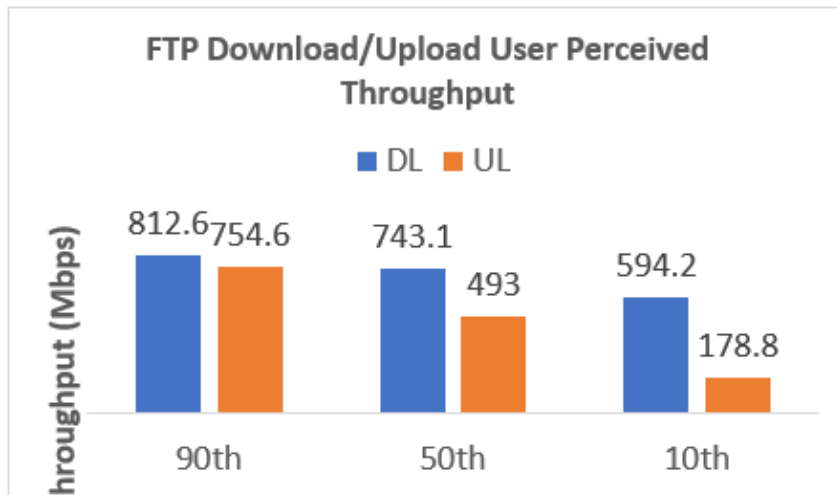


Fig. 8.10. FTP user perceived throughput for a New Jersey enterprise deployment.

For users performing web browsing on the DL or posting content on the UL the 10th, 50th and 90th user perceived throughputs are presented in in Fig. 8.11.

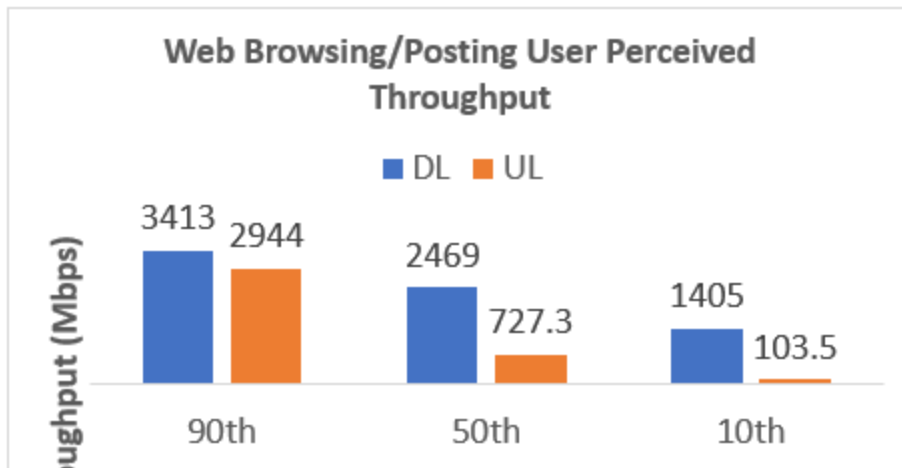


Fig. 8.11. Web browsing/posting user perceived throughput in New Jersey enterprise deployment.

The DL user perceived throughput was as high as 3.4 Gbps for the cell center user and as low as 1.4 Gbps for the cell edge user. On the UL, the cell center users experience data speeds around 2.9 Gbps while the cell edge users experience data speeds around 100 Mbps.

These simulation results demonstrate that 5G NR mmWave enterprise deployments can provide high capacity for unlimited data access fueling laptops, tablets and smartphones.

8.3 Layer Management for Maximum Capacity

In addition to delivering high throughput to users in targeted areas as discussed in Sections 8.1 and 8.2, it is desirable to enable traffic offloading from FR1 and FR2 to maximize network capacity gain. This is indeed the objective of layer management planning. Offloading traffic to FR2 mmWave can be challenging, especially in scenarios with users requiring outdoor-to-indoor coverage.

These challenges are illustrated with a multi-layer simulation using the following scenario:

- FR1 coverage is provided from 4x tri sector macrocells spaced 400 m apart on a hex grid.
- FR2 coverage is from poles on a 200 m hex grid, creating four FR2 nodes per FR1 macro sector node.
- FR1 and FR2 layers are independently modelled, with interfrequency load balancing between them to maximize capacity while meeting minimum throughput objectives.
- The propagation model uses a blended distribution to represent a combined mix of open outdoor, shadowed outdoor, and indoor users, consistent with 80% of the users indoor. Clutter and building losses are random and directional to match statistical models, but do not accurately represent real buildings.
- It is important to note that this system simulation is focused on interband effects from outdoor sites serving mixed outdoor and indoor users, and differs from the assumptions used for high resolution mmWave RF planning-based systems simulations shown in Sections 8.1 and 8.2.

The objective of this simulation is to illustrate and compare capacity of DC and CA approaches to FR1-FR2 load distribution in a somewhat realistic RF environment.

Table 8.7 shows the parameters for the simulation, while Fig. 8.12 shows the basic concept of the model.

Table 8.7: High-Level simulation parameters.

		FR1	FR2
Carrier Frequency	MHz	1900	28000
Carrier Aggregated BW	MHz	60	200
DL Max EIRP/Polarization	dBm	74	60
Antenna Configuration		4TR	512 TR
TDD Configuration		FDD	TDD 3:1
Minimum UL UE throughput	Mbps	2	2
Minimum DL UE throughput	Mbps	50	50
Loading Outage target		5%	5%
Pathloss Model		TR 38.901	TR 38.901
Average building loss	dB	20	40
Average Inter Site Distance	Meters	400	200

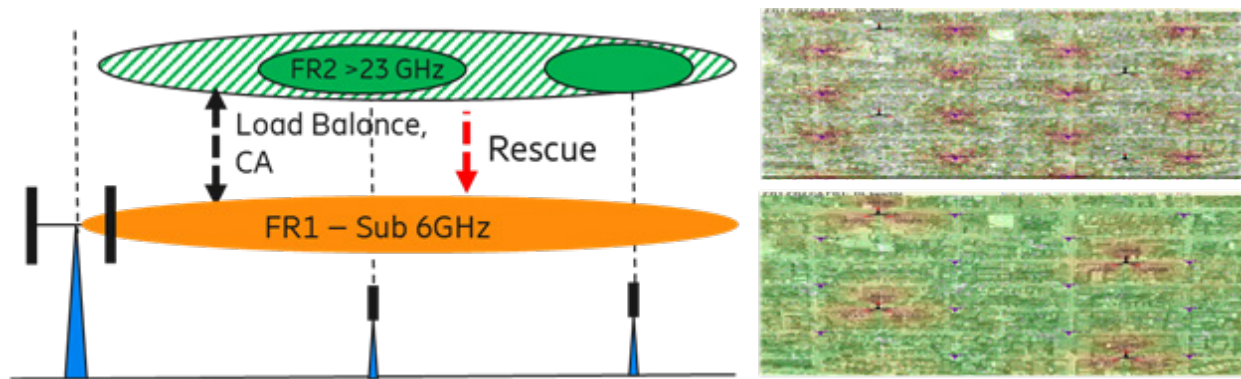


Fig. 8.12. Multi-layer model.

The plots that follow are from the model, loaded to exactly 5% of users falling below target KPIs.

As shown in Fig. 8.13, FR2 plots show many locations without FR2 UL coverage (white) where UEs will depend on FR1 underlay as PCell for service continuity. FR2 DL coverage extends much further than its UL and would be used as an SCell where possible to maximize FR1 offload.

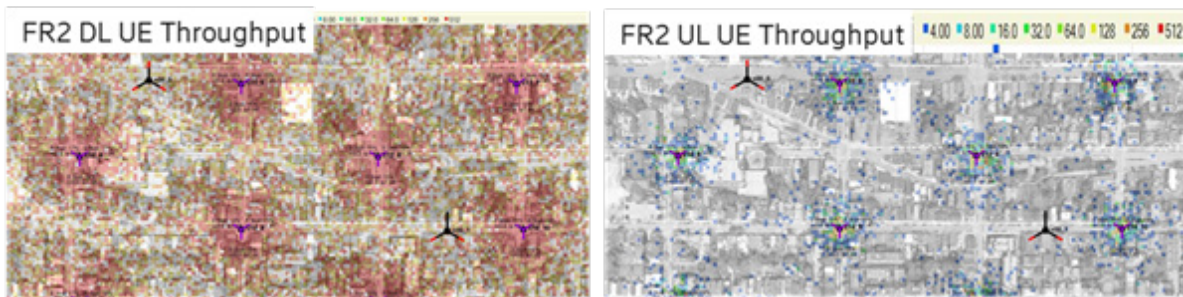


Fig. 8.13: mmWave Downlink (left) and uplink (right) throughput.

In contrast, as shown in Fig. 8.14, FR1 DL and UL coverage is contiguous over the service area and provides service beyond the FR2 range.

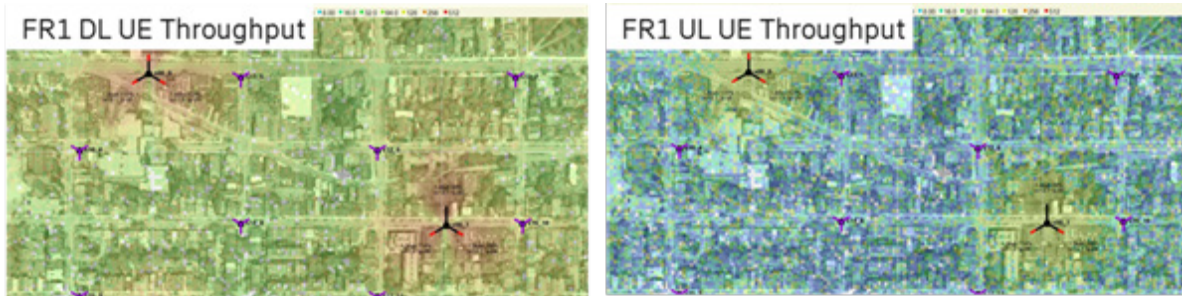


Fig. 8.14. FR1 downlink (left) and uplink (right) throughput.

The load slice diagrams in Fig. 8.15 show how traffic is distributed between FR1 and FR2 relative to the macrocell reach ranked as FR1 pathloss but scaled according to cell area. (e.g. values to the right of 90% represent the 10th percentile of area with highest pathloss).

- **FR1—Only** shows constant DL + UL load per area of 1800 bps/sq m with slight falloff at the extreme cell edge as some UEs with highest pathloss lose coverage, lighter band indicates uplink.
- **FR1+FR2 DC** adds FR2 overlay using dual connectivity. There is useful traffic offload to FR2 where it has UL coverage; however, it does not reach the indoor areas that consume most of FR1 capacity because FR2 is constrained by its uplink. This means that the sustainable network load at the 5% KPI limit is only marginally increased to 2100 bps/sq. m.
- **FR1+FR2 CA** will leverage DL carrier aggregation by using FR1 as PCell with FR2 mmWave as DL SCell. This substantially increases the area over which FR1 -> FR2 DL traffic offload can occur, and gives a good improvement in sustainable network load at the KPI limit to reach 3400 bps/sq. m. Network capacity is still limited by FR1 KPI degradation, often uplink capacity exhaustion due to noise rise.

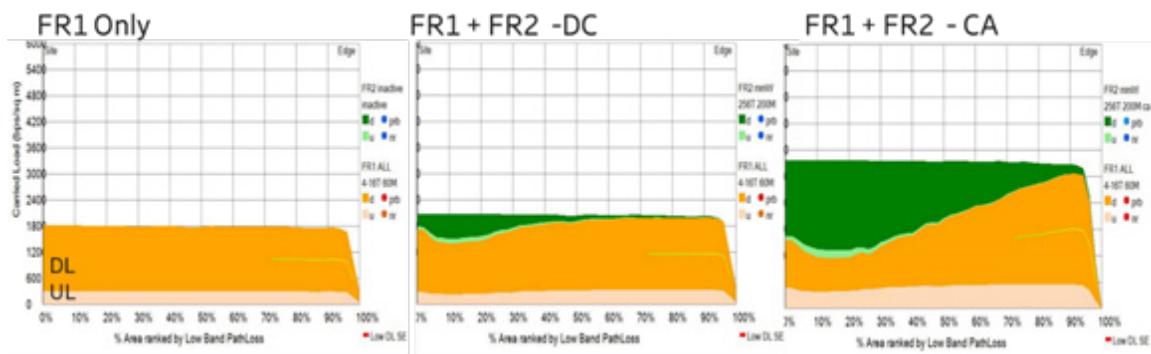


Fig. 8.15. Traffic distribution load slice diagrams.

8.3.1 Traffic Profile and Hotspot Location Sensitivity

The base model applied equal traffic demand per area as observed in most MBB wireless networks, making it harder to leverage the FR2 potential capacity that is concentrated in outdoor areas. The model can be modified to generate higher user activity when FR2 DL and/or UL coverage are available to increase utilization of spare mmWave capacity. As an extreme example, Fig. 8.16 assumes traffic demand is increased by 5x at locations with DL+UL mmWave service for the NR DC case, and at locations with DL mmWave for NR CA case.

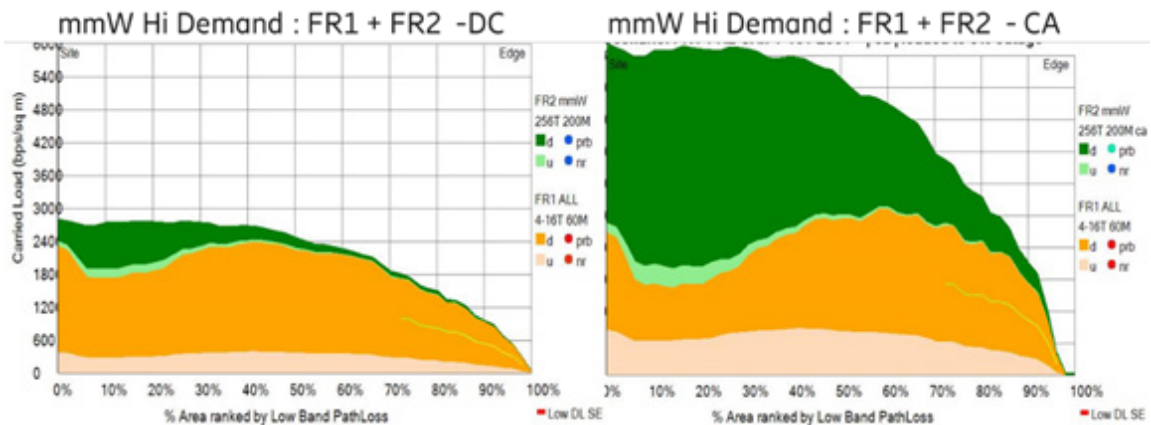


Fig. 8.16: DC vs CA Load Slice Diagrams, assuming 5x traffic demand increase.

Comparing Fig. 8.16 with Fig. 8.15, it can be observed how traffic demand moves to locations with lower pathloss as seen from the macrocell locations, and away from the higher pathloss indoor cell edge served only by FR1. The effect is far greater with CA because the FR2 area over which the traffic increase is applied becomes larger. Achievable capacity density over the inner 50% of FR1 cell area now exceeds 6000 bps/sq. m, which is > 3x the FR1-only baseline.

In some cases, the user behavior may change as connection bandwidth and throughput worsens. In those scenarios, users with FR1+FR2-capable devices may proactively reduce their data consumption when outside of FR2 coverage. Another possibility would be installing FR2-only fixed wireless local loop (FWLL) devices inside the FR2 coverage area.

Another alternative to increase FR2 capacity relief to FR1 is to locate mmWave small cells very close to traffic hotspots that are not close to the FR1 cell center. This works well in a simulation, but the real-world challenges of securing cost-effective site locations with power and high-capacity backhaul exactly where they are most needed, as well as the fact that these hotspots may move over time, will limit the percentage of small cells that capture consistently high offload.

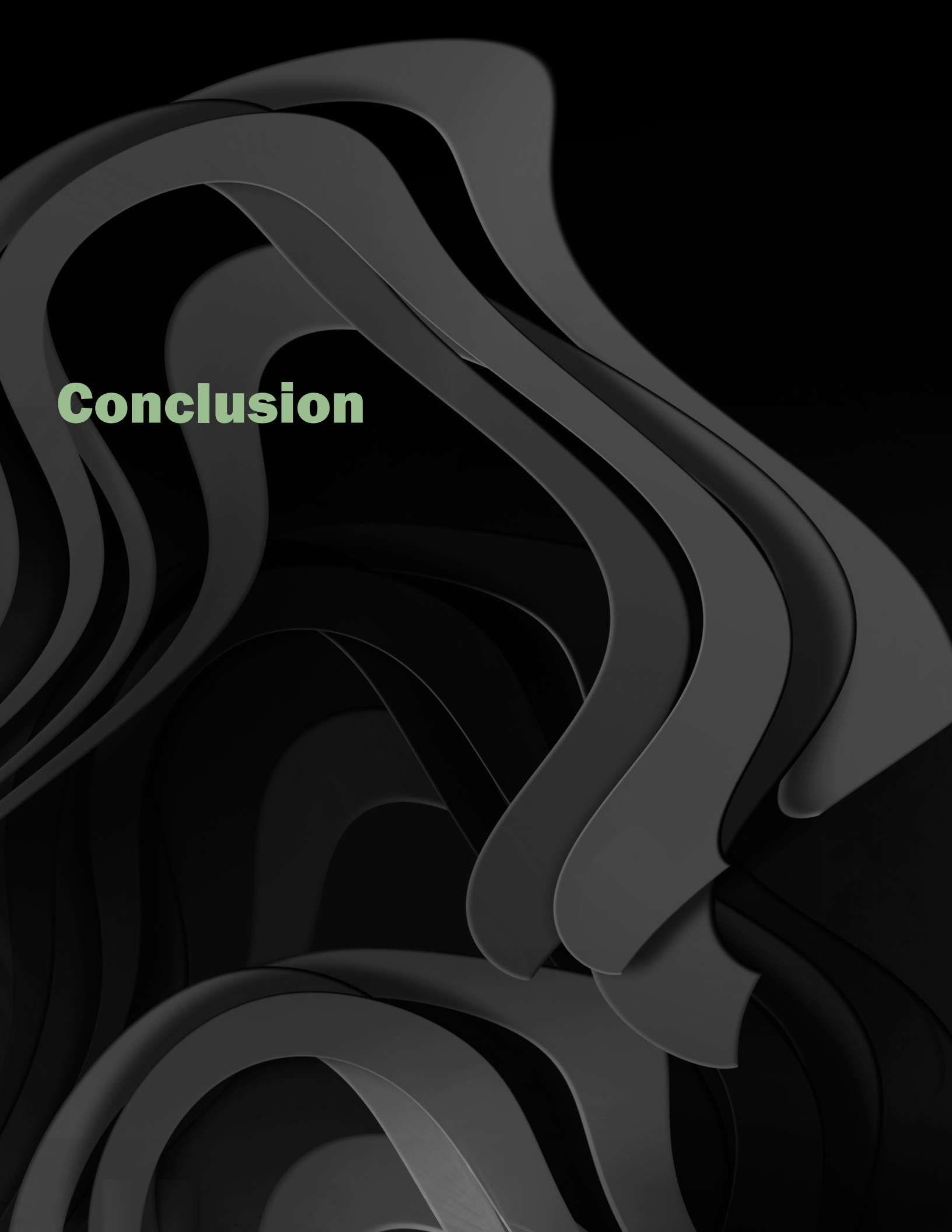
To recap, there are inherent challenges to leverage the overlay capacity of mmWave in scenarios requiring outdoor-to-indoor coverage, especially when the mmWave uplink coverage is limited. It therefore is best to leverage the FR1 uplink to extend the offload area – and carrier aggregation is a more effective mechanism than dual connectivity to do so.

8.4 Evolving Requirements for Future mmWave Technology Developments

The introduction of mmWave frequencies in mobile broadband networks and devices is still in its relative infancy. As of this writing we are only two years into commercialization with 5G NR, and many of the standardized enabling technologies allowing new use cases discussed in Chapter 5 have yet to be or are only just being implemented. The standards also continue to evolve to refine or improve upon processes and methodologies already standardized, as is the case for beam management as discussed in Chapter 6.6.1.1.

The uses discussed for mmWave in this whitepaper are likely just the beginning of being able to make use of this ample spectrum resource. 5G NR will continue to evolve, and “6G” and its use cases are already being conceptualized. As more mmWave and even THz bands are standardized and the ecosystem evolves to support multiple bands working together simultaneously, vast amounts of bandwidth and even lower latency will enable new use cases.

The reader should seek out the 5G Americas whitepaper on Network Evolution for an exciting peek into the future of mobile communications and how mmWave can support a number of exciting new use cases, such as sensing and imaging applications in smart devices, frictionless services, and holographic communications.



Conclusion

Conclusion

As we have seen, millimeter wave on 5G NR has great potential for unlocking new and emerging use cases and serving new customer needs. This is evidenced both by the ongoing standardization efforts within 3GPP and rulemaking by regulatory bodies worldwide to make more of this spectrum available for mobile broadband and other use cases, as discussed in Chapters 2 and 3.

Chapter 4 presents background to understand the propagation characteristics that present challenges in deploying mmWave, including pathloss, blockage, penetration loss, hand and body loss, foliage loss, atmospheric losses and scattering. We present a robust discussion on channel models and how the propagation characteristics are represented in these models. Finally, as there are two sides to every coin, we discussed some of the benefits of mmWave including larger bandwidth, the ability to deploy large beamforming antenna arrays, shorter TTI and the resulting reduced latency, higher densification and channel reciprocity.

Chapter 5 lays out a myriad of use cases where mmWave on 5G NR is a viable solution: serving eMBB applications such as outdoor dense urban capacity hotspots and smart offices, ultra-reliable applications such as factory automation and remote surgery, and fixed wireless applications as home internet replacement. We explore how mmWave can serve as backhaul to mitigate the costs of fiber deployment – either as dedicated backhaul spectrum, or in the exciting use case of integrated access and backhaul, enabling the ample mmW spectrum resource to be used both for OTA backhaul as well as to serve devices. We also look at how mmWave can be leveraged into more traditional use cases of distributed antenna systems and repeater.

Chapter 6 provides a robust discussion on the technologies which allow mmWave to both overcome the challenges and exploit the benefits that were detailed in Chapter 4. We discussed the various CU/DU splits in RAN architecture, the challenges of antenna design for mmWave, both at the cell site and handset, and the all-important concepts of beamforming and beam tracking and their practical design and implementation trade-offs. Finally, we discuss the work in standards to further evolve the mmWave specifications, including improvements to beam refinement procedures.

Chapter 7 discusses practical operational aspects of mmWave, and the challenges of mmW coverage planning and device implementation. We begin with the 3GPP standardized mechanisms to deploy mmWave, starting with the LTE-NR dual connectivity currently deployed, followed by all-5G NR carrier aggregation, just now being commercialized. We then propose that mmWave is best realized in NR carrier aggregation with sub-6 GHz NR, making complimentary use of their strengths. We further discuss the transport topology necessary to accommodate the high bandwidth and low latency requirements that are critical enablers for the coverage extension possible with CA.

Finally, in Chapter 8 we explore the challenges of keeping mmWave deployment costs in check. We present results from studies showing significant coverage can be achieved from co-siting mmWave with outdoor LTE macrocells and small cells, and indoors with Wi-Fi APs. We present network capacity simulation results for both indoor and outdoor environments that lend credence to the promise of 5G on mmWave, with real-world performance that is substantially better than that currently possible on 4G across multiple metrics. The findings also illustrate that these emerging 5G networks will have the capacity and performance to support a whole host of new services and experiences beyond the traditional use cases of browsing, downloading, and streaming.

Appendix

Acronyms

λ	wavelength (meters)
μ s	microsecond
1G	First Generation
10 GigE	10 Gigabit Internet
2G	Second Generation
3G	Third Generation
3GPP	Third Generation Partnership Project
4G	Fourth Generation
5G	Fifth Generation
5GC	5G Core
6G	Sixth Generation Wireless Technology (not yet standardized)
ACK	Acknowledgement
ACMA	Australian Communication and Media Authority
ADC	Analog Digital Converter
AI	Artificial Intelligence
AP	Aperiodic
APA	Analog Phase Array
AR	Augmented Reality
bps	Bits per Second
BBU	Baseband Unit
BFD	Beam Failure Detection
BFR	Beam Failure Recovery
BS	Base Station
BWP	Bandwidth Part
c	speed of light in air (@3 × 10 ⁸ m/sec)
C	Celsius
CA	Carrier Aggregation
CapEx	Capital Expenditure
CC	Component Carrier
CE	Control Element
CEPT	European Conference of Postal and Telecommunications Administrations
CFRA	Contention Free Random Access
cm	centimeter
CMOS	Complementary metal-oxide-semiconductor
CMR	Channel Management Resource
CORESET	Control Resource Set
CP	Control Plane
CPRI	Common Public Radio Interface

CSI	Channel State Information
CSIT	Channel State Information at the Transmitter
CU	Central Unit
d	distance (meters)
DAC	Digital Analog Converter
DAS	Distributed Antenna System
dB	Decibel
dBi	Decibel (Isotropic)
dBm	Decibel
DC	Dual Connectivity
DH	Dense Clutter & High Basestation Height
DL	Dense Clutter & Low Basestation Height
DL	Downlink
DMRS	Demodulation Reference Signal
DoT	Department of Telecom (India)
ds	Symbol Duration
DSS	Dynamic Spectrum Sharing
DU	Distributed Unit
eCPRI	Evolved Common Public Radio Interface
ECG	Electrocardiogram
EIRP	Effective Isotropic Radiated Power
eMBB	Enhanced Mobile Broadband
EPC	Evolved Packet Core
EU	European Union
EVM	Error Vector Magnitude
f	frequency
f _o	carrier frequency
FCC	Federal Communications Service
FDA	Fully Digital Architecture
FDD	Frequency Division Duplex
FoM	Figure of Merit
FR1	Frequency Range 1
FR2	Frequency Range 2
FTP	File Transfer Protocol
FWA	Fixed Wireless Access
FWLL	Fixed Wireless Local Loop
GANT	Antenna Gain
Ge	Embedded Element Gain
Gelement	Element Gain
Gbps	Gigabits per Second
GHz	Gigahertz
gNodeB	gNodeB (5G NodeB)
GR	Receiver Gain

GSPS	Gigabit Sample per Second
GT	Transmitter Gain
H2O	water molecule
HARQ	Hybrid Automatic Repeat Request
HBF	Holographic Beam Former
HetNet	Heterogenous Network
HDTV	Hight Definition Television
HOM	Higher Order Modulation
HPA	Hybrid Phase Array
Hz	Hertz
IAB	Integrated Access and Backhaul
IC	Integrated Circuit
IF	Intermediate Frequency
IMR	Interference Management Resource
InF	Indoor Factory
InH	Indoor Hotspot
I/O	Input/Output
ISED	Innovation, Science and Economic Development Canada
IIoT	Industrial Internet of Things
IoT	Internet of Things
km	kilometer
L1	Layer 1
L2	Layer 2
L3	Layer 3
LAA	License Assisted Access
Lohmic	Ohmic Loss
LNA	Low Noise Amplifier
LO	Local Oscillator
LOS	Line of Sight
LRR	Link Recovery Request
LS	Least Square
LTE	Long Term Evolution
MAC	Medium Access Control
MAPL	Maximum Allowable Pathloss
MCG	Master Cell Group
MEC	Mobile Edge Computing
MIIT	Ministry of Industry and Information Technology (China)
MIMO	Multiple Input Multiple Output
MHz	Megahertz
MMSE	Minimum Mean Square Error
mmWave	Millimeter Wave
MN	Master Node
MNO	Mobile Network Operator

mph	Miles per Hour
ms	Microsecond
MTC	Machine Type Communication
NCC	National Communications Commission (Taiwan)
NFV	Network Function Virtualization
NR	New Radio
NR CA	NR Dual Connectivity
NSA	Non Stand Alone
O2	Oxygen Molecule
NPRM	Notice of Proposed Rulemaking
OFDM	Orthogonal Frequency Division Multiplexing
OFDMA	Orthogonal Frequency Division Multiple Access
OOBE	Out of Band Emissions
OpEx	Operational Expenditure
OTT	Over the Top
PA	Power Amplifier
PAPR	Peak to Average Power Ratio
PC	Power Class
PCB	Printed Circuit Board
PCell	Primary Cell
PDCCH	Physical Downlink Control Channel
PDCCP	Packet Data Convergence Protocol
PDSCH	Physical Downlink Shared Channel
PL	Pathloss
PLL	Phase Lock Loop
PR	Received Power
PT	Transmitted Power
PtMP	Point Multipoint
PTRS	Phase Tracking Reference Signal
PUCCH	Physical Uplink Control Channel
PUSCH	Physical Uplink Shared Channel
QAM	Quadrature Amplitude Modulation
Qos	Quality of Service
RAN	Radio Access Network
RF	Radio Frequency
RIC	Radio Intelligence Controller
RLC	Radio Link Control
RRC	Radio Resource Control
RRU	Remote Radio Head
RS	Reference Symbol
RSPG	Radio Spectrum Policy Group
RSU	Roadside Unit
RU	Radio Unit

PHY	Physical Layer
SA	Standalone 5G NR
SCell	Secondary Cell
SCG	Secondary Cell Group
SCS	Subcarrier Spacing
SDN	Software Defined Network
SH	Sparse Clutter & High Basestation Height
SINR	Signal to Interference Plus Noise Ratio
SL	Sparse Clutter & High Basestation Height
SN	Secondary Node
SNR	Signal to Noise Ratio
SRS	Sounding Reference Signal
SSB	Synchronization Signal Block
UE	User Equipment
UMFUS	Upper Microwave Flexible Use Service
URLLC	Ultra Reliable Low Latency Communication
TB	Terabyte
TCI	Transmission Configuration Indicator
TDD	Time Division Duplex
TR	3GPP Technical Report
TTI	Time Transmission Interval
UL	Uplink
UMa	Urban Macrocell
UMi	Urban Microcell
UP	User Plane
v	velocity (m/s)
VCO	Voltage Controlled Oscillator
VR	Virtual Reality
WiGig	Wireless Gigabyte Standards for 60 GHz Wi
WRC19	World Radiocommunication Conference 2019
XR	Extended Reality
XPIC	Cross Polarization Interference Cancelling Technology
ZP	Zero Power

3GPP Pathloss Models

Table A-1 contains several pathloss models from 3GPP TR 38.901, as referenced in Chapter 4.1.5.

Table A-1 Pathloss between base station (BS) and user terminal (UT) valid up to 100 GHz, taken from 3GPP TR 38.901.

Scenario	Sight conditions	Pathloss (dB) f_c is in GHz & d is in meter (See note 6)	Shadow fading std (dB)	Applicability range, antenna height (default values)
UMa	LOS	$PL_{UMa-LOS} = \begin{cases} PL_1 & 10m \leq d_{2D} \leq d'_{BP} \\ PL_2 & d'_{BP} \leq d_{2D} \leq 5km \end{cases}$, see note 1 $PL_1 = 28.0 + 22 \log_{10}(d_{3D}) + 20 \log_{10}(f_c)$ $PL_2 = 28.0 + 40 \log_{10}(d_{3D}) + 20 \log_{10}(f_c) - 9 \log_{10}((d'_{BP})^2 + (h_{BS} - h_{UT})^2)$	$\sigma_{SF} = 4$	$1.5m \leq h_{UT} \leq 22.5m$ $h_{BS} = 25m$
	NLOS	$PL_{UMa-NLOS} = \max(PL_{UMa-LOS}, PL'_{UMa-NLOS})$ for $10m \leq d_{2D} \leq 5km$ $PL'_{UMa-NLOS} = 13.54 + 39.08 \log_{10}(d_{3D}) + 20 \log_{10}(f_c) - 0.6(h_{UT} - 1.5)$	$\sigma_{SF} = 6$	$1.5m \leq h_{UT} \leq 22.5m$ $h_{BS} = 25m$ Explanations: see note 3
		Optional	$PL = 32.4 + 20 \log_{10}(f_c) + 30 \log_{10}(d_{3D})$	$\sigma_{SF} = 7.8$
UMi - Street Canyon	LOS	$PL_{UMi-LOS} = \begin{cases} PL_1 & 10m \leq d_{2D} \leq d'_{BP} \\ PL_2 & d'_{BP} \leq d_{2D} \leq 5km \end{cases}$, see note 1 $PL_1 = 32.4 + 21 \log_{10}(d_{3D}) + 20 \log_{10}(f_c)$ $PL_2 = 32.4 + 40 \log_{10}(d_{3D}) + 20 \log_{10}(f_c) - 9.5 \log_{10}((d'_{BP})^2 + (h_{BS} - h_{UT})^2)$	$\sigma_{SF} = 4$	$1.5m \leq h_{UT} \leq 22.5m$ $h_{BS} = 10m$
	NLOS	$PL_{UMi-NLOS} = \max(PL_{UMi-LOS}, PL'_{UMi-NLOS})$ for $10m \leq d_{2D} \leq 5km$ $PL'_{UMi-NLOS} = 35.3 \log_{10}(d_{3D}) + 22.4 + 21.3 \log_{10}(f_c) - 0.3(h_{UT} - 1.5)$	$\sigma_{SF} = 7.82$	$1.5m \leq h_{UT} \leq 22.5m$ $h_{BS} = 10m$ Explanations: see note 4
		Optional	$PL = 32.4 + 20 \log_{10}(f_c) + 31.9 \log_{10}(d_{3D})$	$\sigma_{SF} = 8.2$
Indi - Office	LOS	$PL_{Indi-LOS} = 32.4 + 17.3 \log_{10}(d_{3D}) + 20 \log_{10}(f_c)$	$\sigma_{SF} = 3$	$1m \leq d_{3D} \leq 150m$
	NLOS	$PL_{Indi-NLOS} = \max(PL_{Indi-LOS}, PL'_{Indi-NLOS})$ $PL'_{Indi-NLOS} = 38.3 \log_{10}(d_{3D}) + 17.30 + 20 \log_{10}(f_c) - 0.3(h_{UT} - 1.5)$	$\sigma_{SF} = 8.03$	$1m \leq d_{3D} \leq 150m$
		Optional	$PL'_{Indi-NLOS} = 32.4 + 20 \log_{10}(f_c) + 31.9 \log_{10}(d_{3D})$	$\sigma_{SF} = 8.29$

mmE	LOS	$PL_{LOS} = 31.84 + 21.50 \log_{10}(d_{3D}) + 19.00 \log_{10}(f_c)$	$\sigma_{SF} = 4.3$	$1 \leq d_{3D} \leq 600 \text{ m}$
	NLOS	InF-SL: $PL = 33 + 25.5 \log_{10}(d_{3D}) + 20 \log_{10}(f_c)$ $PL_{NLOS} = \max(PL, PL_{LOS})$	$\sigma_{SF} = 5.7$	
		InF-DL: $PL = 18.6 + 35.7 \log_{10}(d_{3D}) + 20 \log_{10}(f_c)$ $PL_{NLOS} = \max(PL, PL_{LOS}, PL_{InF-SL})$	$\sigma_{SF} = 7.2$	
		InF-SH: $PL = 32.4 + 23.0 \log_{10}(d_{3D}) + 20 \log_{10}(f_c)$ $PL_{NLOS} = \max(PL, PL_{LOS})$	$\sigma_{SF} = 5.9$	
		InF-DH: $PL = 33.63 + 21.9 \log_{10}(d_{3D}) + 20 \log_{10}(f_c)$ $PL_{NLOS} = \max(PL, PL_{LOS})$	$\sigma_{SF} = 4.0$	

Note 1: Breakpoint distance $d'_{BP} = 4 h'_{BS} h'_{UT} f_c / c$, where f_c is the center frequency (Hz), $c = 3.0 \cdot 10^8$ m/s is the propagation velocity in free space, and h'_{BS} and h'_{UT} are the effective antenna heights at the BS and the UT, respectively. The effective antenna heights h'_{BS} and h'_{UT} are computed as follows: $h'_{BS} = h_{BS} - h_E$, $h'_{UT} = h_{UT} - h_E$, where h_{BS} and h_{UT} are the actual antenna heights, and h_E is the effective environment height. For UMi $h_E = 1.0$ m. For UMa $h_E = 1$ m with a probability equal to $1/(1+C(d_{2D}, h_{UT}))$ and chosen from a discrete uniform distribution $\text{uniform}(12, 15, \dots, (h_{UT}-1.5))$ otherwise. With $C(d_{2D}, h_{UT})$ given by

$$C(d_{2D}, h_{UT}) = \begin{cases} 0 & , h_{UT} < 13\text{m} \\ \left(\frac{h_{UT} - 13}{10} \right)^{1.5} g(d_{2D}) & , 13\text{m} \leq h_{UT} \leq 23\text{m} \end{cases}$$

where

$$g(d_{2D}) = \begin{cases} 0 & , d_{2D} \leq 18\text{m} \\ \frac{5}{4} \left(\frac{d_{2D}}{100} \right)^3 \exp\left(\frac{-d_{2D}}{150} \right) & , 18\text{m} < d_{2D} \end{cases}$$

Note that h_E depends on d_{2D} and h_{UT} and thus needs to be independently determined for every link between BS sites and UTs. A BS site may be a single BS or multiple co-located BSs.

Note 2: The applicable frequency range of the PL formula is $0.5 < f_c < f_H$ GHz, where $f_H = 100$ GHz.

Note 3: UMa NLOS pathloss is from TR 36.873 with simplified format and $PL_{UMa-NLOS} = \text{Pathloss of UMa LOS outdoor scenario}$.

Note 4: $PL_{UMi-NLOS} = \text{Pathloss of UMi-Street Canyon LOS outdoor scenario}$.

Note 5: Break point distance $d_{BP} = 2\pi h_{BS} h_{UT} f_c / c$, where f_c is the center frequency in Hz, $c = 3.0 \cdot 10^8$ m/s is the propagation velocity in free space, and h_{BS} and h_{UT} are the antenna heights at the BS and the UT, respectively.

Note 6: f_c denotes the center frequency normalized by 1GHz, all distance related values are normalized by 1m, unless it is stated otherwise.

Note: The distance between BS and UT is d , measured either horizontally (d_{2D}) or diagonally along the line between BS transmitter and UT (d_{3D}). Here we removed the rural macrocell (RMA) models from the original table, as those models do not extend into the mmWave regime. The symbol definitions and abbreviations are defined in Chapters 3.2 and 3.3 of TR 38.901.

DAS Background

With more than 80% of mobile data traffic originating or terminating indoors, one enormous opportunity for mobile operators and service providers is to bring mmWave services to indoor locations. The fact that mmWave does not propagate well from the outside to inside is beneficial for deploying mmWave indoors as well, since the same mmWave spectrum can be reused indoors with limited coordination with the outdoor deployment. This benefit opens new possibilities for mobile operators to offer private indoor mmWave networks, in addition to expanding mmWave indoors as part of their public networks. One exciting opportunity for 5G NR mmWave is indoor enterprises. Today, most offices have Wi-Fi connectivity for computers and other enterprise devices. With 5G NR mmWave private networks, enterprises can realize the vision of “mobile office of the future”, bringing enhanced performance, convenience, security, and user experiences not possible with today’s connectivity solutions. The most dominant technology for indoor enterprise is DAS [41].

A Distributed antenna system (DAS) is a network of antennas, connected to a common source, distributed throughout a building or an area to improve network performance. The spacing between antennas is such that each antenna gives full coverage without overlapping with other antennas, hence providing uniform coverage within the building. This network of antennas is also power efficient in comparison to a single, high power base station with a larger antenna covering a wide area.

DAS solutions continue to be popular because they are the most efficient and economical way to provide multi-frequency in-building wireless coverage in larger venues. Small cells are a preferred solution for residences or smaller buildings, but given their current limitations they will not replace DAS at the higher end. Rather, a small cell can be used as signal source for the DAS to reduce the cost of deployments in terms of equipment, cabling and real estate as well as security.

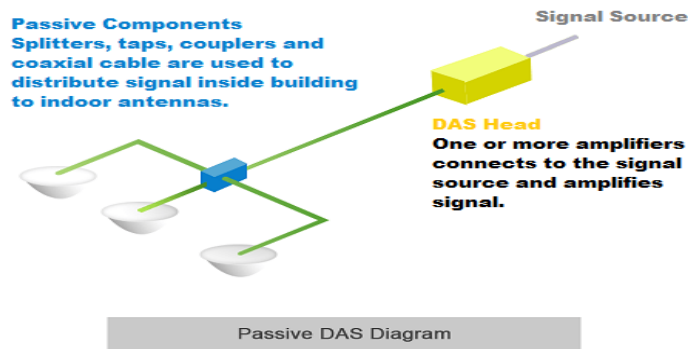
A DAS can be designed for use indoors or outdoors and can be used to provide wireless coverage in hotels, subways, airports, college campuses, sport arenas, hospitals, businesses, roadway tunnels etc. The wireless services typically provided by a DAS include PCS, cellular, Wi-Fi, police, fire, and emergency services.

A DAS has two basic components: a signal source, and a distribution system. The signal source is the input to the DAS network. It can be an on-site macro or small cell base station. It can also be an off-air system (via an antenna on the roof) or remotely located via fiber. The second part of a DAS network would be the distribution system. Once the signal is received by the signal source, it must be distributed throughout the building or the area. There are three types of distribution systems: Passive, analog, and Digital DAS.

DAS Types

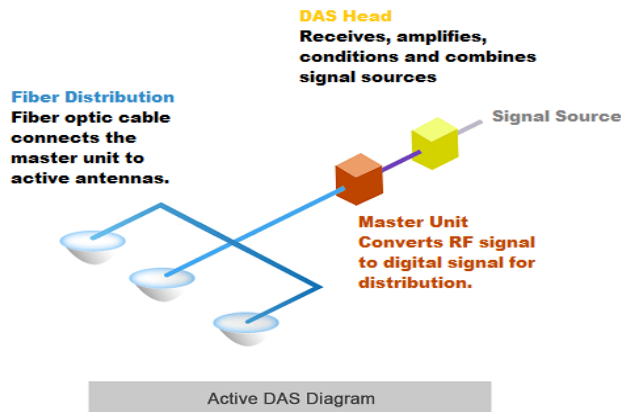
Passive DAS

A passive DAS is a bidirectional RF amplifier connected to a number of passive antennas through a network of passive components. This is an old technology that is seldom used today, and not applicable to mmWave. Fig. 9.1 shows a typical diagram of passive DAS [42].



Analog DAS

The remote antennas are an active unit, comprising of a small power amplifier for down link and a Low Noise Amplifier (LNA) for uplink to keep the noise figure low. There is no digital conversion from the signal source (base station) to the remote units. The RF signal from signal source and through the DAS head-end is amplified and distributed to the remote units. This can be done over the cable or fiber (with optical modem on both ends of the fiber). Fig. 9.2 illustrates a typical analog DAS with fiber distribution [42].



8.4.1.1 Digital DAS

Baseband signal is distributed using (most commonly) CPRI or eCPRI from the signal source to the active DAS remote units using fiber. In this case signal source does not have the radio part but the DAS active remote units become more than a power amp and LNA, because you have to transform the base band to RF. Besides, due to limitation of CPRI capacity, you may be restricted on how many channels or services (bandwidth) you can put on the DAS, with reasonable cost.

As stated above, both digital and analog DAS can use fiber for distribution. In fact that is the most cost effective approach today because cable are heavy, inflexible, and lossy. In mmWave, it is not even a feasible option. The only cable used is where you need to connect the active part of the antenna to the passive antenna. That is usually a very short cable. In mmWave, antennas and transmission/ reception units are integrated.

References

[1]	FCC Lab Office of Engineering and Technology, "Compliance verification/measurement method for part 30 devices," FCC, 2019.
[2]	3GPP, "TR 38.101-2, User Equipment (UE) radio transmission and reception; Frequency range 2 stand-alone," September 2020. [Online]. Available: https://www.iwpc.org/WhitePaper.aspx?WhitePaperID=24 . [Accessed 10 September 2020].
[3]	ETSI, "ETSI Whitepaper No. 9, E band and V band survey on status of worldwide regulation," June 2015. [Online]. Available: https://www.etsi.org/images/files/ETSIWhitePapers/etsi_wp9_e_band_and_v_band_survey_20150629.pdf .
[4]	T. S. Rappaport, R. W. Heath, R. C. Daniels and J. N. Murdock, Millimeter Wave Wireless Communications, 1st ed., Upper Saddle River, NJ: Prentice Hall, 2014.
[5]	I. A. Hemadeh, K. Satyanarayana, M. El-Hajjar and L. Hanzo, "Millimeter-Wave Communications: Physical Channel Models, Design Considerations, Antenna Constructions, and Link-Budget," Second Quarter 2018. [Online]. Available: https://ieeexplore.ieee.org/document/8207426 . [Accessed 10 September 2020].
[6]	S. Sun, T. S. Rappaport, M. Shafi, P. Tang, J. Zhang and P. J. Smith, "Propagation Models and Performance Evaluation for 5G Millimeter-Wave Bands," September 2018. [Online]. Available: https://ieeexplore.ieee.org/document/8386686 . [Accessed 10 September 2020].
[7]	C. Vargas and L. Mello, "Measurements of Reflection and Penetration Loss of Construction Materials at 28 GHz and 38 GHz," in <i>IEEE-APS Topical Conference on Antennas and Propagation in Wireless Communications (APWC)</i> , Catagena de Indias, 2018.
[8]	A. Isa, A. Nix and G. Hilton, "Impact of diffraction and attenuation for material characterization in millimeter wave bands," in <i>2015 Loughborough Antennas & Propagation Conference (LAPC)</i> , Loughborough, 2015.
[9]	F. Schwering, E. Violette and R. Espeland, "Millimeter-Wave Propagation in Vegetation: Experiments and Theory," May 1988. [Online]. Available: https://ieeexplore.ieee.org/document/3037 . [Accessed 10 September 2020].
[10]	H. Xu, V. Kukshya and T. Rappaport, "Spatial and temporal characteristics of 60-GHz indoor channels," September 2000. [Online]. Available: https://ieeexplore.ieee.org/document/995521 . [Accessed 10 September 2020].
[11]	V. Raghavan and et. al., "Spatio-Temporal Impact of Hand and Body Blockage for Millimeter-Wave User Equipment Design at 28 GHz," December 2018. [Online]. Available: https://ieeexplore.ieee.org/document/8570039 . [Accessed 10 September 2020].
[12]	"Adapted from Figure 3, Bulletin Number 70 "Millimeter Wave Propagation: Spectrum Management Implications", Office of Engineering and Technology, Federal Communications Commission," July 1997. [Online]. Available: https://transition.fcc.gov/Bureaus/Engineering_Technology/Documents/bulletins/oet70/oet70a.pdf . [Accessed 10 September 2020].

[13]	“Adapted from Figure 4 of Bulletin Number 70 “Millimeter Wave Propagation: Spectrum Management Implications”, Office of Engineering and Technology, Federal Communications Commission,” July 1997. [Online]. Available: https://transition.fcc.gov/Bureaus/Engineering_Technology/Documents/bulletins/oet70/oet70a.pdf . [Accessed 10 September 2020].
[14]	3GPP, “TR 38.901, Study on channel model for frequencies from 0.5 to 100 GHz. For UMa and UMi scenarios, see Table 7.2-1. For InH, see Table 7.2-2. For InF, see Table 7.2-4,” Jan. 2020. [Online]. Available: https://portal.3gpp.org/desktopmodules/Specifications/SpecificationDetails.aspx?specificationId=3173 . [Accessed 10 Sep. 2020].
[15]	Keysight Technologies, “OTA Test for Millimeter-Wave 5G NR Devices and Systems [Whitepaper],” [Online]. Available: https://www.keysight.com/tw/zh/assets/7018-05940/white-papers/5992-2600.pdf . [Accessed 10 September 2020].
[16]	V. Va, J. Choi and R. Heath, “The Impact of Beamwidth on Temporal Channel Variation in Vehicular Channels and its Implications,” 2016 November IEEE. [Online]. Available: https://ieeexplore.ieee.org/document/7742901 . [Accessed 10 September 2020].
[17]	E. Dahlman, S. Parkvall and J. Sköld, “5G NR: The Next Generation Wireless Access Technology,” London, Academic Press, 2018, p. 125.
[18]	Ericsson, “Cellular networks for Massive IoT [Whitepaper],” January 2020. [Online]. Available: https://www.ericsson.com/48ff1f/assets/local/reports-papers/white-papers/massive_iot_whitepaper.pdf . [Accessed 10 September 2020].
[19]	D. Brin, “The Case for Wideband Transmission: Wideband Channels From Macroeconomics to Standardization (Whitepaper),” Ceragon, 2020.
[20]	Ceragon, “Can 5G hauling capacity requirements be satisfied only by a mmW solution?,” August 2020. [Online]. Available: https://www.ceragon.com/blog/can-5g-hauling-capacity-requirements-be-satisfied-only-by-mmw-solution . [Accessed 10 September 2020].
[21]	NEC, “NEC develops millimeter-wave distributed antenna radio unit improving the channel quality for indoor 5G applications (Press Release),” January 2020. [Online]. Available: https://www.nec.com/en/press/202001/global_20200124_01.html . [Accessed 10 September 2020].
[22]	Ofcom, “An assessment of the effects of repeaters on mobile networks,” Nov. 2015. [Online]. Available: https://www.ofcom.org.uk/research-and-data/technology/telecoms/effects-of-repeaters-on-mobile-networks .
[23]	Pivotal Commware, “Reducing 5G Deployment Costs Using Holographic Beam,” [Online]. Available: https://pivotalcommware.com/wp-content/uploads/2020/05/Reducing-5G-Deployment-Costs-Using-Holographic-Beam-Forming-Repeaters-from-Pivotal-Commware-May-2020-FINAL.pdf . [Accessed 10 Sept. 2020].
[24]	Pivotal Commware, “What Is Holographic Beamforming?,” [Online]. Available: https://pivotalcommware.com/technology/ . [Accessed 10 Sep. 2020].
[25]	Techplayon, “What is RRH (Remote Radio Head), How it is connected to BBU (Base Band Unit)?,” July 2017. [Online]. Available: http://www.techplayon.com/rrh-remote-radio-head-connected-bbu-base-band-unit/ . [Accessed 10 September 2020].
[26]	Keysight Technologies, “O-RAN for 5G: The Path Forward Webinar,” May 2020. [Online]. Available: https://www.keysight.com/us/en/events/america/webinars.html . [Accessed 10 September 2020].

[27]	"Researchgate: Analog Beamforming Architecture image," [Online]. Available: https://www.researchgate.net/figure/Analog-beamforming-architecture_fig1_325465948 . [Accessed 10 September 2020].
[28]	I. Stepanets, G. Forkin and A. Müller, "Beamforming Techniques Performance," March 2019. [Online]. Available: https://www.researchgate.net/publication/332767357_Beamforming_Techniques_Performance_Evaluation_for_5G_massive_MIMO_Systems . [Accessed 10 September 2020].
[29]	5G Americas, "Advanced Antenna Systems for 5G (Whitepaper)," 2019. [Online]. Available: https://www.5gamericas.org/wp-content/uploads/2019/08/5G-Americas_Advanced-Antenna-Systems-for-5G-White-Paper.pdf . [Accessed 10 September 2020].
[30]	ZTE, "BeamHop: A New Member of LTE Base Station Family," November 2012. [Online]. Available: https://www.zte.com.cn/global/about/magazine/zte-technologies/2012/6/en_561/370650.html . [Accessed 10 September 2020].
[31]	"RF GlobalNet Guest Column by Dave Corman, Anokiwave: "A Comprehensive Guide To Active Antennas (Or, "Beamforming 101")," July 2018. [Online]. Available: https://www.rfglobalnet.com/doc/a-comprehensive-guide-to-active-antennas-or-beamforming-0001 . [Accessed 10 September 2020].
[32]	IWPC, "5G Millimeter Wave Frequencies and Mobile Networks v2," 2020. [Online]. Available: https://www.iwpc.org/WhitePaper.aspx?WhitePaperID=24 . [Accessed 10 Sep. 2020].
[33]	M. Rutschlin, "The Simulia Blog: 5G Antenna Design for Mobile Phones," Mar. 2020. [Online]. Available: https://blogs.3ds.com/simulia/5g-antenna-design-mobile-phones/ . [Accessed 10 Sept. 2020].
[34]	O. Castañeda, S. Jacobsson, G. Durisi, T. Goldstein and C. Studer, "High-Bandwidth Spatial Equalization for mmWave Massive MU-MIMO With Processing-in-Memory," 2020 May. [Online]. Available: https://ieeexplore.ieee.org/document/9050632 .
[35]	B. Murmann, "ADC Performance Survey 1997-2020 (ISSCC & VLSI Symposium)," Aug. 2020. [Online]. Available: https://web.stanford.edu/~murmann/adcsurvey.html . [Accessed 10 Sep. 2020].
[36]	J. Preez and S. Sinha, "Millimeter-Wave Power Amplifiers, 1st ed.," New York, Springer, 2017, p. 371.
[37]	Qualcomm Technologies, "Breaking the wireless barriers to mobilize 5G NR mmWave," Jan. 2019. [Online]. Available: https://www.qualcomm.com/media/documents/files/webinar-breaking-the-wireless-barriers-to-mobilize-5g-nr-mmwave.pdf . [Accessed 10 Sep. 2020].
[38]	3GPP, "38.321, NR; Medium Access Control (MAC) protocol specification," Jul. 2020. [Online]. Available: https://portal.3gpp.org/desktopmodules/Specifications/SpecificationDetails.aspx?specificationId=3194 . [Accessed 10 Sep. 2020].
[39]	Qualcomm Technologies, "Mobilizing 5G NR Millimeter Wave: Network Coverage Simulation Studies for Global Sites," Oct. 2017. [Online]. Available: https://www.qualcomm.com/media/documents/files/white-paper-5g-nr-millimeter-wave-network-coverage-simulation.pdf . [Accessed 10 Sep. 2020].
[40]	Qualcomm Technologies, "5G NR mmWave outdoor and indoor deployment strategy," May 2019. [Online]. [Accessed 10 Sep. 2020].
[41]	Qualcomm Technologies, "What new indoor opportunities will 5G NR mmWave bring?," May 2019. [Online]. Available: https://www.qualcomm.com/news/onq/2019/05/08/what-new-indoor-opportunities-will-5g-nr-mmwave-bring . [Accessed 10 September 2020].
[42]	Waveform, "Cellular Distributed Antenna Systems (DAS)," [Online]. Available: https://www.waveform.com/pages/das-distributed-antenna-systems . [Accessed 10 September 2020].

[43]	A. Ghosh, "Microwave Journal, "The 5G mmWave Radio Revolution"," September 2016. [Online]. Available: https://www.microwavejournal.com/articles/27056-the-5g-mmwave-radio-revolution?v=preview . [Accessed 10 September 2020].
[44]	B. Peterson and D. Schnauffer, "Microwave Journal, 5G Fixed Wireless Access Array and RF Front-End Trade-Offs," February 2018. [Online]. Available: https://www.microwavejournal.com/articles/29707-g-fixed-wireless-access-array-and-rf-front-end-trade-offs?v=preview . [Accessed 10 September 2020].
[45]	FCC, "Adapted from Figure 3, Bulletin Number 70 "Millimeter Wave Propagation: Spectrum Management Implications", Office of Engineering and Technology," July 1997. [Online]. Available: https://transition.fcc.gov/Bureaus/Engineering_Technology/Documents/bulletins/oet70/oet70a.pdf . [Accessed 10 September 2020].

Acknowledgments

5G Americas facilitates and advocates for the advancement and transformation of LTE, 5G and beyond throughout the Americas.

5G Americas' Board of Governors members include AT&T, Cable and Wireless, Ciena, Cisco, CommScope, Crown Castle, Ericsson, Intel, Mavenir, Nokia, Qualcomm Incorporated, Samsung, Shaw Communications Inc., T-Mobile USA, Inc., Telefónica and WOM.

5G Americas would like to recognize the significant project leadership and important contributions of group leaders of Intel and Matt Melester of CommScope, along with many representatives from member companies on 5G Americas' Board of Governors who participated in the development of this white paper.

5G Americas would like to recognize the significant project leadership and important contributions of group leaders Rao Yallapragada of Intel, Tao Luo and Lola Awoniyi-Oteri of Qualcomm, Woody Sellers and Ahmad Armand of T-Mobile, along with many representatives from member companies on 5G Americas' Board of Governors who participated in the development of this white paper. The contents of this document reflect the research, analysis, and conclusions of 5G Americas and may not necessarily represent the comprehensive opinions and individual viewpoints of each particular 5G Americas member company. 5G Americas provides this document and the information contained herein for informational purposes only, for use at your sole risk. 5G Americas assumes no responsibility for errors or omissions in this document. This document is subject to revision or removal at any time without notice. No representations or warranties (whether expressed or implied) are made by 5G Americas and 5G Americas is not liable for and hereby disclaims any direct, indirect, punitive, special, incidental, consequential, or exemplary damages arising out of or in connection with the use of this document and any information contained in this document.